Universidade de Lisboa

Faculdade de Ciências

Departamento de Física

Dynamic Functional Connectivity of BOLD fMRI signal during both rest and task execution states

Joana Paula Fontinha de Brito

Dissertação

Mestrado Integrado em Engenharia Biomédica e Biofísica

Perfil em Engenharia Clínica e Instrumentação Médica

2014

Universidade de Lisboa

Faculdade de Ciências

Departamento de Física

Dynamic Functional Connectivity of BOLD fMRI signal during both rest and task execution states

Joana Paula Fontinha de Brito

Dissertação

Mestrado Integrado em Engenharia Biomédica e Biofísica

Perfil em Engenharia Clínica e Instrumentação Médica

Orientadores: Professor Alexandre Andrade e Professor Hugo Ferreira

2014

ACKNOWLEDGMENTS

First of all, I would like to thank to my professors, Alexandre Andrade and Hugo Ferreira, for all the patience, help, availability and learning through my academic journey. Their collaboration was, undoubtedly, very important to me.

I also would like to thank to the Institute of Biophysics and Biomedical Engineering for hosting me during the last years and to the Technical University of Graz for kindly made available all the subjects datasets used on this work.

To my parents, Maria de Fátima Fontinha and Armando Brito I would like to say how grateful I am for all the attention, the emotional support and for all the friendly words of encouragement. With the same love I mention my brother, João Brito, whom I thank for all the silly jokes and chocolate cakes that always animate me. It would not be fair to forget my lovely pet, named Békita, for waking me up with kisses and salute me every day with the same affection and joy. I also would like to thank to my grandmother Idolinda for all the education and prayers in my name.

A special thankful to my best friend and sister, Vânia, with whom I shared so many moments. One of the most important things that I carry from my academic life is our friendship. I am deeply thankful to you for always being there for me.

I don't want to forget anyone so I would like to thank to all people who somehow contribute and help me. I consider my academic journey and my personal journey as our journey.

And, although you are no longer with us, I not only thank you, but also dedicate all my work, all my effort and all my wins up to today. I know you are smiling for me. I will miss you forever.

This research was supported by Fundação para a Ciência e Tecnologia (FCT) and Ministério da Ciência e Educação (MCE) Portugal (PIDDAC) under grants PTDC/SAU-ENB/120718/2010 and PEst-OE/SAU/UI0645/2014.

Fundação para a Ciência e a Tecnologia
MINISTÉRIO DA EDUCAÇÃO E CIÊNCIA

"Gratitude is the only treasure of the humble"

William Shakespeare

RESUMO

A conectividade cerebral é um tema muito atual na área das neurociências. A dinâmica da conectividade tem sido um tema muito explorado ultimamente com o objetivo de se descobrir mais sobre os processos cerebrais relacionados com sinais neuronais em bandas restritas de frequência e ainda compreender as diferenças entre repouso e execução de tarefas. O objetivo principal do presente trabalho consistiu no desenvolvimento de um procedimento para o estudo da conectividade dinâmica baseado na análise da coerência através da Transformada "Wavelet" que proporciona especificidade no tempo e na frequência. A abordagem implementada baseou-se em duas hipóteses diferentes de comunicação neuronal. A primeira considera que dois sinais neuronais oscilatórios comunicam durante períodos de coerência de magnitude elevada e a segunda considera que a comunicação neuronal ocorre em períodos de acoplamento de fase. O uso das duas hipóteses permitiu obter, respectivamente, dois perfis de comunicação neuronal. Uma vez que, as distribuições nulas dos perfis de coerência de magnitude e de acoplamento de fase são desconhecidas, e que os dados provêm de "single-trials" (ou seja, provêm de experiências únicas, sem repetição para um mesmo estado) foi construído um teste estatístico baseado em simulação de dados. A partir deste teste foi possível, para um dado nível de significância, distinguir períodos de comunicação neuronal significativa. Como a interação entre cada par de regiões é analisada através de janelas temporais, ao longo das séries temporais, os períodos de comunicação significativa correspondem a janelas onde há interação. Para os períodos de comunicação significativa foi calculado um valor médio de atraso temporal. A informação obtida a partir do método implementado pode ser expressa sob a forma de matrizes de conectividade funcional para todas as regiões do cérebro e sub-matrizes para regiões pertencentes a redes cerebrais específicas, usando ambas as medidas de comunicação como métricas de conectividade. Este método origina também mapas cerebrais para uma análise baseada numa região de referência onde são apresentados, através de mapas de cores, os valores médios de atrasos temporais entre a região referência e todas as restantes regiões do cérebro, ou para um conjunto mais específico. A partir da análise dos valores médios de atrasos temporais é possível estabelecer uma cronometria da passagem de informação. Se o valor obtido para o atraso temporal entre a região A e a região B é positivo, então, a região A é ativada primeiro e considera-se que precede a região B. A partir deste método é obtida uma análise detalhada entre cada duas regiões cerebrais através da observação dos perfis de interação para as duas hipóteses de comunicação neuronal e pela observação das distribuições de fases e atrasos temporais nas janelas de comunicação. Em relação às distribuições de fase um dos objetivos é conseguir identificar casos em que haja intervalos de fase preferidos para comunicação. A análise dos perfis de coerência de magnitude e acoplamento de fase permitem constatar que há flutuações

na comunicação ao longo das várias janelas temporais o que demostra uma dinâmica na conectividade funcional. Para ambos os perfis foi feita uma análise de correlação e de informação mútua. Para todos os casos analisados concluiu-se que há uma forte semelhança entre as medidas de coerência de magnitude e acoplamento de fase ao longo de todas as janelas temporais, com e sem comunicação significativa. Para testar e ilustrar a metodologia desenvolvida utilizou-se um conjunto de dados de três sujeitos, pelo que não há intenção de formalizar conclusões universais sobre a dinâmica de conectividade cerebral. Para todos os sujeitos a análise focou-se numa gama restrita de frequências, centrada nos 0.1 Hz, de forma a estudar a dinâmica da conectividade ao nível das oscilações lentas da resposta BOLD ("Blood Oxygenation Level-Dependent") que é obtida através de Ressonância Magnética funcional. Estas oscilações estão identificadas como características destes sinais, no entanto, a sua origem ainda não foi descoberta, o que causa um grande interesse na sua exploração.

Ao nível de significância de 95% os resultados mostram uma forte correlação positiva entre as duas métricas de comunicação utilizadas. Em relação á análise de informação mútua, entre as duas variáveis de comunicação, concluiu-se que ambos os perfis contêm 80% de informação comum. Os dados utilizados consistem num paradigma com aquisição em repouso e durante a execução do movimento de um dedo de forma voluntária e de forma estimulada, através de um estímulo auditivo. As matrizes de conectividade obtidas para os três sujeitos, durante todos os momentos de aquisição, e para as duas medidas de conectividade estudadas, revelam uma maior interação global entre as regiões cerebrais para os momentos de execução de tarefa do que para os momentos de repouso. Ou seja, maiores valores de conectividade funcional, para ambas as variáveis estudadas, entre um maior número de regiões para movimento voluntário e estimulado do que para repouso. Uma análise mais pormenorizada em regiões pertencentes à rede motora frontal-cognitiva e á rede parietal-premotora, ambas associadas ao movimento, mostram interações muito elevadas para ambos os movimentos, em todos os sujeitos analisados. Na análise mais detalhada entre regiões específicas, para dois sujeitos em movimento voluntário, detectou-se que os valores obtidos de fase entre a região motora primária esquerda, SMA, e o cíngulo anterior bem como a insula anterior, estão confinados ao intervalo $[-\frac{\pi}{2}; 0]$ durante as janelas temporais de comunicação, sugerindo uma preferência nos valores de fase para ambas as hipóteses de comunicação neuronal. Em relação ao estabelecimento da cronometria da passagem de informação entre regiões cerebrais, obteve-se, para todos os sujeitos, que a ínsula é ativada primeiro que o SMA durante as duas aquisições de execução de tarefa. Para dois dos três sujeitos analisados obteve-se, em movimento voluntário, que os gânglios da base, também envolvidos no controlo motor, são ativados antes da área SMA, pelo que a passagem de informação ocorre nesse sentido, como já foi reportado em estudos anteriores. Um tópico muito interessante e que tem sido o centro de muita discussão científica recai sobre a causa dos atrasos

temporais em fMRI. O grande foco tem sido sobre estes atrasos se deverem a diferenças hemodinâmicas ou a diferenças neuronais. O método implementado e apresentado neste trabalho não permite uma análise direta sobre este assunto mas, apesar de não fornecer uma forma de distinguir as duas hipóteses, alguns dos resultados obtidos corroboram a hipótese de que os atrasos temporais têm origem neuronal. A obtenção de diferentes latências entre as aquisições em repouso e as aquisições durante a execução de tarefas, de forma voluntária e estimulada, apoiam a hipótese de que os atrasos temporais não se devem apenas a atrasos hemodinâmicos. Se os resultados temporais apenas se devessem a atrasos hemodinâmicos, então, não seriam esperadas diferenças entre os valores obtidos para repouso e execução de tarefa. Também a descoberta de atrasos temporais diferentes entre regiões homólogas, em repouso e tarefa, apoia a ideia da origem neuronal uma vez que, seria esperado que os parâmetros fisiológicos que governam as latências hemodinâmicas fossem comparáveis entre regiões homólogas (e regiões vizinhas), com suplemento arterial e drenagem venosa comum.

A partir da metodologia implementada foi possível analisar redes cerebrais relacionadas com repouso, movimento voluntário e movimento estimulado, em termos de períodos de comunicação neuronal e atrasos temporais. Uma vez que, há consistência entre resultados obtidos com a abordagem utilizada e resultados descritos na bibliografia, conclui-se que a metodologia implementada para análise da conectividade funcional foi bem sucedida. Para concluir, de forma a melhorar e complementar o método desenvolvido, outras análises podem ser aplicadas, como uma análise de "clustering" (ou seja, uma análise de agrupamento) de forma a agrupar regiões cerebrais com perfis de comunicação semelhantes ou uma análise de periodicidade para analisar periodicidades nas flutuações dos mesmos perfis. De forma a complementar este método também medidas de conectividade anatómica e efetiva devem ser exploradas.

PALAVRAS-CHAVE

Conectividade dinâmica, Comunicação neuronal, BOLD fMRI, Oscilações lentas, Coerência Wavelet.

ABSTRACT

Brain connectivity is a very active topic in neuroscience. The main goal of the present work consisted on the development of a dynamic connectivity procedure based on wavelet coherence analysis which provides time-frequency specificity. The implemented approach was based on two different neuronal communication hypotheses. One considering that two oscillating neural signals communicate during periods of high magnitude coherence and the other considering that neuronal communication occurs during phase locking periods. Using both hypotheses two different profiles of neuronal communication were obtained. To deal with unknown null distributions, for single-trial data, a surrogate- based statistical test was performed to distinguish significant periods of communication. For those periods, an averaged temporal delay was computed. To test and illustrate the developed methodology a three subjects dataset is used including resting, voluntary and stimulus-driven action states. From functional connectivity matrices it is observed higher global interaction for both action conditions than for resting state. During tasks both frontal-cognitive and parietal-premotor networks have high connectivity values. The method also provides brain maps for temporal delays among specific brain regions. From temporal delays, the chronometry of information flow between brain regions and during voluntary action can be established. The most consistent observation is that the basal ganglia leads the SMA. The results show a strong similarity between both neuronal communication hypotheses. Regarding the discussion about neuronal or hemodynamic causes of fMRI temporal delays same latencies differences found between rest and task conditions support the theory that latencies are not due only to hemodynamic delays.

In conclusion the implemented methodology provides useful information about neuronal communication and temporal delays. To improve this work other approaches can be applied such as Clustering analysis and Periodicity analysis. To achieve a more comprehensive method also anatomical and effective connectivity measures should be explored.

KEYWORDS

Dynamic connectivity, Neuronal communication, BOLD fMRI, Slow oscillations, Wavelet coherence.

CONTENTS

LIST OF FIGURES

LIST OF TABLES

LIST OF ACRONYMS

ACC Anterior Cingulum Cortex

AIC Anterior Insular Cortex

BG Basal-Ganglia

BOLD Blood Oxygen Level Dependent

BP Blood Pressure

CBV Cerebral Blood Volume

DCA Dynamic Connectivity Analysis

DC-EEG Direct-current Electroencephalogram

deoxyHb Deoxyhemoglobin

DMN Default-mode- network

DTI Diffusion Tensor Imaging

EEG Electroencephalogram

fMR Functional Magnetic Resonance

fMRI Functional Magnetic Resonance Imaging

HRF Hemodynamic Response Function

ICN Intrinsic connectivity network

ISF Infra- slow Fluctuations

ISO Infra-slow Oscillations

M1 Primary motor cortex

MC Magnitude Coherence

MCS Magnitude Coherence Statistic

MCV Magnitude Coherence Value

MPF Medial Prefrontal cortex

NIRS Near-Infrared Spectroscopy

oxyHb OxyHemoglobin

PCC Posterior Parietal cortex

PL Phase-Locking

PLS Phase-Locking Statistic

PLV Phase-Locking Value

ROI Region of Interest

RSN Resting State Network

SMA Supplementary Motor Area

WTC Wavelet Transform Coherence

1- INTRODUCTION

1.1- Brain Imaging Techniques

Neuroimaging includes the use of different techniques which provide information about both structural and functional imaging without invasive neurosurgery. Nowadays there is a considerable number of safe brain imaging techniques allowing the detection of problems within the human brain and the research of how the human brain works. The investigation of how and where in the brain a cognitive process occurs is performed based on tasks and tests varying the level of demand on the cognitive, sensory or motor capacities of the participant. The performance of a task is correlated with physiological measures in a way to relate functions to areas of the brain. Functional imaging deals with the diagnosis of metabolic diseases and lesions such as Alzheimer's disease, with neurological and cognitive research such as the identification of multiple regions and their temporal relationships associated with the performance of a well designed task and also with brain-computer-interfaces. Some of the most known and used functional neuroimaging techniques are: Electroencephalogram, EEG; Near-Infrared Spectroscopy, NIRS, and functional Magnetic Resonance Imaging, fMRI (Raichle 2003).

1.1.1- EEG, NIRS and fMRI

In a brief description EEG refers to the recording of the electrical activity of the brain (more precisely, post-synaptic potentials), over a period of time, resorting to electrodes that are placed on the subject's scalp. Time dependent signals such as the EEG can be decomposed into a sum of pure frequency components which allows the exploration of the signal in terms of its power spectrum at each frequency. The EEG spectrum includes frequencies from 0 Hz to the limits of the recording equipment (usually the signal is high-passed filtered above 0.1 Hz). The analysis is typically made below 100Hz because it is the band where most of the power of the EEG signal is contained. Within the range from 0.1Hz to 100Hz the analysis is often made by sub-bands, depending on the application. The most commonly used bands are Delta (0.1 – 3.5 Hz); Theta (4.0- 7.5Hz); Alpha (8.0- 13.0 Hz); Beta (14.0 – 30.0 Hz), and Gamma (30.0 – 100 Hz or above) (Niedermeyer & Lopes da Silva 2005). DC-EEG, *direct current-EEG*, is adopted for a very slow changing EEG signal. The application of a DC amplifier implies that no low frequencies are omitted and thus it is essential when the signal of interest refers to very slow oscillating neurocortical activity such as signal with frequencies below 1Hz (Saab 2009).

NIRS is a brain imaging technique known as near-infrared spectroscopy based on oxyHemoglobin, oxyHb, and deoxyHemoglobin, deoxyHb, concentrations as an indirect measure of brain activity thanks to the relationship between focal brain activity and regional cerebral blood flow. This neurovascular coupling means that increased activity, that requires

additional metabolic supplies such as oxygen and glucose, is accompanied by local vasodilatation and increased blood flow and oxygenation. This metabolic response known as the hemodynamic response function, HRF, follows neural activity by several seconds. (Gervain et al. 2011)

Nowadays Functional Magnetic Resonance Imaging, fMRI, is a powerful technique which is very popular since it can give high quality visualization of the location of activity in the brain resulting from sensory stimulation or cognitive function. Therefore, it allows the study of how the healthy brain works, how it is affected by diseases and how it recovers after damage, and also how drugs can modulate activity (Strother 2006). So research on fMRI has been undergoing a quite considerable increase.

1.1.2- Hemodynamic BOLD- fMRI Response

Brain activity produces neurological signals that can be monitored and fMRI can be used to measure the hemodynamic response of brain in relation to neural activities. Such measurement is achieved by the detection of changes in blood oxygenation since there is a level dependence between the activation of a brain area and the demand of blood flow. When a specific region of the brain is used, there is an increase of blood flow to that same area. So fMRI research is typical focused on the blood oxygenation level-dependent signal named BOLD signal (Damoiseaux et al. 2006). The BOLD response depends on oxygen uptake, cerebral blood volume, CBV, and cerebral flow velocity. During neural activity there is an increase of blood flow causing an increase of oxyhemoglobin which is detectable with functional magnetic resonance imaging techniques. The magnitude and latency of the hemodynamic responses are affected by changes on neural activity associated (Pfurtscheller et al. 2012). After a sensorial stimulation or even after a mental imagery there is an increase in oxygen and glucose consumption supplied by the vascular system. In the most frequently used form of fMRI, the brain's responses to stimulation or task performance are inferred from the effects of local hemodynamic changes that influence microvascular oxygenation and, thus, measurable levels of MR signal strength. Since arterial blood is essentially oxygenated, this method measures the changes occurring on venous blood oxygenation. The relationship between the blood oxygenation level and the signal strength gives, to this form of functional imaging, the name Blood Oxygenation Level Dependent, BOLD. Using this concept the changes in MR strength are mapped and registered into an anatomical image and can specify the functional response to stimulation or task performance (Mcintyre et al. 2003).

The hemoglobin molecule has magnetic properties that differ depending upon whether it is bound to oxygen or not. The oxygenated hemoglobin (Hb) has no unpaired electron and no magnetic moment (it is diamagnetic). In contrast, deoxyhemoglobin (dHb) has unpaired electron

and magnetic moment (it is paramagnetic). Thus, because blood deoxygenation affects magnetic susceptibility, MR pulses used in fMRI should show more signal for blood with oxygen and less signal for blood deoxygenated. Following Figure 1, during neural activity, there is an increase of blood flow which causes an increase of oxyhemoglobin. Such increase is measured by T2*-weighted MRI (Aizenstein et al. 2004) and it is seen in the intensity of MR signal.

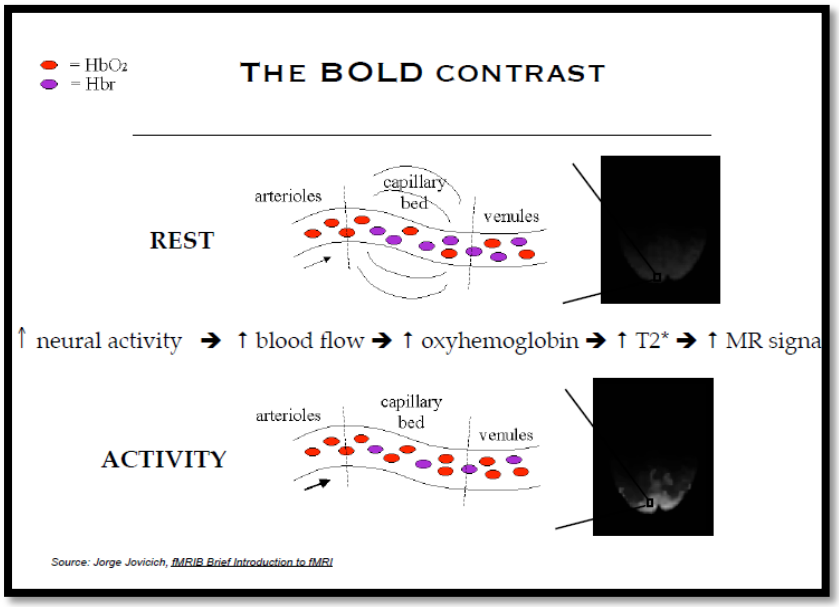

Figure 1- Illustration of the BOLD contrast which measures inhomogeneities in the magnetic field due to changes in the level of O_2 in blood. Difference between rest and activity states. During neural activity there is an increase of blood flow which causes an increase of oxyhemoglobin which is seen in the intensity of MR signal.

Functional neuroimaging using MRI, based on BOLD contrast, allows the evaluation and identification of brain regions that respond to task-induced activation and are functionally connected to other regions (Chang et al. 2009).

1.1.3- Ongoing slow oscillations

The combination of both electrophysiological and neuroimaging data reveals that mammalian brain dynamics is governed by spontaneous modulations of neuronal activity levels in cortical and sub cortical structures that occur in different frequency bands, 0.01-0.1Hz, 0.1-1 Hz, and <0.01 Hz (Palva & Palva 2012). Fluctuations on the lower frequency range are named slow fluctuations or slow oscillations and represent an interesting property of the brain that has been reported in studies with NIRS, EEG and BOLD fMRI signals. These fluctuations are a prominent feature of the mentioned signals, however, their origin is still not known. According to Pfurtscheller (2012) there are a few possibilities such as the firing of neurons in the reticular formation of the brain stem with a 10 seconds period, or alternatively, neurons may slowly modulate their activity level because of intrinsic excitability changes. Additionally, slow

systemic fluctuations may also be caused due to the dynamics of cerebral auto-regulation (Pfurtscheller et al. 2012).

The discovery that slow fluctuations in BOLD signals are correlated among specific constellations of brain regions, which constitute intrinsic connectivity networks and define the dynamic architecture of spontaneous brain activity at large, cause a resurgence in interest towards this frequency band (Palva & Palva 2012). It is known that intrinsic activity measured with BOLD fMRI and EEG in the resting brain is organized in multiple highly specific functional networks that fluctuate at frequencies between 0.01 and 0.1 Hz (Fox et al. 2005; Pfurtscheller et al. 2012; Yuan et al. 2013). All the findings on slow oscillations cause an increase of investigation on the respective frequency band and the examination of brain activity is not only made to understand differences between rest and task performance but also to explore the spontaneous brain activity present during resting-state (Biswal et al. 1995). Biswal and colleagues were the first to show that these spontaneous fluctuations were coherent within specific neuro-anatomical systems such as the somato-motor system. Such results were then confirmed and extended to other systems as visual, auditory and language processing networks (Biswal et al. 1995; Greicius et al. 2008).

Over time the human cortical activity has been studied in an intensive way at frequencies ranging from 0.5 Hz to several hundred Hz with EEG. The interpretation of the mechanisms and functions of neuronal events can be done in the context of the ongoing large-scale activity taking into account the full bandwidth of cortical oscillations which includes both very fast and infraslow frequencies. Human cortex may generate infraslow oscillations which are not detectable by conventional EEG because its inferior limit of recording bandwidth of ~0.5 Hz. Vanhatalo et al. used DC-coupled EEG scalp recordings to analyze infraslow oscillations, ISOs, and suggested that such oscillations may represent a slow and cyclic modulation of cortical gross excitability. Previous studies (Gilden et al. 2001) have reported that cortical evoked responses and cognitive performance oscillate at an infraslow rate which supports Vanhatalo et al. to suggest that ISOs are not restricted to sleep states and may rather reflect a continuous oscillatory behavior of wide range of brain functions (Vanhatalo et al. 2004).

Pfurtscheller (2012) hypothesized that these slow oscillations reflect the excitability dynamics of cortical networks. The results suggest that slow oscillations are important in movement and decision making (Pfurtscheller et al. 2012).

1.1.3.1- EEG and NIRS signals recordings

Fluctuations around 0.1Hz in the resting brain were previously found in the EEG (Vanhatalo et al. 2004; Witte et al. 2004) and in both HbO_2 and Hb concentrations (Roche-Labarbe et al. 2007; Zheng et al. 2010; Sasai et al. 2012). The combination of NIRS, near-infrared

spectroscopy, EEG, BP, blood-pressure, respiration and heart rate in the same study allowed the identification of a short-lasting coupling between prefrontal oxyhemoglobin (HbO_2) and central EEG alpha and/or beta power oscillations in the frequency band 0.07 Hz-0.13 Hz with an approximate 100 seconds of duration (Pfurtscheller, Daly, et al. 2012). Pfurtscheller et al. (2012) also provide support for the idea of Mantini et al. (2007) that resting state networks fluctuate with frequencies between 0.01Hz-0.1Hz.

1.1.3.2- Relation between NIRS and BOLD recordings

NIRS recordings during awake rest have demonstrated slow oscillations with dominance at 0.1Hz (Sasai et al. 2012; Zheng et al. 2010). Both NIRS and fMRI- BOLD signals are based on the detection of hemodynamic response caused by neuronal activity and since ISOs have been discovered in NIRS studies it is also expected that fMRI- BOLD show the same specific feature. There are reports of fMRI-BOLD signal fluctuations on the frequency band 0.01 Hz-0.1 Hz, (Palva & Palva 2012) however, there are no reports referring dominance of 0.1 Hz oscillations.

1.1.4- fMRI confounds

The BOLD contrast does not directly measures the neural activity since it depends on cerebral blood flow, blood volume and oxygenation which are coupled with the ongoing neural processes. There are other physiological processes that can affect the brain`s BOLD response such as the cardiac pulsation and the respiration, which can cause confounding signal fluctuations that are generally considered as physiological noise. (Yuan et al. 2013)

This type of physiological noise translates into non-periodic low frequency fluctuations which overlap with BOLD components. These fluctuations can contribute to a significant variance of BOLD signal. Han Yuan et al. investigated whether the low-frequency fluctuation in physiological noise reflects neuronal activities. The observation of correlation between respiration and electrophysiological recordings suggest that the fluctuation of respiration, that is commonly assumed to be the source of physiological noise in BOLD, may be of neural origin. It is important to note some conclusions of Han Yuan et al. which emphasize that when removing the low-frequency respiratory fluctuation from the BOLD signal, a common substrate of neural activity is also removed and therefore any interpretation requires caution. In contrast if choosing not to remove the respiratory- related low-frequency noise in the BOLD signal, such fluctuation remains a source of confound in fMRI data and the yielded functional connectivity results should also be carefully interpreted. So, unfortunately, slow fluctuation can also be related with physiological noise and not only with neural activity. (Yuan et al. 2013)

1.2- Brain Connectivity

Brain connectivity refers to a pattern of anatomical links, statistical dependencies and causal interactions, between different units within nervous system, from which the terms of

Anatomical, Functional and Effective connectivity arise respectively. Brain connectivity is crucial to elucidate how neurons and neural networks process information and the investigation of connectivity patterns plays a crucial role to determine the functional properties of neurons and neuronal systems. The brain is a complex system whose components organize themselves into dynamic patterns and form networks of interactive components. No single nerve cell can carry out the actions that the human brain is able to perform, however, a large number of nerve cells, linked together into networks inherently provided with dynamic connectivity patterns, make possible all the brain functions such as memory, behavior, thought and consciousness. To understand these integrative functions it is required an understanding of brain networks and the complex dynamic patterns created by them (Sporns 2011).

It seems likely that anatomical variability is one of the sources of functional variability, expressed in neural dynamics and behavioral performance. So, brain connectivity refers to a set of different aspects of brain organization and as it was mentioned before there is a fundamental distinction among structural or anatomical connectivity, effective connectivity and functional connectivity (Sporns 2007).

1.2.1- Types of Connectivity

Anatomical connectivity is related to biophysical processes for the signal transmission. It refers to a network of connections, synaptic connections, which link sets of neurons or neuronal elements and it is usually analyzed with parameters such as synaptic strength or effectiveness. Nowadays diffusion weighted imaging techniques, such as Diffusion Tensor Imaging, DTI, are useful as whole brain in vivo markers of temporal changes in fiber tracts, however, they have insufficient spatial resolution. Effective connectivity describes networks of directional effects of one neural element over another one and so it can be seen as a combination of both anatomical and functional connectivity. It attempts to extract networks of causal influences of one neural element over another (Sporns 2007). Functional connectivity is fundamentally a statistical concept that captures deviations from statistical independence between distributed and often spatially remote neuronal units. It measures dynamic and stochastic characteristics as correlation or covariance, spectral coherence and phase-locking among signals of different brain regions over the cerebral information processing to estimate statistical dependence. It is often calculated among all elements of a system like all brain regions, regardless whether these elements are connected by direct structural links. Functional connectivity is highly dependent on time unlike anatomical connectivity. Statistical patterns between neuronal elements fluctuate on multiple time scales, some as short as tens or hundreds of milliseconds. Functional connectivity can be studied using non-invasive techniques such as electroencephalogram, EEG, near-infrared spectroscopy, NIRS, and functional magnetic resonance, fRMI (Sporns 2007; Vieira 2011).

1.2.2- BOLD-fMRI based connectivity

Nowadays BOLD-fMRI technique is very commonly used to investigate the functional connectivity of the human brain. The degree of functional connectivity can provide information regarding to the engagement of brain areas during both resting and task performance states.

1.2.2.1- Resting State

Recent neuroimaging studies based on BOLD-fMRI signal have lead to the proposal that rest is characterized by an organized default mode network, formed by specific brain regions, that is modulated or deactivated during specific goal-oriented mental activity. The so called default-mode-network, DMN, includes cingulate cortices, inferior parietal regions and medial prefrontal regions (Fox et al. 2005) and shows strong functional connectivity between those regions. The default mode theory also predicts that engagement between these regions diminishes during cognitive tasks, because of the suppression of the circuit during task execution (Hampson et al.,2006). This resting-state organization is also seen as baseline level of activity characteristic of the human brain which seems to be consistent across different subjects and exhibits significant temporal dynamics (Damoiseaux et al. 2006).

The default mode of brain function hypothesis is readdressed from the perspective of the presence of low-frequency BOLD-fMRI signal changes on the frequency band 0.012–0.1 Hz in the resting brain (Fox et al. 2005; Bluhm et al. 2007). Slow network dynamics characterize neuronal activity also during cognitive tasks (Fox et al. 2005).

Spatial-temporally organized low-frequency fluctuations observed in BOLD-fMRI signal during rest states suggest the existence of underling dynamics networks that emerge spontaneously from intrinsic brain processes (Cabral et al. 2011).

Common networks are quantified in terms of their expected percentage BOLD signal change which provides a measure of the dynamics of the fluctuations. The calculation of the typical amount of variation, in percentage, at each voxel's location of the brain allows the association of coherent networks (Damoiseaux et al. 2006). Previous research reported consistently coherent fluctuations in BOLD fMRI signal within neuroanatomical systems (Biswal et al. 1995; Beckmann et al. 2005). Demoiseaux et al. (2006) reported coherent resting fluctuations in regions involved in motor function, visual processing, executive functioning, auditory processing, memory and also in the default-mode-network, DMN.

1.2.2.2- Task execution

When an attention-demanding cognitive task is taking place there are two possible opposite types of response to be observed. A specific set of frontal and parietal cortical regions routinely exhibit activity increases (Andrew & Pfurtscheller 1996; Cabeza 2000; Corbetta, M & Shulman

2002) whereas a different set of regions, including posterior cingulate, medial and lateral parietal, and medial prefrontal cortex (MPF), routinely exhibit activity decreases (Simpson et al. 2001). As the attention demand of the task is increased the activity in positive regions is further increased whereas activity in negative regions is further decreased (McKiernan et al. 2003). Cognitive tasks can recruit processes of attention and working memory which increase frontal and parietal regions activity (Corbetta, M & Shulman 2002). The repetition of the task can create an episodic memory which can attenuate the decrease of activity. This means that self-referential aspects of a task can modulate the activity intensity. Increased activity is expected in response to attention-demanding cognitive tasks in regions whose function supports task execution and decreased activity in regions supporting unrelated or irrelevant processes (Gusnard & Raichle 2001).

A number of networks has been reported in several studies involving motor cortex, visual cortex and not only regions involved in sensory-related processing but also regions involved in higher cognitive functions have been identified (Biswal et al. 1995). During a task execution there are regions from different networks that seem to activate each other (Damoiseaux et al. 2006).

Functional neuroimaging studies commonly use finger tapping tasks to study the human motor system since its simplicity facilitates the study with both normal control subjects and subjects with neuropathologies affecting the motor system. Finger tapping tasks can vary in the complexity of the tapping and also in the presence or absence of a stimulus which makes it flexible to variations of paradigms. Regarding the presence of a pacing stimulus, the studies usually use visual or auditory regularly paced and repetitive stimulus. A stimulus-paced finger tapping performed in the absence of an external stimulus is internally guided (named self-paced finger tapping). Other variations of finger tapping studies is the performance of a single finger movement, performed by the dominant hand; multi-finger sequence and bimanual movements (Witt et al. 2009).

In Witt (2009), a voxel-wise, coordinate-based meta- analysis was performed on 685 sets of activation foci in Talairach space gathered from 38 published studies employing finger tapping tasks, activation on bilateral sensorimotor cortices, supplementary motor areas (SMA) , left ventral premotor cortex, bilateral inferior parietal cortices, bilateral basal ganglia and bilateral anterior cerebellum. Studies investigating both auditory and visual pacing stimulus have reported different networks of active brain regions without consistency across studies. The variations in the experimental paradigms used and the few specific neural regions analyzed on those studies can justify such inconsistency across studies.

Voluntary action

Voluntary action is one of the most characteristic features of the human brain. Nowadays neuroscience is focused on viewing such actions as a complex set of specific brain processes, rather than a transcendental feature of human nature. To investigate these brain processes, neurocientists apply the classic engineering principle of intervening to control inputs and then measure the outputs. Well-designed studies can provide new insights into the volitional brain. For voluntary actions the stimulus-independence causes difficulties on the experimental study of human volition (Haggard 2008).

To capture the concept of voluntary actions being independent on the stimulus, the most common approaches are not adequate because they use a stimulus as an input to measure the system`s output. The most used experimental solution to this problem, according to Haggard (2013) is to provide a stimulus that only partly determines what the participant should do, in one of three ways: the participant performs a fixed action but chooses "when" to perform it; the participant performs an action at a specific time but chooses the number of repetitions of the actions or the participant chooses whether to perform an action or not.

Another important concept is that a voluntary action is not the same as a reflex action. The first one involves the cerebral cortex whereas the second one is purely spinal. It is known that a voluntary action matures late in individual development whereas a reflex can be present at or before birth (Haggard 2008).

The voluntary action involves two distinct subjective experiences which are the "intention" of performing an action, (the planning of doing something) and the experience of "agency" which is the latest feeling that the action performed as indeed cause an external event (Haggard 2008).

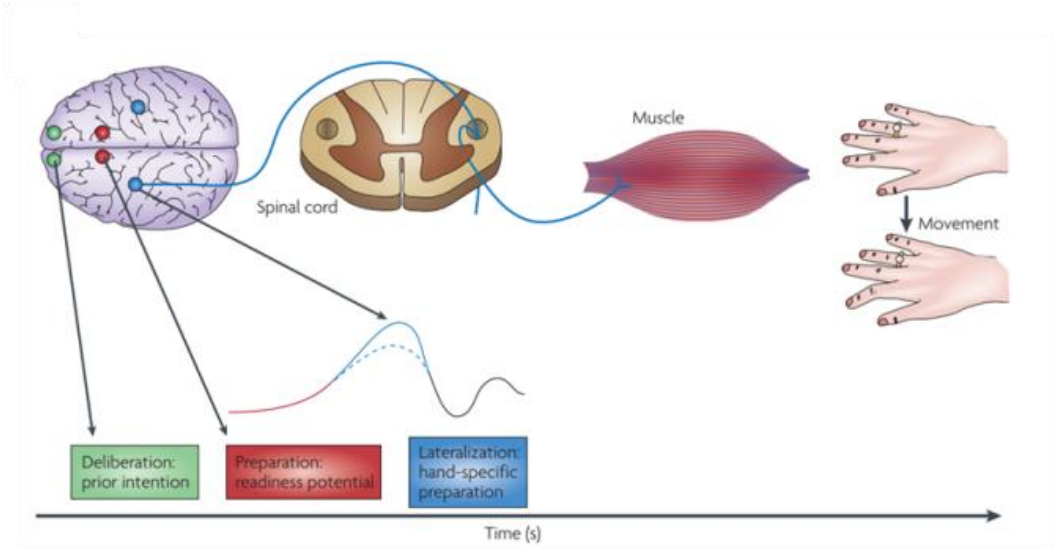

Figure 2- Brain activity preceding a voluntary action of the right hand. The frontopolar cortex (showed in green) forms and deliberates plans and intentions. The pre-SMA (in red) begins the preparation of the action, with other premotor areas, generating the readness potencials, red trace, which can be recorded from scalp. Immediately before the action takes place, M1, (in blue), becomes active. In later stages of preparation the contralateral hemisphere is more active than the ipsilateral hemisphere of the brain (solid and dotted traces). Finally, signal leaves M1 for the spinal cord and to contralateral hand muscles. Addapted from (Haggard 2008).

Based on Haggard (2008) during the execution of a voluntary finger movement the frontopolar cortex is responsible for the formation and deliberation of plans and intentions, the pre-SMA begins the preparation of the action with other motor areas and immediately before the action takes place the primary motor cortex, M1, becomes active. Then the signal leaves M1 to the spinal cord and then to the contra lateral hand muscles, as shown on Figure 2. According to the results presented by (Jenkins et al. 2000; Brass & Haggard 2007) it is also expected that regions such as the supplementary motor area, SMA, anterior cingulate cortex, ACC and anterior insular cortex, AIC, are activated during self-initiated movements.

Brain Circuits for Voluntary and Stimulus-driven finger movement

Activity on SMA has been linked to higher motor processing functions such as the initiation of movement, motor planning, motor learning and selection of movement. Activation in the basal ganglia has been associated with the performance of simple repetitive movements. Activity on both SMA and basal ganglia has been preferentially linked to internally generated movements over externally generated movements, however this distinction has not been consistently reported (Cunnington et al. 2002). The premotor cortex has been shown to play an important role in the transformation of sensory information into appropriate motor behavior, especially regarding to sequential movements (Ghuman et al. 2013). The parietal cortex has also been shown to be active during auditory-cued movements (Haggard 2008). Dum (2002) suggested that cortical motor areas show similar preferences for voluntary and for stimulus-driven actions,

suggesting that there is a distinction in cortical organization of action (Dum et al. 2002). Several neuroimaging investigations have focused on the comparison between brain activity during manual actions performed as a free will action and performed as a stimulus-dependent action.

The human brain contains different relevant cortical motor circuits converging on the primary motor cortex (M1) responsible for the transmission of motor commands to the spinal cord and muscles. M1 receives two broad classes of inputs which subserve voluntary and stimulus-driven actions, such as the finger movement, see Figure 3. According to Haggard (2008) the studies applied on similar manual action based on external stimulus response and based on voluntary response at a time of the participant choice showed stronger activation on pre-SMA for the volition case than for stimulus-driven action. The role of such brain area on voluntary action is confirmed by recordings of electrodes on the scalp showing an activation occurring 1 s or more before the voluntary movement. The onset readiness potential is seen as the initiation of a cascade of neural activity that spreads from the pre-SMA to M1, causing movement. The pre-SMA belongs to a wider frontal cognitive-motor network, see left-hand panel on Figure 3, which includes the premotor, the cingulate and the frontopolar cortices (Haggard 2008). This network is expected on voluntary action and by contrast the parietal-premotor circuit, see right-hand panel on Figure 3, seems to guide stimulus-driven action, however it has also a contribution to voluntary behavior. Another relevant circuit is the basal ganglia-preSMA which can be more involved on immediate action instead of the parietal-premotor circuit since the basal ganglia-preSMA is more directed to the initiation of action than the parietal-premotor circuit which might arbitrate among alternative action. So the basal ganglia-preSMA has a key role on voluntary action (Haggard 2008).

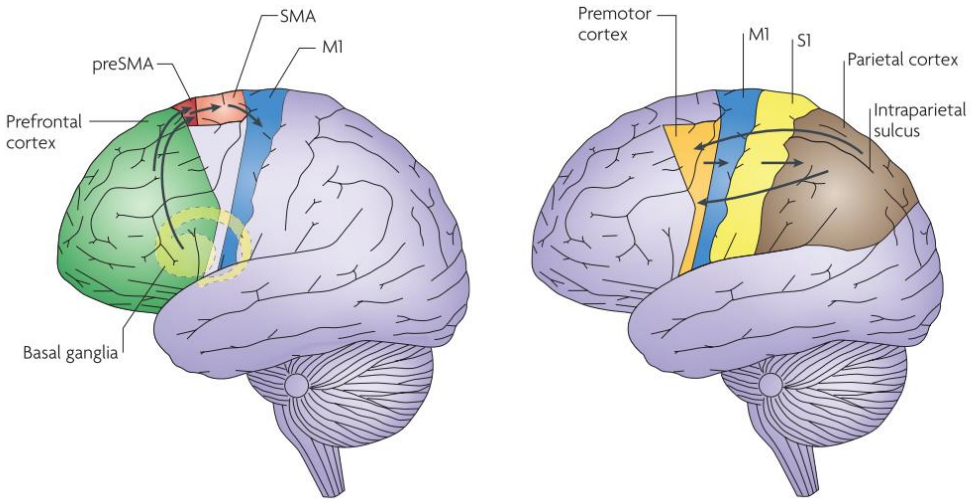

Figure 3- Left-hand panel: The primary motor cortex, M1, receives one key input from the supplementary motor area, SMA, and preSMA, which in turn receives inputs from the basal-ganglia and the prefrontal cortex. Right-hand panel: information from early sensory cortices, S1, is relayed to parietal cortex and from there to the lateral part of the premotor cortex, which projects in turn to M1. Adapted from (Haggard 2008).

1.3- Measures of functional Connectivity

To understand how the human brain works it is crucial to study the mechanisms of processing and interaction among many active neuronal groups focusing on how their communication occurs. It is also essential to investigate the flexibility of the modulation of communication among different brain regions which are the basis of the dynamics of the human brain. Neuronal processes integrate numerous functional areas widely distributed over the brain that are in constant interaction. Since oscillatory activity plays an important role in neuronal processes, the interest of such feature has extended to higher integrative processes. Lachaux et al. (1999) highlighted the possibility that such large-scale integration could be mediated by neuronal groups, oscillating on specific narrow frequency bands, entering into a precise phase-locking over a limited period of time. Before that, Roelfsema et al. 1997 had reported evidence for long-range synchronizations between widely separated brain regions which was in accordance with the notion that phase synchronization should subserve overall integration of all dimension cognitive acts, including associative memory, emotional tone and motor planning, already suggested by Varela (1995).

In overall terms, the most common model of neuronal communication is based on the sending of a message by a neuron, encoded as action potential, down its axons to all neurons which are anatomically connected with it. Then the receiving neurons combine all the different inputs received from all neurons to which they are anatomically connected. If the communication was performed based on such model then the distribution and reception of neural signals crucially depended on the anatomical connections structure meaning that communication was imposed by anatomical connectedness. However, cognitive functions require a flexible effective communication structure on top of the anatomical communication (Fries 2005). Fries (2005) hypothesized that such effective communication structure is due to a pattern of coherence among neuronal groups, in other words the communication is due to a pattern of phase-locking among oscillations in the communicating neuronal groups. Fries addressed the hypothesis of "communication-through-coherence", CTC, where the neuronal communication between two neuronal groups depends on coherence between them and the absence of neuronal coherence prevents communication. According to CTC hypothesis, the two neuronal groups must have oscillatory properties and those oscillations must constitute rhythmic modulations in neuronal excitability. Thus rhythmic excitability peaks create rhythmically reoccurring temporal windows for communication and only coherently oscillating (or phase-locked) neuronal groups can communicate effectively, because their communication windows for input and for output are open at the same times. So different groups of neurons can only communicate effectively with each other if the rhythmic opening of their communication windows is coordinated between the

groups. This hypothesis suggests that brain dynamic relies on dynamic communication structure based on flexible neuronal coherence patterns.

The large-scale integration of neuronal groups oscillating in a narrow frequency band during processes such as the planning and movement execution involves the understanding of synchrony between signals. Phase synchrony refers to phase-locking over a limited period of time. The analysis of synchrony has been focused on the detection of correlations in the phases of the oscillators while discarding the effects of amplitude fluctuations (Lachaux et al. 1999). Phase synchronization of coupled nonlinear oscillations might occur even in the absence of amplitude correlations. The analysis performed using methods that mix both phase and amplitude can miss the type of event where correlations exist in timing alone while amplitude varies independently. A reliable approach to detect synchrony occurring in oscillatory neural signals must take into account that timing correlations are better evaluated in the phase of oscillators (Hurtado et al. 2004). Phase synchronization is a mechanism for optimal communication between brain regions (Cabral et al. 2011).

1.3.1- Neuronal Signal Synchrony

To measure the neuronal signal synchrony, estimators of synchrony between time series of brain activity that return low values for independent time series and high values for correlated time series can be used. There are different approaches to quantify the degree of synchronization based on both linear and nonlinear techniques. The most commonly used measures are the cross correlation and the spectral coherence function whereas the most usually nonlinear measures used are the mutual information, the transfer entropy, the Granger causality and the phase synchronization measured by averaging phase coherences.

In a brief introduction to linear measures, the cross correlation has been widely used in time domain allowing the classification of complete or lag synchronizations, uncorrelated signals and linear independent signals. Linear correlations are also able to quantify the frequency domain using the cross spectrum, which is a complex function, to obtain the so called coherence function, corresponding to the amplitude normalized by the power spectrum of the two signals. This measure is frequency-dependent and so, it is useful for synchrony quantification in only certain frequency ranges such as the classical EEG bands. Coherence is obtained by averaging processes over subintervals, known as time-windows, of equal length by the Welch method based on Fourier transform. The coherence function can also be applied in a time-frequency domain using the Wavelet transform (Torrence C., Compo 1998).

Regarding nonlinear measures, the mutual information quantifies not only linear but also nonlinear dependencies between two systems. This measure stems from information theory and is based on Shannon entropy. The transfer entropy extends the concept of mutual information to

detect the direction of information exchange between two systems (Damoiseaux et al. 2006) and is based on the same principle as Granger causality as a directional approach incorporating information about the system's past, introduced by Granger (1969). At last, the phase synchronization measure has been found widespread used in neurosciences since its features allows for restricted analysis in certain frequency bands reflecting specific brain rhythms which can be related to cognitive processes, states of vigilance and others. This measure is time-resolved, with much better time resolution than coherence, and is only sensitive to the phases, irrespective to the amplitude of the signals. To obtain the phase synchronization it is necessary to determine the instantaneous phases from time series x and y, $\emptyset_x(t)$ and $\emptyset_y(t)$. This is commonly achieved based on the analytic signal approach. To a specific time series, for example time series x, the analytic signal is given by $Z_x(t) = x(t) + i\tilde{x}(t) = A_x^H e^{i\emptyset x^H(t)}$, where $\tilde{x}(t)$ corresponds to the Hilbert transform. From $Z_x(t)$ it is obtained the Hilbert phase: $\emptyset_x^H(t) = \arctan\left(\frac{\tilde{x}(t)}{x(t)}\right)$ (Gabor 1945). The same reasoning is followed for y time series to achieve the instantaneous phases of a time series. Another widely used method to quantify the phase synchronization is based on wavelet transform from which is the phase component extracted, allowing for the computation of phase coherence (Lachaux et al. 1999), as detailed later on.

To evaluate the interactions between brain regions both time-invariant spectral and time-frequencies analysis to get both magnitude and phase coherences across signals which are indeed measures of functional connectivity have been applied. (Sun et al. 2005).

1.3.2- Time-invariant analysis

A common measure used on functional connectivity is the correlation between brain signals from different regions, however, correlation techniques cannot differentiate between frequency and phase information. Information complementary to temporal correlation can be obtained from separate analysis of frequency and phase. So, in addition to temporal correlation, coherence analysis has been applied in order to investigate both amplitude and phase similarities (Biswal 2012).

The concept of coherence is fundamental for fluctuations quantities investigation. Gardener (1988) presented a precise meaning of the coherence concept for statistical signal processing and time-series analysis. From his work the mathematical definition of coherence for two non-zero random processes x and y, at frequency f, is defined by Equation 1, and is based on a Fourier analysis as mentioned before.

$$\varrho(f) = \frac{|S_{xy}(f)|}{[S_{xx}(f) \cdot S_{yy}(f)]^{1/2}} \qquad \text{Equation 1}$$

Where $S_{xy}(f)$ is the cross-spectral density between x and y. This measure provides a time-invariant analysis of coherence between time series. Several studies recorded considerable temporal displacements of BOLD response between brain regions within a subject. Miezin et al showed differences of more than one second for the onset of BOLD response and both Rosen et al and Buckner et al characterized the temporal behavior of BOLD signal as within-subject variable. In previous studies the phase shift between fMRI time series was computed using the cross-spectral density matrix (Muller et al. 2001; Muller et al. 2003; Koopmans 1974 and Priestley 1981). However, such measure assumes that the phase shift does not change over time and consists on the temporal displacement average between fMRI time series in different brain regions. So spectral methods are restricted to stationary processes which are so called since their mean value is constant and the covariance does not change over time.

Using the concept of coherence Sun et al (2005) investigated latency differences among a set of brain regions, functionally connected, based on phase-delays in functional magnetic resonance imaging data. Previous studies used the magnitude coherency, as a spectral measure of the linear time-invariant relationship between regions. Sun et al presented a work based on the phase component of such coherency between regions to estimate the linear delay between them. The calculation of the phase-delays can be used to examine the temporal properties of functional networks associated to specific tasks. The work presented by Sun et al. shows that phase-delay values are crucial to determine lag and leads on activation of different brain regions within a network, allowing to establish conclusions about the temporal dynamics of brain networks during a specific paradigm of analysis.

1.3.3- Time-frequency analysis

Time series of BOLD fMRI response exhibit non-stationary and non-periodicity on their signals which means they can vary in both amplitude and frequency over long periods of time leading to a constraint of spectral methods (Chang & Glover 2010). Coherence based on Fourier analysis has been commonly used as a first approximation to track coupling between two oscillatory neural signals. However, a measure that also describes the temporal variability of the phase shift is crucial, since the temporal dynamics of brain regions can change over time. The wavelet coherence provides a description of the temporal behavior of the BOLD fMRI signal even for non-stationary cases. Wavelet coherence, in contrast to Fourier analysis, can detect short and significant episodes of coherence between nonstationary signals by quantifying the instantaneous coherency among neural signals (Lachaux et al 2001).

Following van Milligen et al. (1995), in a wavelet coherence analysis, BOLD-fMRI signals are commonly decomposed along the Morlet wavelet family, while many other wavelets may be chosen, since this wavelet mother has the advantage of simplicity and it is well suited for such

spectral estimations. The Morlet wavelet, $\Psi_{\tau,f}(u)$, is defined for frequency f and time t by Equation 2.

$$\Psi_{\tau,f}(u) = \sqrt{f} \cdot \exp\left(i2\pi f(u-f)\right) \cdot \exp\left(-\frac{(u-\tau)^2}{\sigma^2}\right) \qquad \text{Equation 2}$$

$\Psi_{\tau,f}(u)$ is the product of a sinusoidal wave at frequency f, with a Gaussian function centered at time τ, with a standard deviation σ proportional to the inverse f, such that the number of cycles of the wavelet is the same for all frequencies. Figure 4 shows an example of the application of the Morlet wavelet for two different frequencies using 5 cycles. Since the length of the segments decreases with frequency it can be seen by comparing a) and b) that the length of the integration window decreases with frequency, thus improving the temporal resolution of the coherence estimate. In wavelet coherence the standard deviation σ varies with frequency f and the relation σf remains constant.

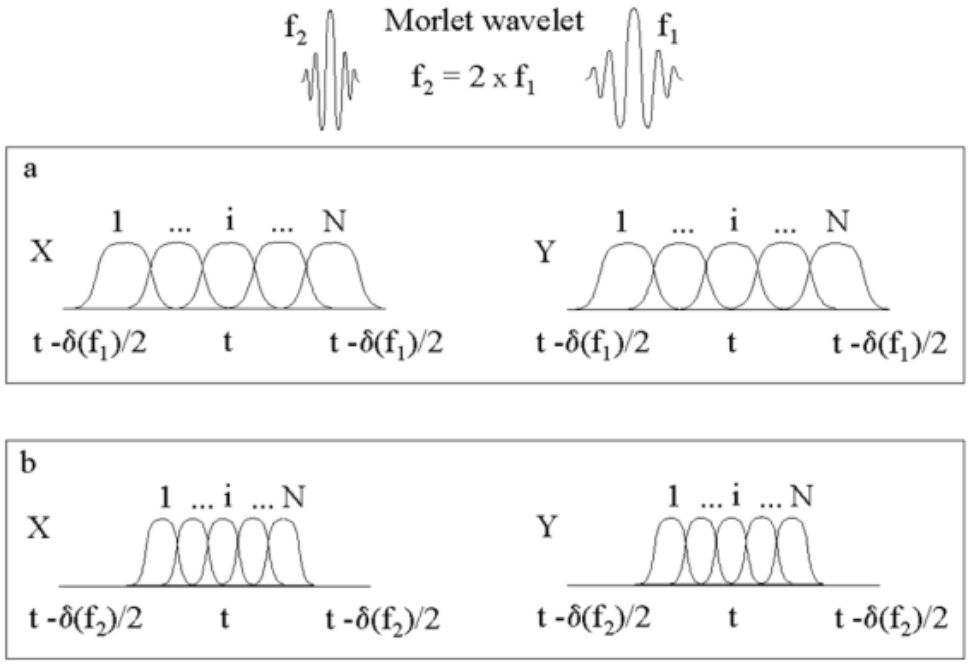

Figure 4- Application of the wavelet coherence for two different frequencies. For time $\boldsymbol{t}$ and frequency $\boldsymbol{f}$, the Morlet wavelet is defined as the product of a sinusoid at frequency $\boldsymbol{f}$, by a Gaussian window with a standard deviation such that the number of cycles of the wavelet is the same for all frequencies (upper plots, 5 cycles). Since the length of the segments decreases with frequency, it can be seen by comparing (a) and (b) that the length of the integration window decreases with frequency, thus improving the temporal resolution of the coherence estimate. Figure taken from (Lachaux et al. 2002).

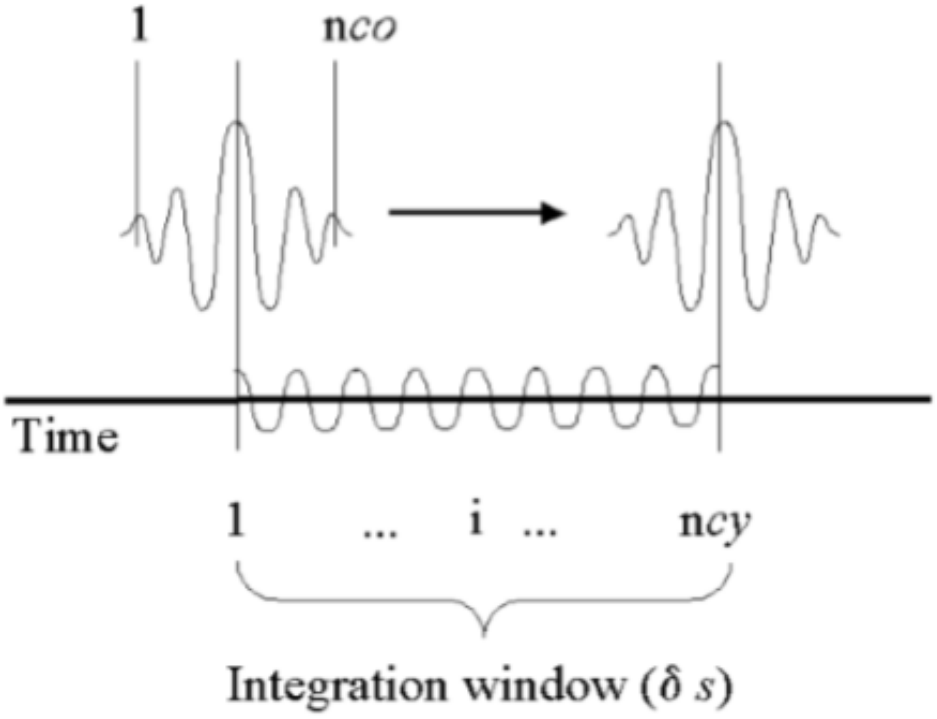

Figure 5- By the convolution of the signal and sucessive nco-cycle Morlet wavelets, the wavelet-coefficients are computed. For each frequency, the wavelet coherence averages the wavelet coefficients over an interval size of $\boldsymbol{\delta}$ that adapts to $\boldsymbol{f}$. $\boldsymbol{\delta}$ corresponds to a constant number of oscillations cycles: $\boldsymbol{\delta = ncy}$. Figure taken from (Lachaux et al. 2002).

In wavelet coherence, δ defines the temporal resolution and it can be adapted to the frequency of interest, so small values can be chosen for higher frequencies making possible to follow the variations of coherence in time. For each frequency, the wavelet coherence averages the wavelet coefficients over an interval of size δ that adapts to f, see Figure 5. δ corresponds to a constant number of oscillations cycles, ncy so $\delta = \frac{ncy}{f}$. The wavelet-coefficients are computed by convoluting the signal with successive cycles Morlet wavelets, nco.

The wavelet transform of a signal $x(u)$ is a function of time τ and frequency f given by the convolution of $x(u)$ with the Morlet wavelet as in the following equation 3 where * denotes the complex conjugate,

$$W_x(\tau, f) = \int_{-\infty}^{+\infty} x(u) \cdot \Psi_{\tau,f} * (u) du \quad \text{Equation 3}$$

$$W_x(\tau, f) = A_x^W(t) e^{i\emptyset x^W(t)} \text{ Equation 4}$$

and based on the relation of equation 4, the instantaneous phases by $\emptyset_x^W(t) = \arctan\left(\frac{ImW_x(\tau,f)}{ReW_x(\tau,f)}\right)$ is extracted. The same logic is followed for time series y.

From the wavelet transforms of the two signals x and y, the wavelet cross-spectrum between both around time t and frequency f can be defined:

$$SW_{xy}(t,f) = \int_{t-\delta/2}^{t+\delta/2} W_x(\tau,f) \cdot W_y{}^*(\tau,f)d\tau \qquad \text{Equation 5}$$

Finally, analogous to the Fourier-based coherence previously introduced, the wavelet coherence $WCo(t,f)$ is defined at time t and frequency f by equation 6:

$$WCo(t,f) = \frac{|SW_{xy}(t,f)|}{\left[SW_{xx}(t,f)\cdot S_{Wyy}(t,f)\right]^{1/2}} \qquad \text{Equation 6}$$

On Figure 6 it is showed the time-frequency maps that result from Wavelet Coherence analysis. On the left the coherence was computed between two independent signals whereas on the right the coherence was computed for two simulated signals with a well defined synchronous period. The high values of coherence are obtained for such time-frequency period, on the right time-frequency map. From this figure, it is seen a thick black line, known as the influence cone, which limits the region where the wavelet coherence is computed showing same temporal resolution limitation. The computation cannot be performed for the entire time-frequency region since it involves an integration window which requires a data recording before and after time t, in an interval that depends on frequency f: $[t - \frac{(nco+ncy)}{2f};\ t + \frac{(nco+ncy)}{2f}]$.

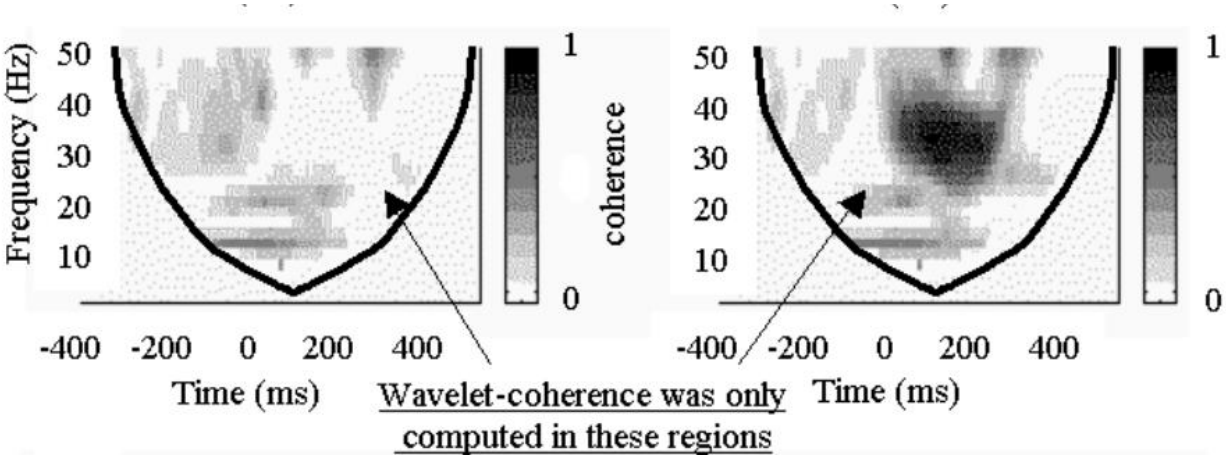

Figure 6- Time-frequency maps for wavelet coherence analysis. On the left: coherence result between two independent signals; on the right: coherence between two signals with a well defined synchronous period. The coherence could not be computed in the regions outside the thick black line because it required data before -400ms or after +600ms outside the recorded interval. Coherence ranges from 0 to 1. Image adapted from (Lachaux et al. 2002).

The work of Lachaux et al (2002) also provided a mathematical form to calculate the Phase Coherence over time periods to achieve the phase synchronization between two signals, equation 7, which corresponds to the Phase-Locking measure to quantify the phase synchronization defined as the global entrainment of the phases, while the amplitudes may remain uncorrelated. A more detailed explanation about the wavelet transform coherence computation is presented on Lachaux et al.

$$PC(f,t) = \left| \frac{1}{\delta} \int_{t-\frac{\delta}{2}}^{t+\frac{\delta}{2}} \exp\left(j(\emptyset_y(f,\tau)) - \exp\left(j\left(\emptyset_x(f,\tau)\right)\right)\right) d\tau \right| \quad \text{Equation 7}$$

The resulting Phase-Locking indexes vary from 0 to 1 and are averaged values for each $[t-\frac{\delta}{2}; t+\frac{\delta}{2}]$ time-window.

The knowledge about cerebral networks dynamics depend on the investigation of the temporal variations in the coupling between neural signals. Both Wavelet and Fourier coherence analysis use a time window analysis and the most relevant difference between both methods is the fact that the window is fixed to Fourier analysis whereas for Wavelet analysis the window is automatically adapted to the signal frequency. The wavelet coherence is used to analyze the coherence and phase lag between two time series as a function of both time and frequency (Torrence C., Compo 1998) and, therefore, it is well suited to investigate non-stationary changes in coupling between fMRI time series. The wavelet coherence phase of two time series can be considered as a measure of the delay of the BOLD response function in one brain region with respect to another allowing the investigation of temporal changes of phase shifts (Muller et al 2004). Therefore, wavelet coherence can be used to explore the temporal dynamics of blood

oxygenation-level dependent, BOLD, signal in the human brain based on the hypotheses that temporal dynamics may change over time (Chang & Glover 2010) .

1.4- Thesis Hypothesis and Goals

The purpose of this thesis work is to present a methodological approach to analyze functional connectivity among different brain regions on a specific narrow frequency band and for single trial data, and to quantitatively assess time delays between the regions involved. A time-frequency framework based on Wavelet Transform Coherence is used to account for the fact that functional connectivity exhibits dynamic changes across several frequencies. Thus, the computation of phase and time-delays statistics measures will be confined to periods where a) phase-locking occurs in accordance with the hypothesis of "communication through coherence" postulated by Fries (2005) or b) to periods of high common magnitude since it is hypothesized as a marker of meaningful interaction on the work performed by Lachaux (2002). The method also consists on a statistical test to distinguish between significant periods of both Magnitude Coherence and Phase-Locking for single scans. The presented work also tests whether Phase-Locking and Magnitude Coherence are indeed correlated, using both Pearson correlation and Mutual Information.

To test and illustrate the obtained analysis method, a set of functional magnetic resonance data is used that was acquired during a specific paradigm hypothesizing the presence of significant interaction/communication between regions belonging to networks related to voluntary and stimulus-driven action such as the frontal-cognitive motor network, the basal ganglia pre-SMA network and parietal-premotor network. This leads to a discussion of whether time-delays involving key regions such as SMA and insula are consistent with expectations.

The acquired paradigm also contains resting state acquisition used to investigate functional connectivity on regions belonging to the default-mode network. The present work is focused on slow (~0.1 Hz) oscillations due to their importance in movement and decision making (Pfurtscheller et al. 2012).

2- MATERIALS AND METHODS

2.1- Materials

2.1.1- Datasets

A dataset: composed by three right-handed healthy subjects as determined by the Edinburgh Handedness Inventory. Data acquisition comprised an experimental design of five distinct states. The paradigm consists on a first moment of resting state followed by a voluntary task execution denominated self-paced finger movement where subjects pressed a button at free will with the right hand, then another resting state acquisition was taken followed by a stimulus-driven movement named auditory-paced finger movement where the subjects were stimulated with an auditory sound as an indicator to press the button and receive no information about the timing of such stimulus. The last paradigm of acquisition was again a resting moment.

B dataset: One dataset composed of 3 subjects acquired during resting state. For each subject the acquisition was performed for two different TR values: a short TR (=0.92s) and a longer TR (=2.5s) were used.

Both datasets were acquired in and kindly made available by the Technical University of Graz, Austria, in the context of an ongoing collaboration with the Institute of Biophysics and Biomedical Engineering.

2.1.2- Image acquisition and Data Pre-Processing

A dataset: Functional images were acquired on a 3.0-T scanner (MagnetomSkyra, Siemens) with a voxel size of 3.5 x 3.5 x 3.5 mm^3, TR/TE=1830/30ms, FOV=240x240 mm^2 and for 32 interleaved slices. For all resting sessions 160 functional echo-planar images were taken during 5 minutes whereas for both self-paced and auditory-paced finger movements 330, 366 and 337 volumes were taken for each subject, respectively, (during ~10 minutes scanning period). Pre-processing of the data was accomplished using the DPARSF toolbox (Chao-Gan & Yu-Feng 2010) and included removal of the first 10 time points (to allow the participants to adapt to the situation inside the scanner and to allow the signal to reach the state of equilibrium), slice timing correction, motion correction, normalization to MNI space using EPI template provided by SPM, resampling to 3mm isotropic voxels, spatial smoothing with a 4 mm FWHM Gaussian kernel and linear detrending. Then the nuisance covariates were regressed out. Lastly, the BOLD time courses of 116 regions from AAL atlas (Tzourio-Mazoyer et al. 2002) were extracted.

B dataset: Functional images were acquired on a 3.0-T scanner (MagnetomSkyra, Siemens) with a voxel size of 3.5 x 3.5 x 3.5 mm^3, TR/TE=902/30ms or TR/TE=2500/30ms, FOV=240x240

mm^2 and for 32 interleaved slices. For the shorter TR acquisition 372 volumes were taken and for the longer TR acquisition 130 volumes were taken. The data pre-processing was the same as for *A* dataset.

2.2- Methods

In the current study a methodology is presented, implemented on MATLAB, to achieve functional connectivity measures based on the Wavelet Analysis, a time-frequency approach. The following scheme, Figure 7, summarizes the three main steps of the analysis.

By computing both Magnitude Coherence, MC, and phase differences, between two fMRI BOLD time series, one is able to determine the Phase Locking, PL, indexes during a specific period of time as described on the 1st section.

Then the methodology consists on joint MC and PL-based statistical approach to differentiate significant periods of Magnitude Coherence and Phase-Locking between the two time series, which is described on the 2nd section. This section is divided into three subsections (1, 2 and 3) where the first presents the *surrogate data scheme* computed to the achieve a statistic analysis, the second subsection refers to the calculation of both MC and PL indexes based on the surrogates ensembles in order to get the *statistic testing* for both variables and the last subsection presents the *decision taken* on significant statistical values for both MC and PL measures. The outcome is both phase and time-delays between the time series, across periods of time defined by the time-window analysis performed using the wavelet transform.

On 3rd section it is explained the phase and time-delay calculation based on two different concepts: first the computation is limited to periods of time where there is significant magnitude coherence between time series and second the computation is restricted only to periods where the time series are in statistical significant phase-locking.

The 4th section is dedicated to the relationship between Magnitude Coherence and Phase-Locking profiles using both Pearson Correlation and the Mutual Information theory. The last section, 5th section, presents an output illustration.

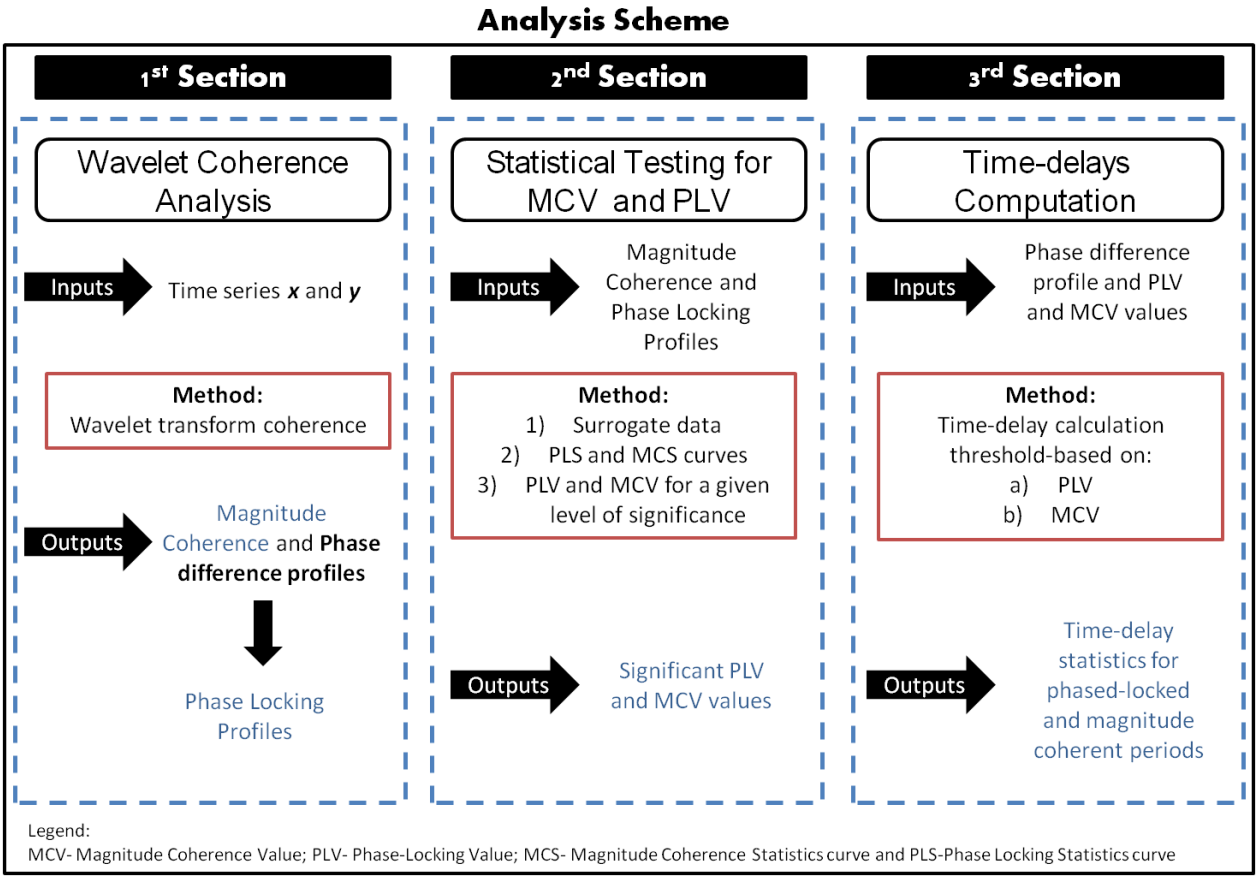

Figure 7- Analysis scheme for the three main steps of the presented methodology. The first section is based on Wavelet coherence computation for two chosen time series, *x* and *y*. The outputs from this step are both Magnitude Coherence, MC and Phase differences profiles from which the Phase Locking, PL profiles are obtained. On the second section a statistical test is performed for both MCV and PLV using the outputs from the first step as inputs to this section. There is a surrogate data process followed by statistical curves for both PL and MC known as PLS and MCS curves and finally it is applied a statistical decision based on a chosen level of significance to achieve the mentioned outputs. At last, the third section refers to the time-delays computation from the significant statistical PLV and MCV already obtained. Here two different hypothesis of communication are studied , one based on a) PLV and the other on b) MCV as introduced before. The outputs from this analysis are Time-delay statistics for periods of communication between the time series x and y.

2.2.1- 1st Section: Wavelet Transform Coherence

The Wavelet Transform Coherence introduced on section 1.3.3- Time-frequency analysis, provides a description of the temporal behavior of non-stationary signals and it is used to analyze the magnitude coherence and phase lag between two time series as function of both time and frequency (Torrence C., Compo 1998). In the present work the "Crosswavelet and Wavelet Coherence Toolbox" implemented on MATLAB and provided by A. Grinsted is used (Grinsted et al. 2004). After the extraction of the BOLD time courses, on data pre-processing, the time courses are used as inputs on the *WTC* function, provided by the mentioned toolbox, to obtained time-frequency maps for both common power, also known as magnitude coherence, and phase difference to analyze all 116 AAL brain regions. The *WTC* function computes the

referred maps for two time courses, named time series x and y, see Figure 8, meaning that one gets the magnitude coherence and phase differences maps for each two brain regions allowing the analysis of connectivity between region pairs.

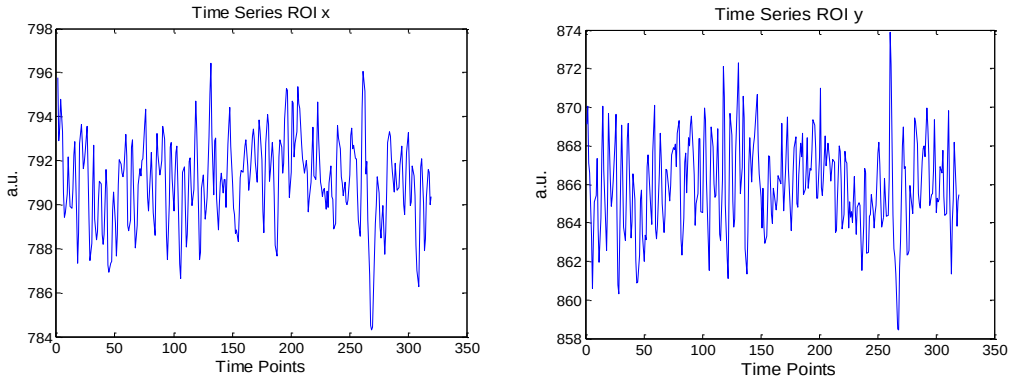

Figure 8- BOLD time courses/time series for two random AAL regions, time series $\boldsymbol{x}$ and $\boldsymbol{y}$,obtained from the pre-processing of data performed on DPARSF toolbox.

The computation of *WTC* function for the pair of BOLD time courses showed on Figure 8 originates as outputs the maps showed on the following Figure 9 for both magnitude coherence and angle difference variables. Both magnitude coherence and angle difference matrices, or maps, are obtained in function of both time and frequency. The wavelet transform for a specific time course of length N, number of time points, is calculated with the corresponding TR.

2.2.1.1- Magnitude Coherence and Angles difference maps

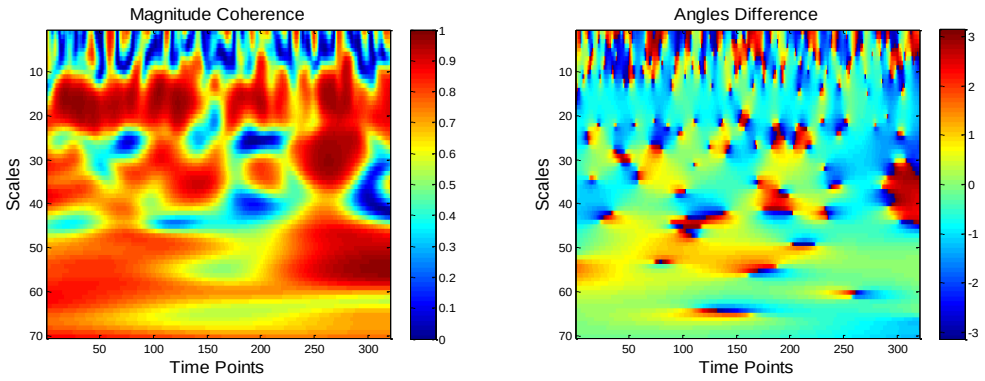

Figure 9- Outputs from WTC function. On the left: matrice for the magnitude coherence values, scaled between [0;1] for both time (time points) and frequency (scales) domains. On the right: matrice for angle difference values, scaled between $[-\boldsymbol{\pi};\boldsymbol{\pi}]$ for both (time points) and frequency (scales) domains. The values of both magnitude coherence and angle difference are plotted by colormap.

Analyzing the magnitude coherence map presented on the left of Figure 9 the resulting values are scaled between [0-1] interval, where a zero value means no magnitude coherence between the analyzed time series x and y, and a maximum value means maximum magnitude coherence

between signals, on the corresponding time point. On the right of Figure 9 it is presented the angles difference map where the values vary between $[-\pi; \pi]$. Each time point is associated to a value that corresponds to a time window whose dimension varies depending on the corresponding frequency.

2.2.1.2- Phase-Locking computation

Through phase difference values, obtained by wavelet transform coherence, Figure 9 on the right, it is computed a phase locking measure, that reveals the level of phase difference stability, by the computation of the Phase Coherence integration, equation 6, between the signals across a defined time-window, as provided on (Lachaux et al. 2002). The definition of the time-window depends on the number of cycles, *ncy*, a parameter which is explained on introduction section 1.3.3- Time-frequency analysis. Figure 10 shows the Phase Locking matrix obtained from angle difference matrix, presented on the right panel of Figure 9. The phase locking increases when the phase/angle difference shows small variations in time. The phase locking values are also scaled from [0-1] interval. A zero value means low phase locking/phase coherence between time series. Whereas one means constant phase difference across the time-window and so, for such specific period of time, the signals are phase-locked. With Phase Locking indexes we are able to analyze the concept of phase synchronization between fMRI BOLD acquired signals.

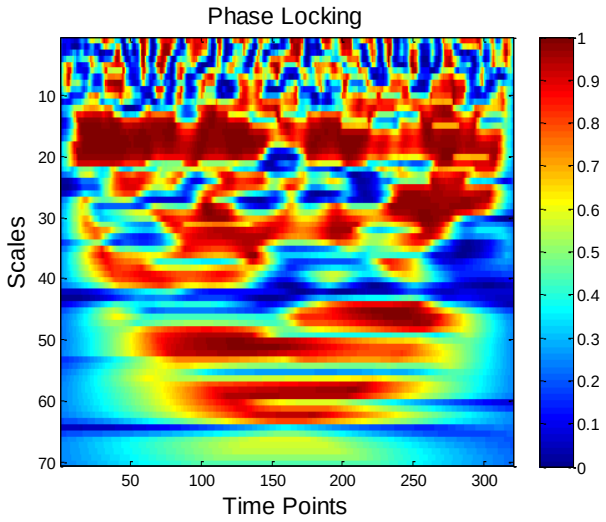

Figure 10- Phase Locking matrice obtained from Angle difference matrice, Figure 9 on the right, by applying the Phase Coherence integration provided by Lachaux (2002), see equation 6.

2.2.1.3- Magnitude Coherence and Phase-Locking profiles

After the computation of both magnitude coherence and phase-locking matrices, over time and frequency, the goal of the algorithm is to get the magnitude and phase locking indexes for a specific narrow frequency band. For that the user specifies the frequency intervals in *Hz* units.

The algorithm performs an average over scales values corresponding to the narrow frequency band selected. Another relevant topic is the time-points that are rejected from the analysis. *WTC* function itself determines which time points are not statistically significant and such time points are mentioned as time points outside the influence *coi* on the time-frequency maps. Summarizing, from both magnitude coherence and phase-locking matrices it is performed an average, time point by time point, for the scales values corresponding to the selected frequency band and only for significant time points (time points inside the influence cone, *coi*). On Figure 11 it is represented both Magnitude Coherence and Phase Locking Profiles for a narrow frequency band, 0.07-0.13 Hz.

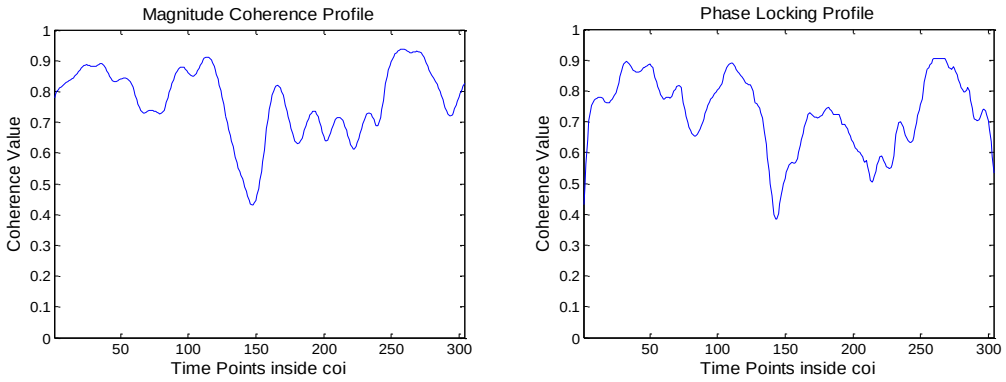

Figure 11- Magnitude Coherence Profile, on the left, and Phase-Locking Profile, on the right - plot of the averaged magnitude coherence/phase locking indexes for a specific narrow frequency band, 0.07-0.13 Hz, and for time points inside influence cone, ***coi***.

2.2.2- 2nd Section: Statistical testing for both MCV and PLV

This step of the present method consists on building a statistical test to differentiate both significant magnitude coherence value, MCV, and phase-locking value, PLV. Since we are dealing with single-trial data we can`t determine the null distribution by shuffling trials and we also cannot make analytical inferences on the distribution of both magnitude coherence and phase-locking values because we have no a prior knowledge about their statistics.

Following the work performed by Lachaux (1999) and Hurtado (2004) a surrogate based statistical test is build for the distinction of significant magnitude and phase locking values, between two time series. This approach consists on the generation of a large set of surrogates, in order to achieve a distribution under the null hypothesis of independent pairs of oscillatory activity, which rely on a randomization technique, once the sampling distribution is unknown. Then only values that significantly depart from what would be expected for independent oscillators can be considered as revealing meaningful magnitude and meaningful phase locking. To accomplish a valid distribution the statistical tests must be adapted to our particular set of data, and so, the surrogate data must share some features with the original data. The obtained distribution of magnitude coherence and, the obtained distribution of phase-locking indexes,

known as magnitude coherence statistic curve, MCS, and phase-locking statistic curve, PLS, computed for pairs drawn randomly from the surrogates ensembles, can be considered as an approximation of the null distribution of each case. Hurtado (2004) showed that the null hypothesis based on random techniques depend on the method used to generate the surrogate data. So, preserving the power spectrum of the instantaneous frequency by randomization of the power spectrum phase evolutions are computed.

2.2.2.1- Surrogate data Scheme

The generation of a surrogate ensemble is performed for a specific time series, ROI x, in order to achieve a set of N surrogates based on the instantaneous frequency of the ROI x.

Figure 12 represents the surrogate ensemble procedure. From the angles it is obtained the instantaneous frequency vector by differentiation. The second step is the random permutation of the instantaneous frequency vector by N times to obtain N frequency vectors to create N surrogates having the same power spectrum as the ROI x. The third step is the phase reconstruction. As it can be seen on Figure 12, the phase evolution is considered as a walk in the unit circle. For each time point, t_k, the phase advance is given by $\Delta\emptyset_k = w_k \Delta t$, where Δt is the time resolution, $\Delta t = TR$, and w_k is the step size which is a surrogate of instantaneous frequencies, $k = 1,2,3 \ldots N$. To compute the surrogate phase evolution the equation 8 is used.

$$\emptyset_{k+1} = \emptyset_k + w_k \Delta t \quad \text{Equation 8}$$

The statistical test is repeated for all time series for the analysis of both magnitude coherence and phase synchrony between each time series and the ROI x. This means that the surrogate ensemble procedure is seed-based, the seed corresponds to the ROI x. For a different seed all the procedure must be repeated.

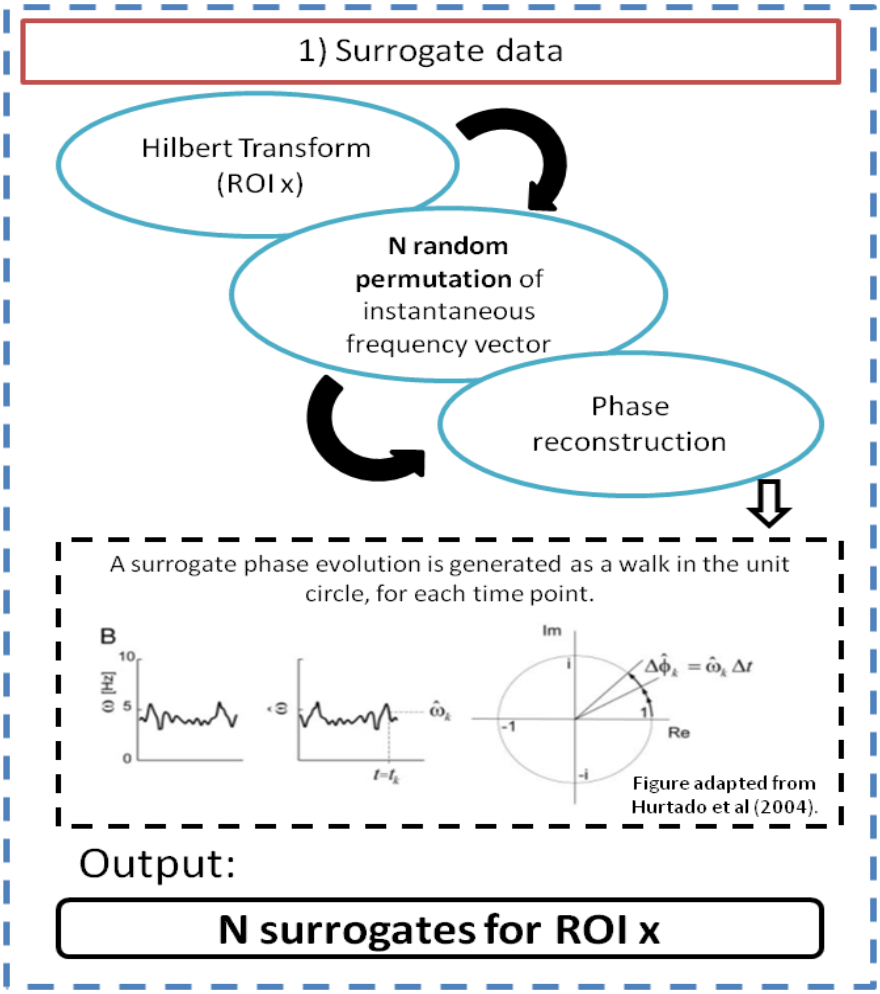

Figure 12- The surrogate ensemble is performed to a chosen time series named ROI x. It consists on applying the Hilbert Transform to achieve the instantaneous frequencies values from which is made a random permutation N times. This allows one to get a phase reconstrution following Hurtado' s work. The phase is seen as a walk in the unit circle. From the N random permutation of the power spectrum one gets N surrogates for ROI x.

2.2.2.2- MCV and PLV indexes based on Surrogate data

After the achievement of the surrogate ensemble for the seed ROI x it is calculated both magnitude coherence and phase locking values, for all time points, using the method described before, on section 2.2.1- 1st Section: Wavelet Transform Coherence. The WTC function is applied over all N surrogates for ROI x in relation to another chosen ROI. For each time point of the ROI x signal is obtained magnitude coherence and a phase locking value from each surrogate time series. This means that, for example, for a pair of time series named seed ROI x - ROI y we obtained N surrogate magnitude coherence profiles and N surrogate phase locking profiles, as seen on Figure 13. For each time point results N Magnitude Coherence Values, MCV, and N Phase-Locking Values, PLV.

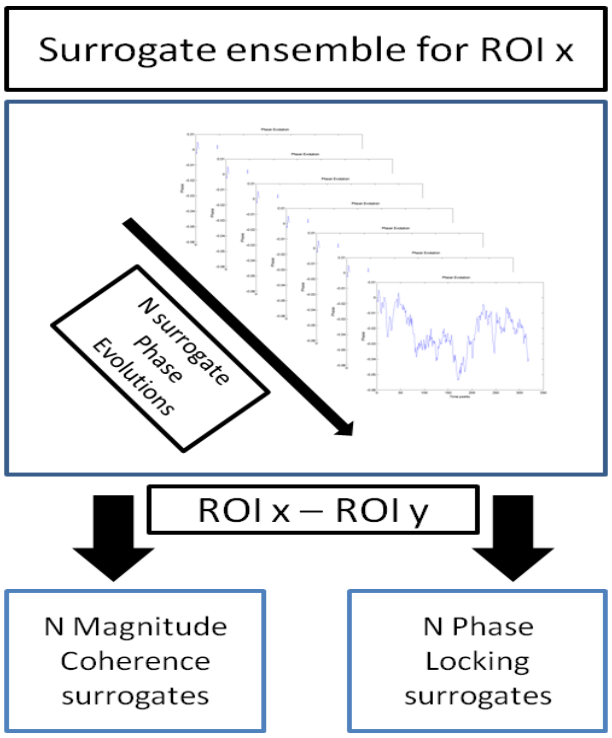

Figure 13- Representation of the MCV and PLV procedure. After the computation of the surrogate ensemble for a seed ROI x, it is obtained both N Magnitude Coherence and N Phase-Locking profiles for a ROI pair x and y.

2.2.2.3- Statistical Decision on significant MCV and PLV

From the N MCV and PLV surrogates, for a specific pair of ROI signals, a distribution for the MC and a distribution for the PL values, for each time point, are obtained. Each time point corresponds to a time-window, and each distribution of each time-window has N surrogate values.

After computation of the distributions for all MCV and PLV time points a percentile curve is calculated. To obtain, for example, a 95% cutoff value one gets the 95^{th} percentile curve from the distribution of each time point, for both MC and PL variables. The percentile curves are named Magnitude Coherence Statistic curve and Phase Locking Statistic curve, MCS and PLS curves. On Figure 14, the blue lines represent the Phase Locking and Magnitude Coherence profiles and the green lines represent both PLS and MCS curves for a chosen p-value. Then for each time point there is a significant Phase Locking Value, PLV, and a significant Magnitude Coherence Value, MCV.

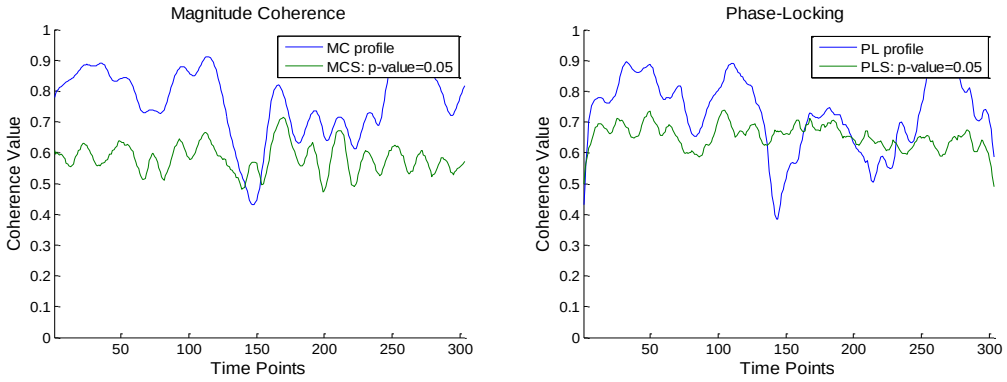

Figure 14- Phase Locking and Magnitude Coherence Analysis for significant MCV and PLV. In blue: Phase Locking and Magnitude Coherence profiles for a specific pair of ROI signals. In green: PLS and MCS curves for p-value=0.05.

The decision on significant MCV/PLV is performed for each time point/window. If, for each time-point, the magnitude coherence/phase locking value, (blue lines on Figure 14), is equal or higher than the respective 95% cutoff curve, (green lines on Figure 14), those time points have statistical significant Magnitude Coherence/Phase-locking. The resulting values are then used as threshold values to differentiate among periods with significant magnitude coherence/ significant phase-locking.

2.2.3- 3rd Section: Time-delay calculation

The time-delay calculation is obtained by wavelet coherence-based computation of phase delays. The phase differences between a pair of time series obtained by *WTC* analysis allows the calculation of time-delays by dividing the angles, time point by time point, by $2\pi F$, where F is the centered frequency from the narrow chosen frequency band. From the resulting values of time-delays, which are obtained in seconds units, for all time points we can calculate time-delay statistics for a pair of time series, such as average, median and standard deviation. The computation of time-delays statistics will be limited to periods where:

a) Phase-locking occurs on a given level of significance;
b) Magnitude of coherence is statistically significant on a given level of significance.

in order to test both neuronal communication hypothesis already mentioned. This methodology also allows the quantification of time-frequency bins with Phase-Locking above threshold and/or Magnitude Coherence above threshold. These bins correspond to periods of significant neuronal communication, based on a) and b).

2.2.4- 4th Section: Relationship between Magnitude Coherence and Phase-Locking

This work addresses the relationship between MC and PL variables, over time-points, using both Pearson correlation and Mutual information to investigate the similarity between both.

Regarding to Pearson Correlation analysis one gets a linear measure for the relation between the variables, whereas, the Mutual Information analysis allows the investigation of common information.

2.2.4.1- Pearson Correlation Analysis

The Pearson Correlation analysis was performed based on seed-analysis to get a set of both Magnitude Coherence and Phase-Locking indexes to be used as inputs. The correlation is computed for each pair of Magnitude Coherence and Phase-Locking indexes for the same pair of ROI signals. The goal is to have a value of correlation for each pair of signals chosen. Since this analysis is performed on a set of ROI signals the result is a set of correlation values with different p-values associated, so it is necessary to perform a correction of those p-values for multiple comparisons. Methods for dealing with multiple testing frequently call for adjusting the level of significance in some way, so the probability of observing at least one significant result due to chance remains below the chosen level of significance. It means that it is necessary to adjust a new cut off level equivalent to the chosen p-value. To perform such correction it is applied the Bonferroni Correction, where the $Corrected\ p\_value = \frac{p\_value}{\#cases}$, where p_value is the value chosen to the analysis before the correction, $\#cases$ is the number of comparisions and the $Corrected\ p\_value$ is the used value to distinguished among significant correlations (Curtin & Schulz 1998; Ossadtchi et al. 2013).

2.2.4.2- Mutual Information Analysis

Information theory was first introduced by Claud E. Shannon on a Mathematical Theory of Communication (Shannon & Weaver 1964). Mutual information measures the amount of common information between two random variables x and y and it is given by equation 8.

$$MI(x,y) = \sum_{x\in X}\sum_{y\in Y} p(x,y)\log\left(\frac{p(x,y)}{p(x)p(y)}\right) \quad \text{Equation 8}$$

where $p(x,y)$ corresponds to the joint probablility distribution function and $p(x)p(y)$are the marginal probability distribution functions (Pluim et al. 2003).

Since mutual information varies on the interval: $0 \leq MI \leq \min\left(H(x), H(y)\right)$, where H corresponds to entropy measure, it was applied a simply modification on *mutualiformation* function for MATLAB provided by Mon Cheng (2012) to achieve a normalization on MI values. In the presented work it is used to investigate the mutual dependence between Magnitude Coherence and Phase-Locking variables in order to investigate the degree of common information given by both variables.

2.2.5- 5th Section: Output illustration

This section presents an illustration of the methodology outputs for the study of human brain functional connectivity. The illustration is only performed for same examples to show the variety of analyses and results that the developed method allows for.

A) Input Parameters Setting

To give an illustration of the outputs produced by the presented analysis method it is necessary to set input parameters. From *A* dataset it is used the data acquired and pre-processed for one subject during a unique state of the paradigm. The results illustration is based on a single subject analysis. So, to give rise to the following results the chosen input parameters values are described on Table 1.

Inputs	Values
TR- sampling rate	1.83s
f1-f2-frequency band	0.07-0.13 Hz
Ncy- number of cycles for time-window integration	4
N- number of surrogates	1000
p-value-statistical level of significance	0.05

Table 1- Table for inputs parameters values for the application illustration of the presented methodology.

As presented on Table 1 a time-window of 4 cycles is computed for phase locking indexes calculation meaning that phase locking is evaluated across ~40 seconds intervals since the frequency band selected is centered on ~0.1 Hz. For the selected subject the narrow frequency band used to the Wavelet Transform Coherence step is 0.07-0.13Hz. The statistical test performed on both magnitude coherence and phase locking values is based on a surrogate ensemble of 1000 simulations and a p-value of 0.05.

B) Functional Connectivity Matrices

A common way to show the relation among all brain regions is the functional connectivity matrix. The presented methodology produces both Magnitude Coherence, MC, and Phase-Locking, PL, matrices. Each value on each matrix entry is the averaged value of magnitude coherence or phase-locking over all time points, for each pair of brain regions, ROIs. Figure 15 shows an illustration of MC and PL functional connectivity matrices outputs.

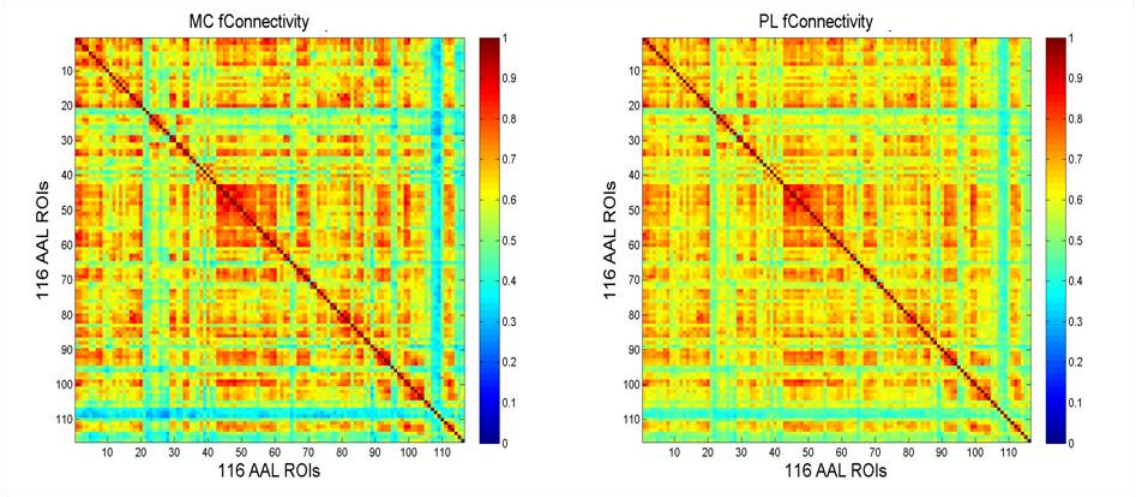

Figure 15-A On the left: Magnitude Coherence-based functional connectivity matrix. On the right: Phase-Locking -based functional connectivity matrix. Each matrix entry presents an averaged value of MC/PL for each ROIs pair for all 116 AAL list of brain regions used on pre-processing (see Appendix 1- AAL brain regions used on DPARSF).

Similar to these matrices the presented method also provides functional connectivity matrices for specific sets of brain regions giving rise to sub-matrices where instead of a full brain analysis, specific networks such as the DMN, the PPN and FCMN are considered.

C) Brain mapping for averaged time-delays

Regarding time-delay results obtained for both studied hypotheses, see 2.2.3- 3rd Section: Time-delay calculation, the presented methodology produces brain mappings for seed-based analysis. This means that the user must choose a seed brain region and a set of target brain regions where the target set can be composed from 1 or all 116 AAL ROIs. The output brain maps show the averaged time-delays for all time-windows selected as significant periods of MC/ PL. To illustrate a seed-based analysis for averaged time-delays, the chosen seed brain region is the left supplementary motor area, SMA, and the areas selected as target regions to be studied in relation to the seed are the sensorimotor areas, (M1 and S1), the premotor cortex, right SMA, and the parietal cortex areas. The output brain maps for both Magnitude Coherence and Phase-Locking time-delay-based calculation are presented on Figure 16. The images were obtained overlapping the time-delays values of communication, functional information, on an anatomical template, MNI template, using the *xjview* toolbox for MATLAB, resulting on brain maps with both anatomical and functional information.

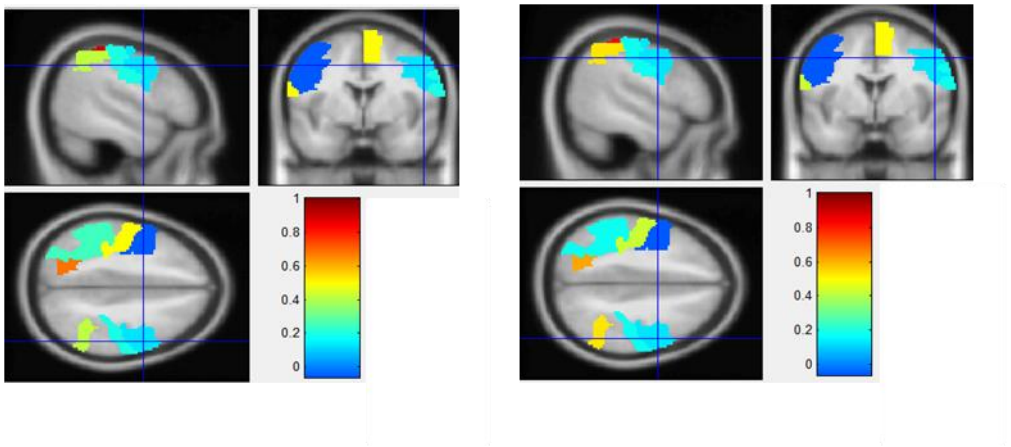

Figure 16- Brain Mapping for averaged time-delays, in seconds (represented by *hot* colormap), between a seed region (Left SMA) and a target set of regions. For this example all time-delays have positive values. On the left: brain mapping for communication on significant magnitude coherence periods for 95% level of significance. On the right: brain mapping for communication on significant phase-locked periods for 95% level of significance. The images were obtained overlapping the time-delays values on an anatomical template, MNI template, using the *xjview* toolbox for MATLAB.

D) Magnitude Coherence and Phase Locking profiles

The Magnitude Coherence and Phase Locking indexes profiles and the respective MCS and PLS, for a specific p-value, are also outputs of the implemented algorithm, allowing a more detailed inspection of the connectivity between two specific brain areas. The Left SMA-Left Insula brain regions pair is used to show the mentioned profiles outputs, see Figure 17. Analyzing both MC and PL variations over time points allows the inspection of communication fluctuations between the brain regions analyzed.

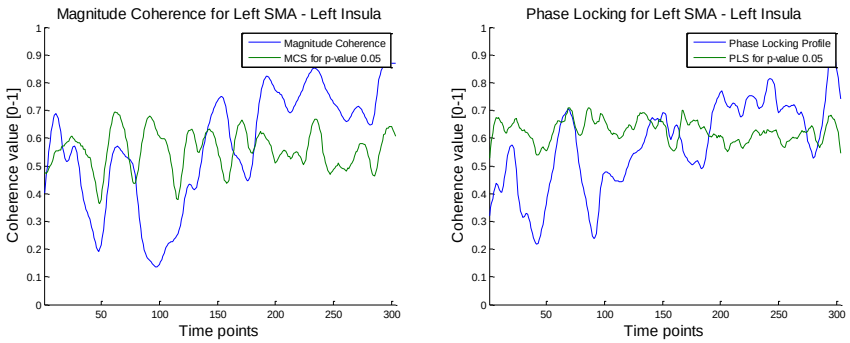

Figure 17- On the left: Magnitude Coherence profile for Left SMA-Left Insula regions. Blue line: Magnitude Coherence profile for the frequency band 0.07-0.13Hz. Green line: Magnitude Coherence Statistical curve for p-value=0.05. On the Right: Magnitude Coherence profile for Left SMA-Left Insula regions. Blue line: Magnitude Coherence profile for the frequency band 0.07-0.13Hz. Green line: Magnitude Coherence Statistical curve for p-value=0.05.

E) Time/Phase-delays statistics

The presented methodology gives a set of statistical parameters for both hypothesis of communication. The time-delays between brain regions presented as a final result and displayed on brain maps consist on average values over all time points above the threshold for significant statistical values. However, the analysis also takes into account other statistical measures as the median and standard deviation and displays them to a more detailed analysis. Table 2 contains, for the brain regions used, the statistics values of time-delay and also the number of time points with significant values of MC and PL at 95% level of significance, named significant bins. Each significant bin (or time point) corresponds to a 40 seconds period.

Measure\Hyphothesis	Significant MC	Significant PL
Mean	-1.429 s	-1.484 s
Median	-1.490 s	-1.509 s
Standard deviation	0.767 s	0.795 s
Significant bins/ Total bins	163/303	133/303

Table 2- Statistical measures(mean, median and standard deviation) for time-delays (in seconds) for both significant MC and significant PL periods at a p-value=0.05 and number of significant bins.

It is also important to take into account the phase and time delay distribution over all time points above MCS and PLS curves, for the specific interesting ROI pair under analysis. Using the *rose* function implemented on MATLAB one gets the phases distribution over the trigonometric circle which allows the analysis of such distribution. Having both time and phase delay histograms is important to inspect if the periods of time considered as significant communication periods have similar phases delays and if there is any relation between communication and the phase values associated. The following figures,

Figure 18 and Figure 19, illustrate the mentioned histograms for both PL and MC statistical significant bins/time points for both phase and time-delays.

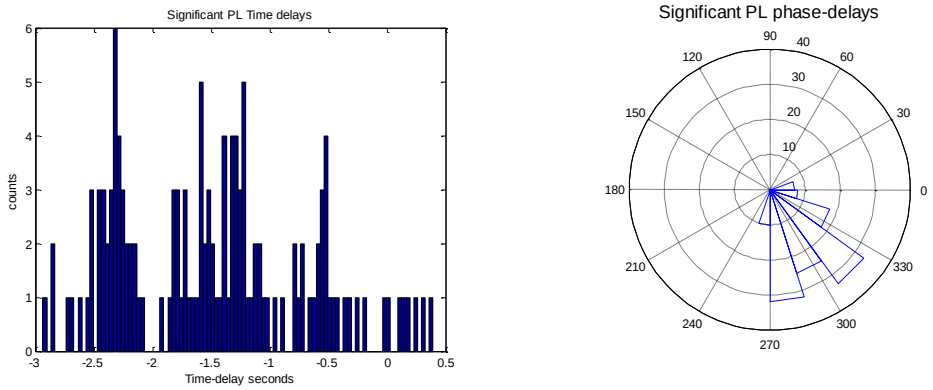

Figure 18- On the left: Histogram for time-delays, in seconds; on the right: Histogram for phase-delays, in degrees, for significant Phase-Locking periods.

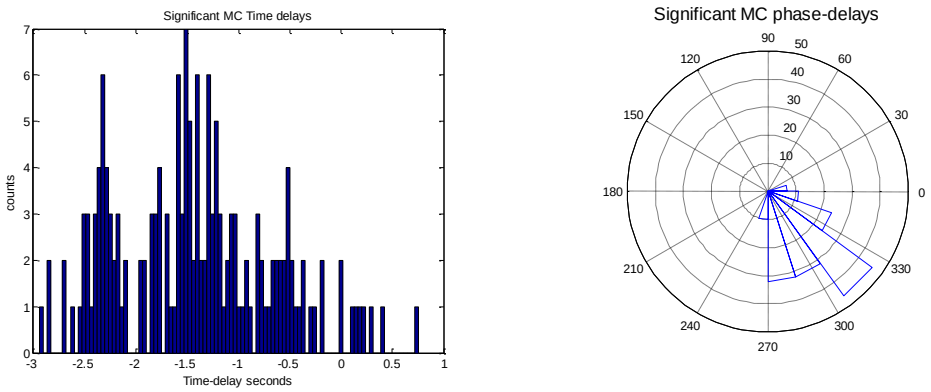

Figure 19- On the left: Histogram for time-delays, in seconds; on the right: Histogram for phase-delays, in degrees, for significant Magnitude Coherence periods.

F) Pearson Correlation and MI statistics plots

To evaluate the relationship between Magnitude Coherence and Phase-Locking indexes variables it is applied the Pearson Correlation and Mutual Information measures at 95% level of significance. Indeed this analysis can be performed for a specific pair of brain signals or for a chosen set of brain regions. For example, for Left SMA-Left insula pair, whose MC and PL profiles are shown on Figure 17, the Pearson correlation and the MI values during voluntary action, are 0.82 and 0.94, respectively. Such results mean a strong linear correlation between the MC and PL profiles and that both variables have an high degree of common information. For a set of brains regions analysis, such as the L_SMA-PPN regions, instead of a unique pair of signals, the results are plotted as shown on Figure 20 allowing to take conclusions about the relationship among different pairs.

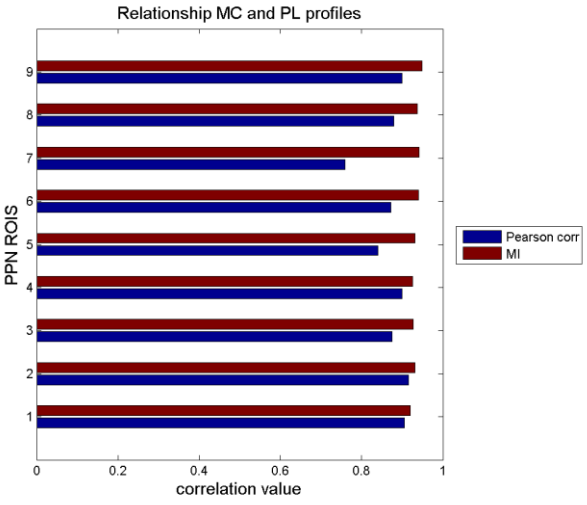

Figure 20- Values of Mutual Information, ploted with a red color, and values of pearson correlation, ploted with a blue color, for a set of brain regions bellonging to the Parietal-premotor network, PPN. These results correspond to the self-paced finger movement acquisition state.

3- RESULTS

Both Magnitude Coherence and Phase-Locking indexes, over time-windows, are averaged to give rise to matrices showing functional connectivity between all ROI pairs. Focus on a small subset of ROIs allows one to focus attention on specific networks known from the literature.

The results are based on dataset *A*. Since the used dataset is formed only by three subjects the main goal is not to make universal inferences about functional connectivity or neuronal communication. The presented results are used to show the potential of the method and to allow for a discussion on the advantages and disadvantages of the implemented analysis approach. The focus is on specific regions and circuits presumed to support resting state, voluntary finger movement and stimulus-driven finger movement, and on narrow frequency bands close to 0.1Hz. Table 3 shows the selected frequencies for each subject. Using the three subjects it can be performed a comparison among results searching for similarity or variability on the human brain connectivity within subjects.

Subject	frequency band
1	0.07-0.13Hz
2	0.07-0.13Hz
3	0.06-0.11Hz

Table 3- Narrow frequency bands selected for each subject of A dataset.

3.1- Connectivity matrices for all ROIs

In this section the results are presented for all 116 ROI signals obtained after data pre-processing. As shown before the outputs for all brain regions analysis are the functional connectivity matrices based on both studied hypothesis represented by MC and PL measures. On Figure 21 and Figure 22 connectivity matrices for subject 1 are presented. The corresponding results for subjects 2 and 3 are presented on Appendix 2- Functional connectivity matrices for subject 2 and 3. Figure 21 contains the resting state functional connectivity matrices whereas Figure 22 presents the same matrices for volunatry and stimulues-driven action. For both figures, the left column presents the functional connectivity matrices based on Magnitude Coherence metric and the right column refers to the Phase-Locking metric.

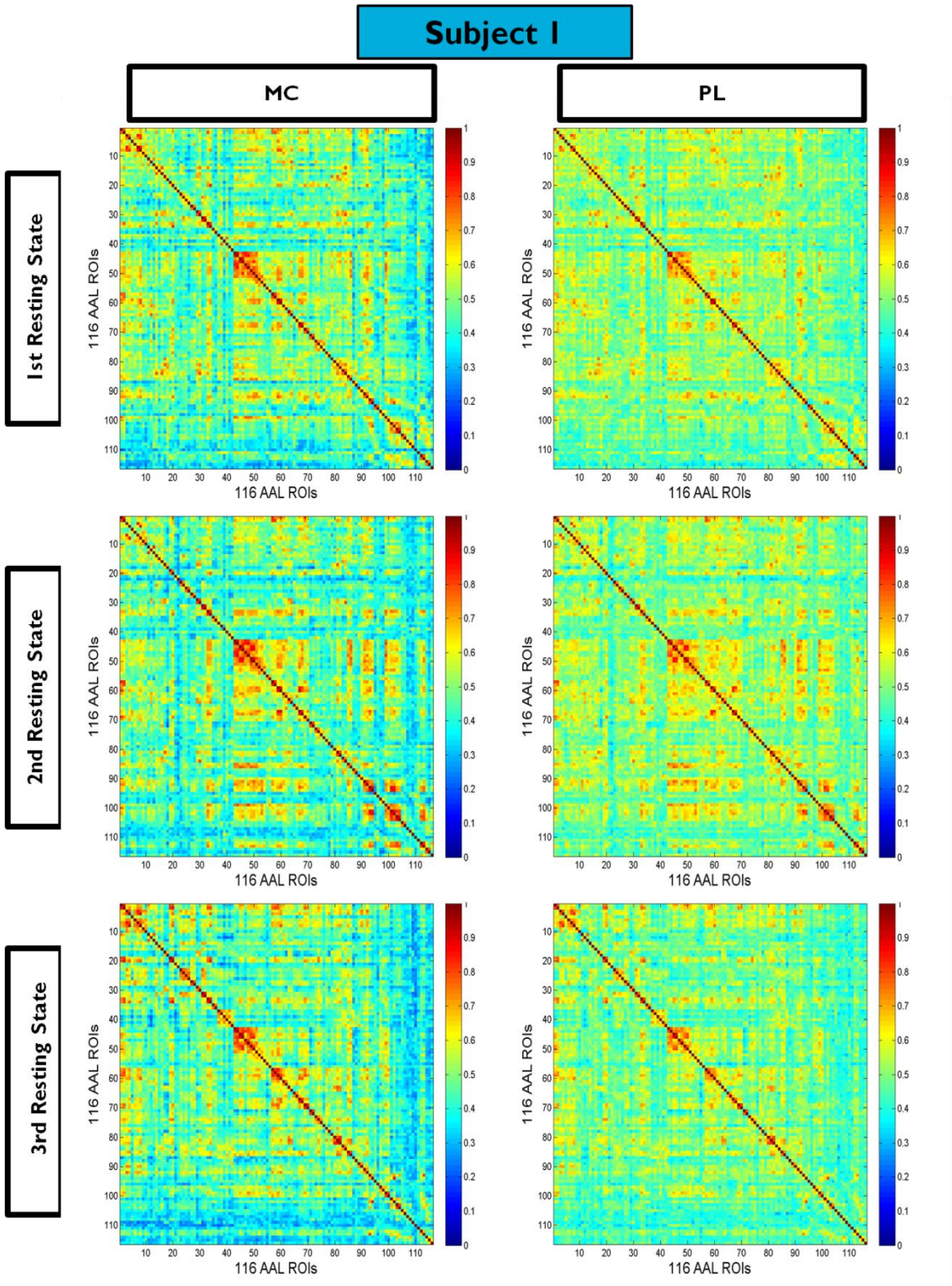

Figure 21- Functional Connectivity matrices for all resting states (for subject 1). On the left: functional measure based on Magnitude Coherence metric and on the right: functional measure based on Phase-Locking. From top to bottom: 1st resting state; 2nd resting state; and 3rd resting state moment of the analyzed paradigm.

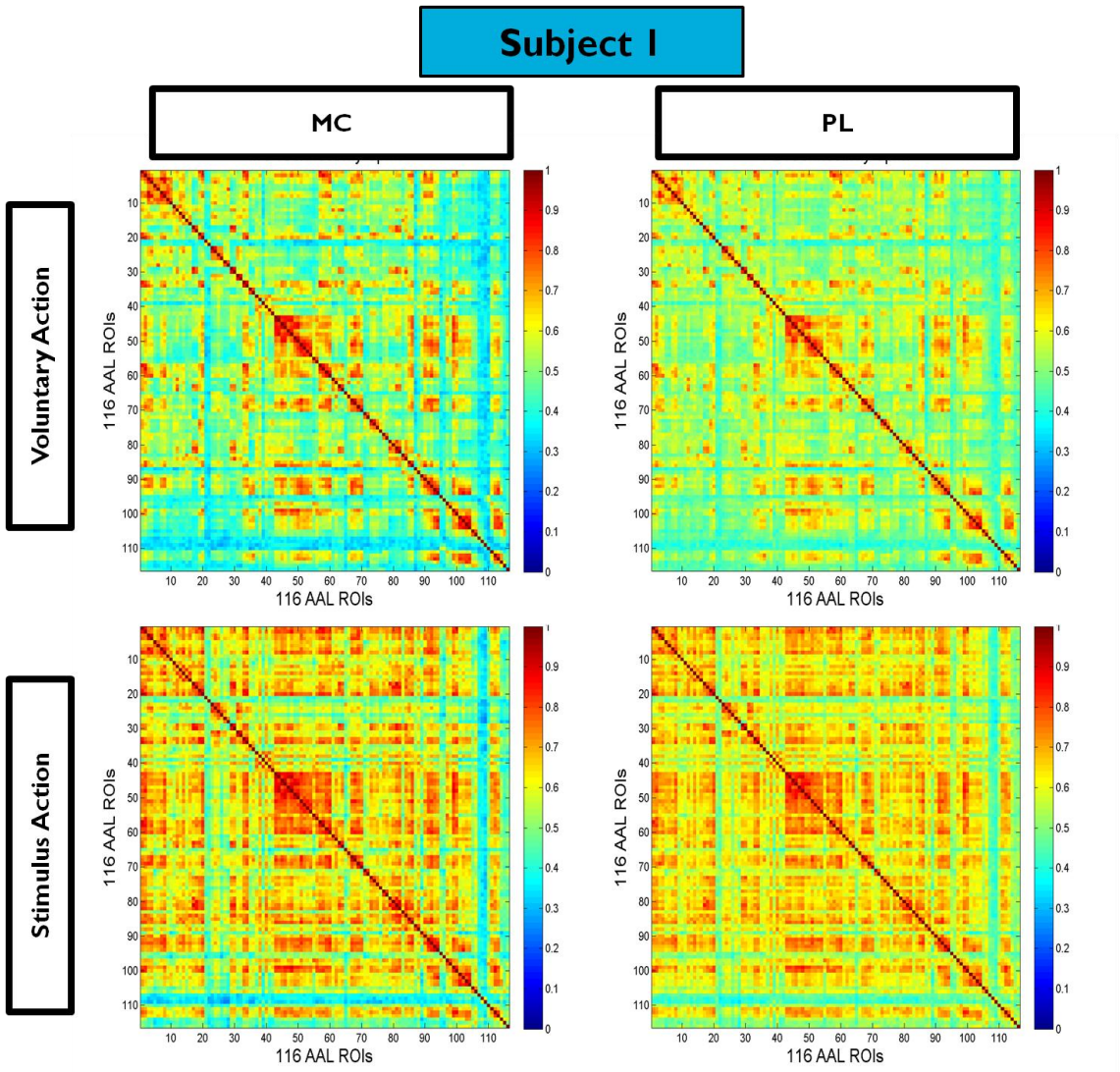

Figure 22- Functional Connectivity matrices for action states (for subject 1). On the left: functional measure based on Magnitude Coherence metric and on the right: functional measure based on Phase-Locking metric. From top to bottom: Voluntary action corresponding to self-paced finger movement and Stimulus action corresponding to auditory-paced finger movement.

For subject 1 it is easy to identify high values of Magnitude Coherence-based functional connectivity and Phase-Locking-based functional connectivity during the voluntary action acquisition moments. For subject 2 the mentioned matrices show high values in comparison with the other moments of paradigm but, it is clear that such values are not so high as they are for subject1. For the third subject both action states show high values of functional connectivity, based on both MC and PL measures, for a large number of brain regions pairs. In relation to the resting state acquisition, the obtained matrices show lower global functional connectivity values in comparison with the action moments. However, it is noted that the first subject has considerable higher connectivity values during rest moments contrary to what is observed for subject 2 and 3.

3.2- DMN, FCMN and PPN sub-matrices

As mentioned on 1- Introduction there are different circuits for the execution of a voluntary action which means that each subject is able to activate different brain patterns to perform the same action. From functional connectivity matrices, for all 116 brain regions, one is able to get sub-matrices for sets of ROIs focusing only on the brain regions expected to be involved on specific paradigm states. The analysis of all ROIs matrices is considerably difficult and, therefore, the following analysis is focused on sub-matrices, concerning to specific networks, which are the default mode network, DMN, for all resting states, the frontal cognitive-motor network, FCMN, for voluntary action (self-paced finger movement), and the parietal-premotor circuit, PPN, which is expected to guide the stimulus-driven action (auditory-paced finger movement), and also contributes to the voluntary movement. Table 4 summarizes the AAL brain regions belonging to these networks which are used on the presented work and the corresponding numbering used for functional connectivity sub-matrices.

Brain Networks	Brain Regions	AAL region Number	Functional Connectivity matrix number
Default Mode Network-DMN	Medial prefrontal areas;	7,8,9,10	1,2,3,4
	Posterior cingulate cortex;	35,36	5,6
	Hippocampus;	37,38	7,8
	Inferior parietal cortex;	61,62	9,10
	Lateral temporal cortex.	85,86	11,12
Frontal Cognitive-motor Network-FCMN	M1	1,2	1,2
	Prefrontal cortex;	3,4,7,8	3,4,5,6
	SMA	19,20	7,8
	Basal-ganglia	71,72,73,74,75,76	9,10,11,12,13,14
Parietal-Premotor Network-PPN	M1	1,2	1,2
	Premotor cortex	19,20	3,4
	S1	57,58	5,6
	Parietal cortex	59,60,61,62	7,8,9,10

Table 4- Brain regions belonging to the default mode network, the frontal-cognitive motor network and parietal-premotor network; the corresponding AAL region number and the corresponding functional connectivity matrix number. The AAL list of regions is on **Appendix 1- AAL brain regions** .

The following figures,Figure 23 and Figure 24, show functional connectivity sub-matrices based on Magnitude Coherence, MC, and Phase-Locking, PL, measures for DMN brain regions. The default-mode network consists on a set of brain regions, see Table 4, identified as being activated during resting state acquisition moments and so, it is expected, on rest, significant connections among them. These figures present the obtained functional connectivity for the three resting states of the studied paradigm for all the subjects. By observation of Figure 23 it is seen for all resting states, and for both metrics of connectivity, that values higher than 0.5 show up in almost all brain region pairs. Regarding to Figure 24, for both subject 2 and 3 the results are not so high among DMN brain regions.

Figure 25 presents the sub-matrices, for all three subjects, focusing on the FCMN brain regions, see Table 4. It can be seen that functional connectivity measures have high values for almost all brain region pairs belonging to the frontal-cognitive motor network. It is also observed that both subject 1 and 3 present higher values then subject 2.

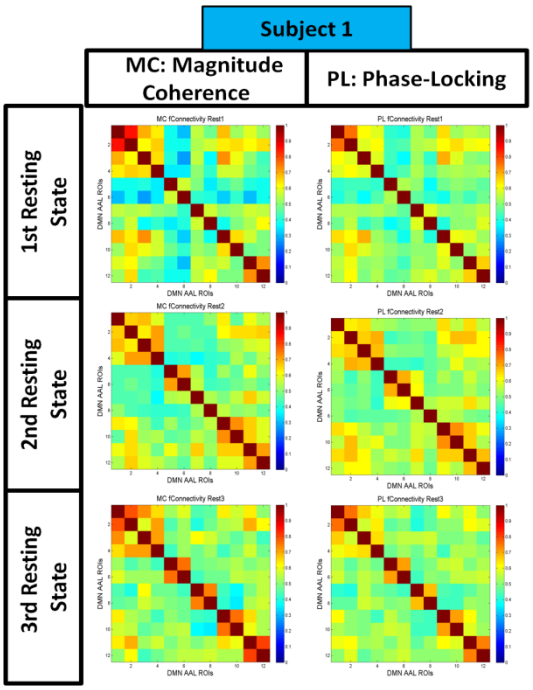

Figure 23-Functional connectivity sub-matrices focusing the DMN brain regions, presented on **Table 4**, for subject 1.On the left: Magnitude Coherence metric; on the right: Phase-Locking metric. From top to bottom: 1st resting state; 2nd resting state and 3rd resting state

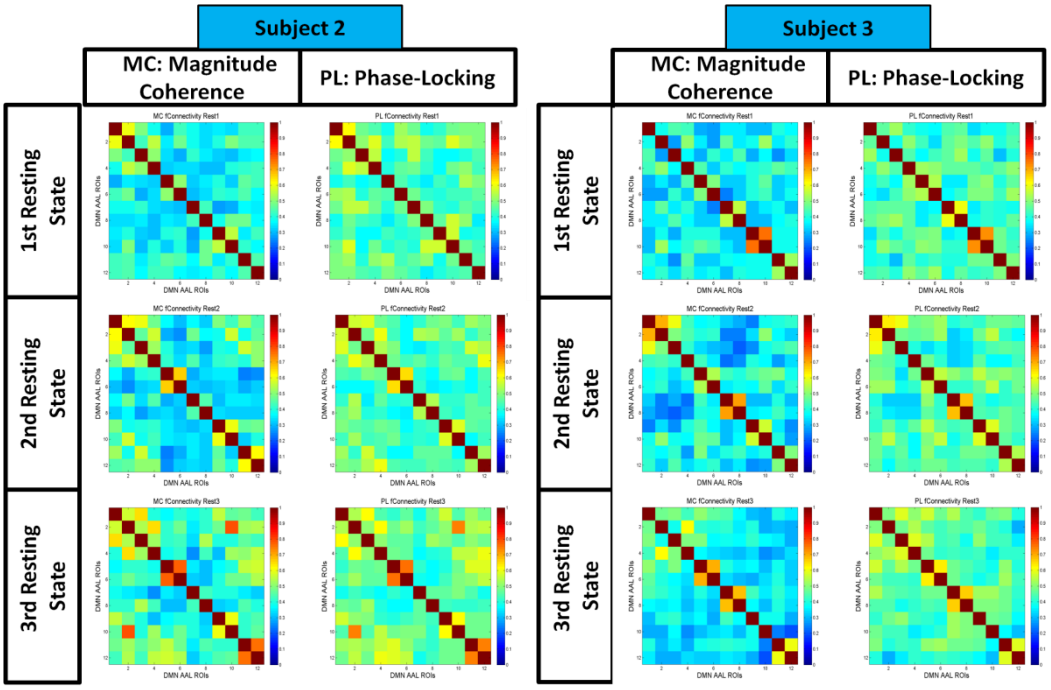

Figure 24- Functional connectivity focusing the DMN brain regions presented on **Table 4**. Left panel: sub-matrices for subject 2; Right panel: sub-matrices for subject 3. For both panels: on the left: Magnitude Coherence metric; on the right: Phase-Locking metric. From top to bottom: 1st resting state; 2nd resting state and 3rd resting state.

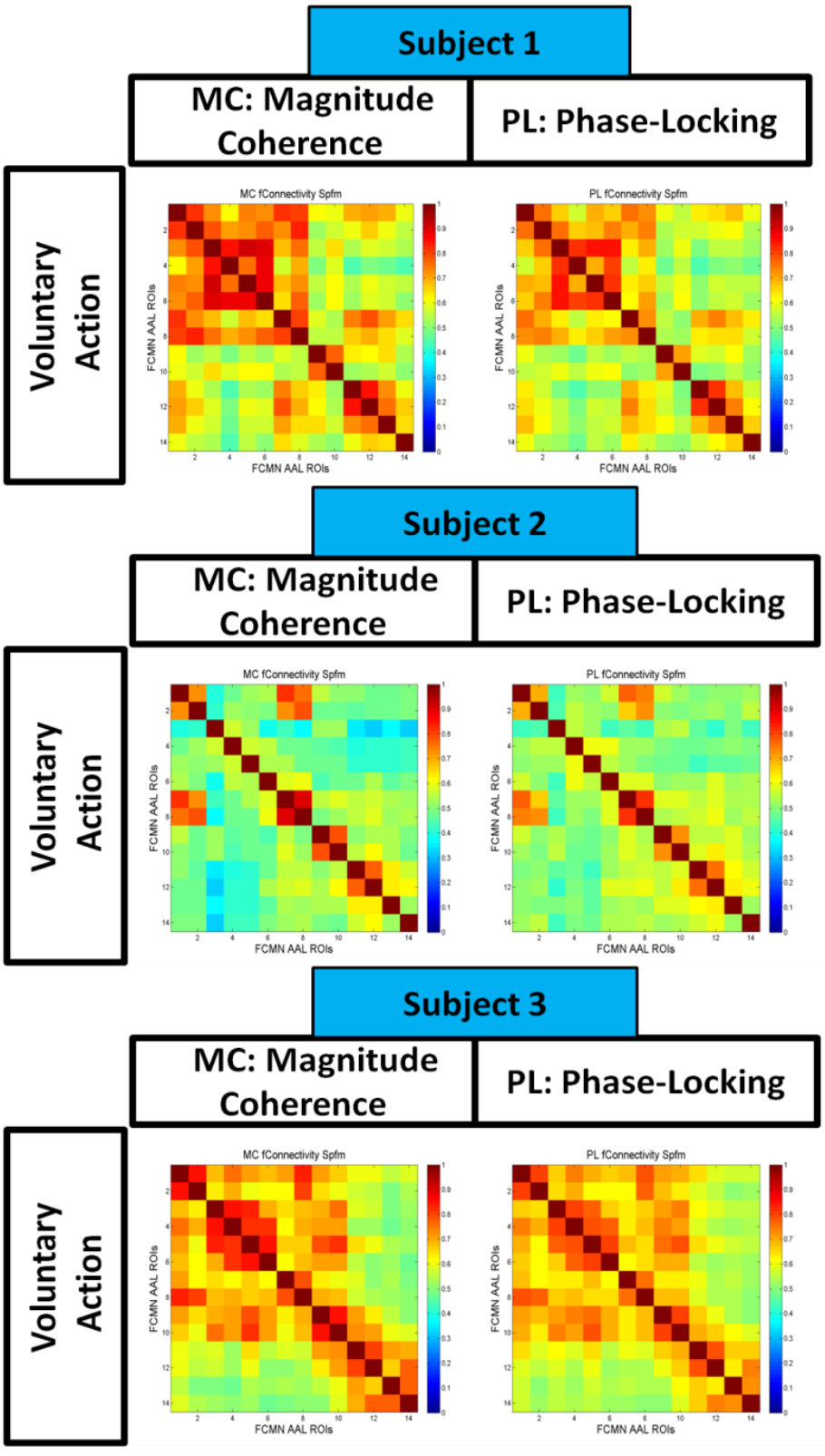

Figure 25- Functional connectivity focusing FCMN brain regions, presented on **Table 4**. From top: sub-matrices for subjects 1, 2 and 3, respectively. On the left: Magnitude Coherence metric; on the right: Phase-Locking metrics.

Finally, Figure 26 shows the obtained sub-matrices for PPN regions, see also Table 4, for the three subjects of the analyzed dataset during both action states, voluntary versus stimulus-driven action. By comparing each subject, for both actions, the results suggest a similar contribution of

PPN regions on both voluntary and stimulus action. For subject 1 and 3 the PPN regions seem to be all highly connected, however, for subject 2, observing both MC and PL measures, it seems that inside the PPN network there are regions more connected with each other, still keeping the similarity between MC and PL results.

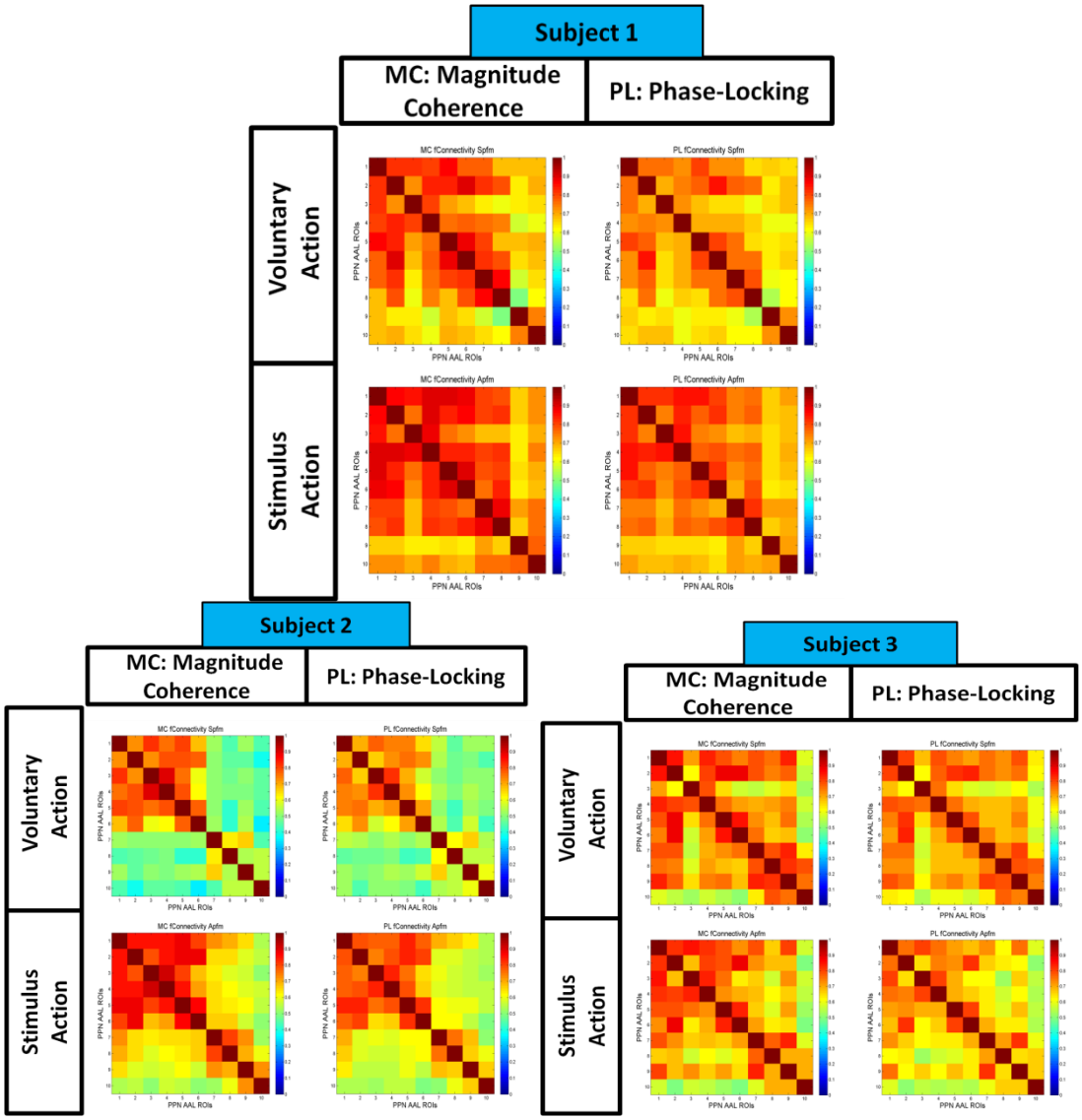

Figure 26- Functional Connectivity focusing PPN brain regions presented on **Table 4**. On the left top: sub-matrices for subject 1 during both voluntary and stimulus action and for both MC and PL metrics. On the right top: sub-matrices for subject 2. On bottom: sub-matrices for subject 3.

3.3- Brain maps for communication delays

From the presented matrices for functional connectivity measured by MC and PL metrics it can be seen a large set of brain regions which can involve resting, voluntary and/or stimulus-driven action states. Using the developed methodology and based on such key role brain regions a seed-based analysis was performed to assess the temporal delays of neuronal communication

between them. In this section the averaged time-delays for both hypothesis of neuronal communication are presented by brain maps focusing both voluntary and stimulus-driven actions.

Since the performed actions are finger movements performed with the right hand for all subjects, the used seed is the left supplementary motor area, L_SMA. By creating the brain maps presented on Figure 27 it is possible to analyze differences on time-delays for the PPN regions in relation to the Left SMA.

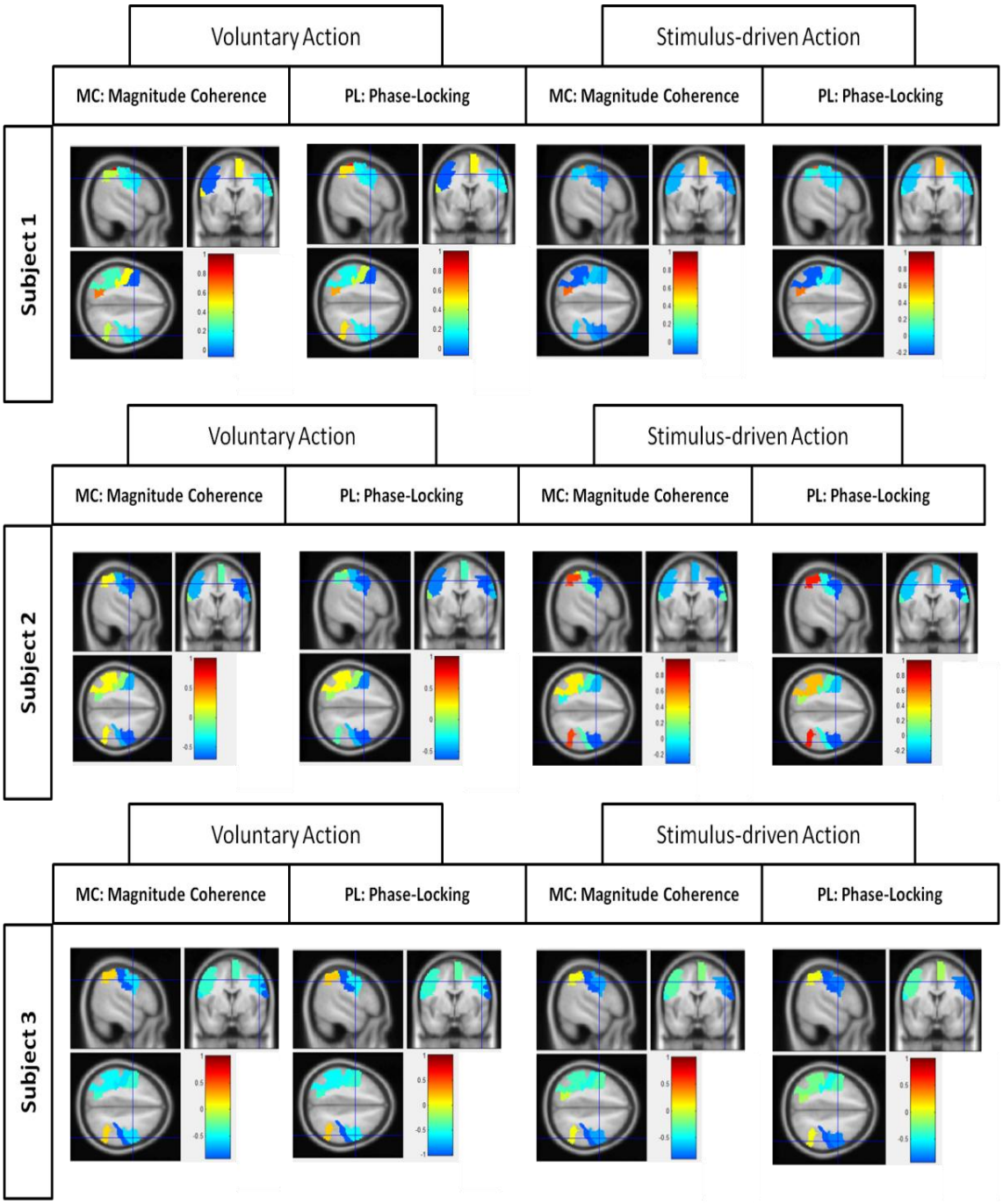

Figure 27- Time-delays, in seconds, between Left SMA and PPN regions, for both voluntary and stimulus-driven actions and based on both MC and PL measures of neuronal communication periods.

Observing Figure 27, for both voluntary and stimulus-driven action, and for all subjects, similar averaged time-delays on both magnitude coherence and phase-locking periods of neuronal communication at a 95% level of statistical significance are observed. The averaged time-delays for left SMA and PPN regions, see Table 4, vary on a maximum range of -1 to 1 second, on all presented cases.

3.4- ROI pairs Analysis

3.4.1- Temporal delays statistics

To demonstrate temporal delays statistics analysis, for specific brain regions signals pairs, it is used the Left SMA and a set of bilateral regions known as being related to finger movement tasks, described on Table 5.

Brain Area	ROI name*
Sensory-motor areas	
M1	Precentral areas
S1	Postcentral areas

Table 5- Set of bilateral brain regions used on a single-subject analysis for a detailed inspection of neuronal communication. *See **Appendix 1- AAL brain regions** .

The next figures, Figure 28-Figure 31, show the obtained results for the pairs L_SMA-M1/S1 bilateral areas, respectively. The figures present the Magnitude and Phase-Locking profiles, time-delays and phase-delays distributions for significant periods of neuronal communication, during the voluntary and stimulus-driven finger movement (p-value=0.05).

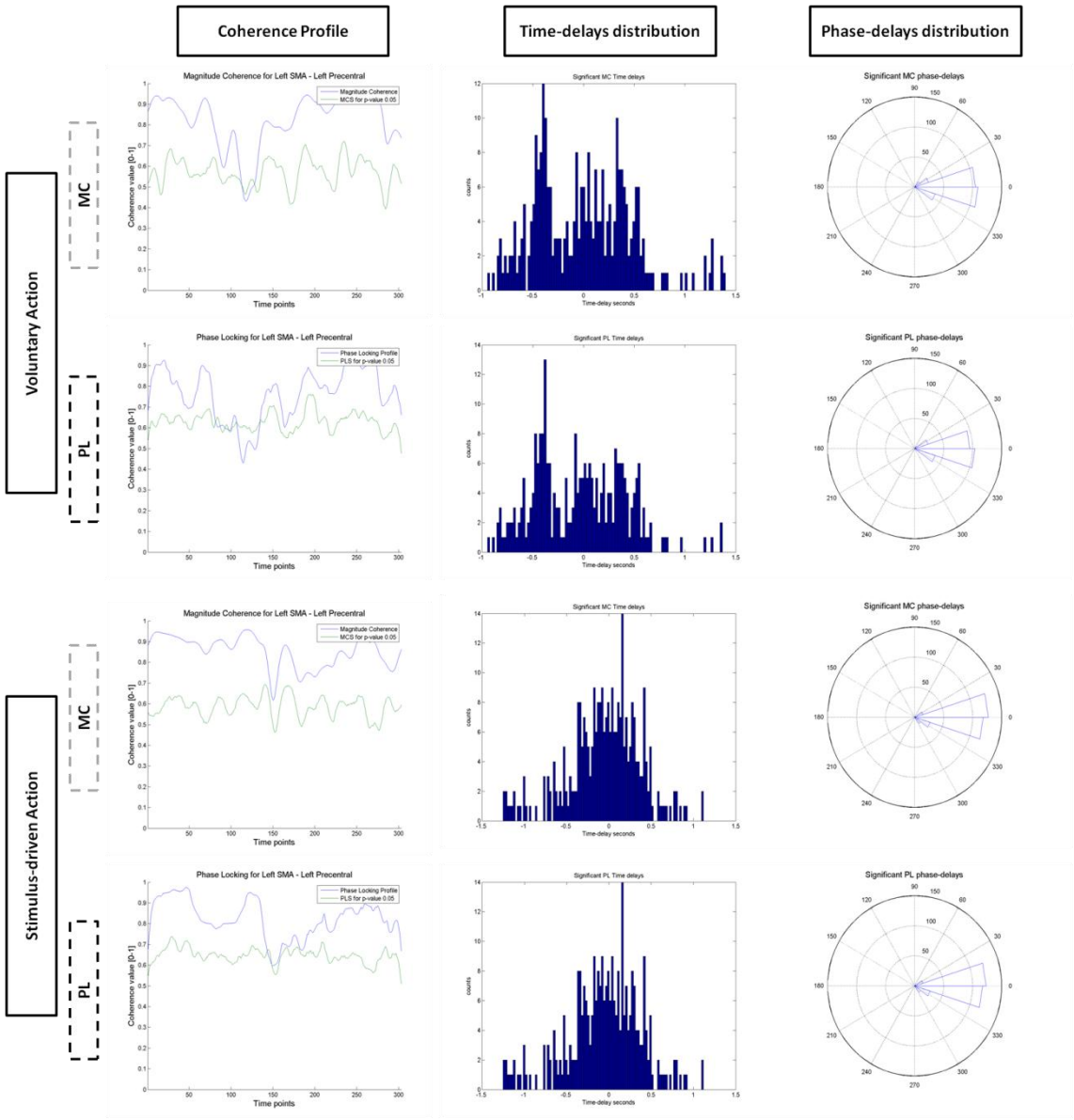

Figure 28- Results for L_SMA-L_precentral area during voluntary and stimulus-driven finger movement states. On the left column: Magnitude and Phase-Locking profiles over all time-points; on the middle column: time-delays distribution for both MC and PL measures; on the right column: phase-delays distribution for both MC and PL measures.

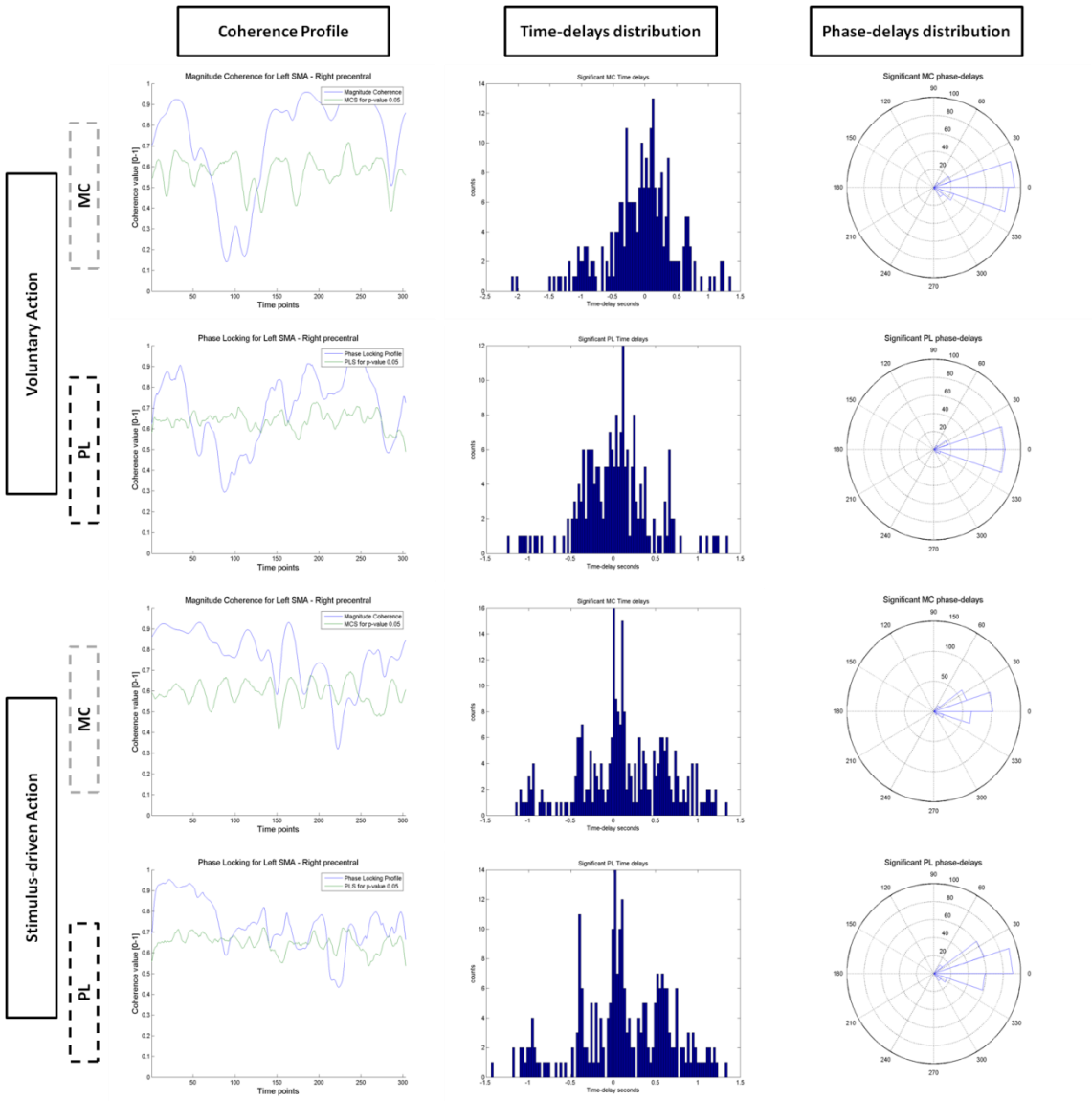

Figure 29- Results for L_SMA-R_precentral area during voluntary and stimulus-driven finger movement states. On the left column: Magnitude and Phase-Locking profiles over all time-points; on the middle column: time-delays distribution for both MC and PL measures; on the right column: phase-delays distribution for both MC and PL measures.

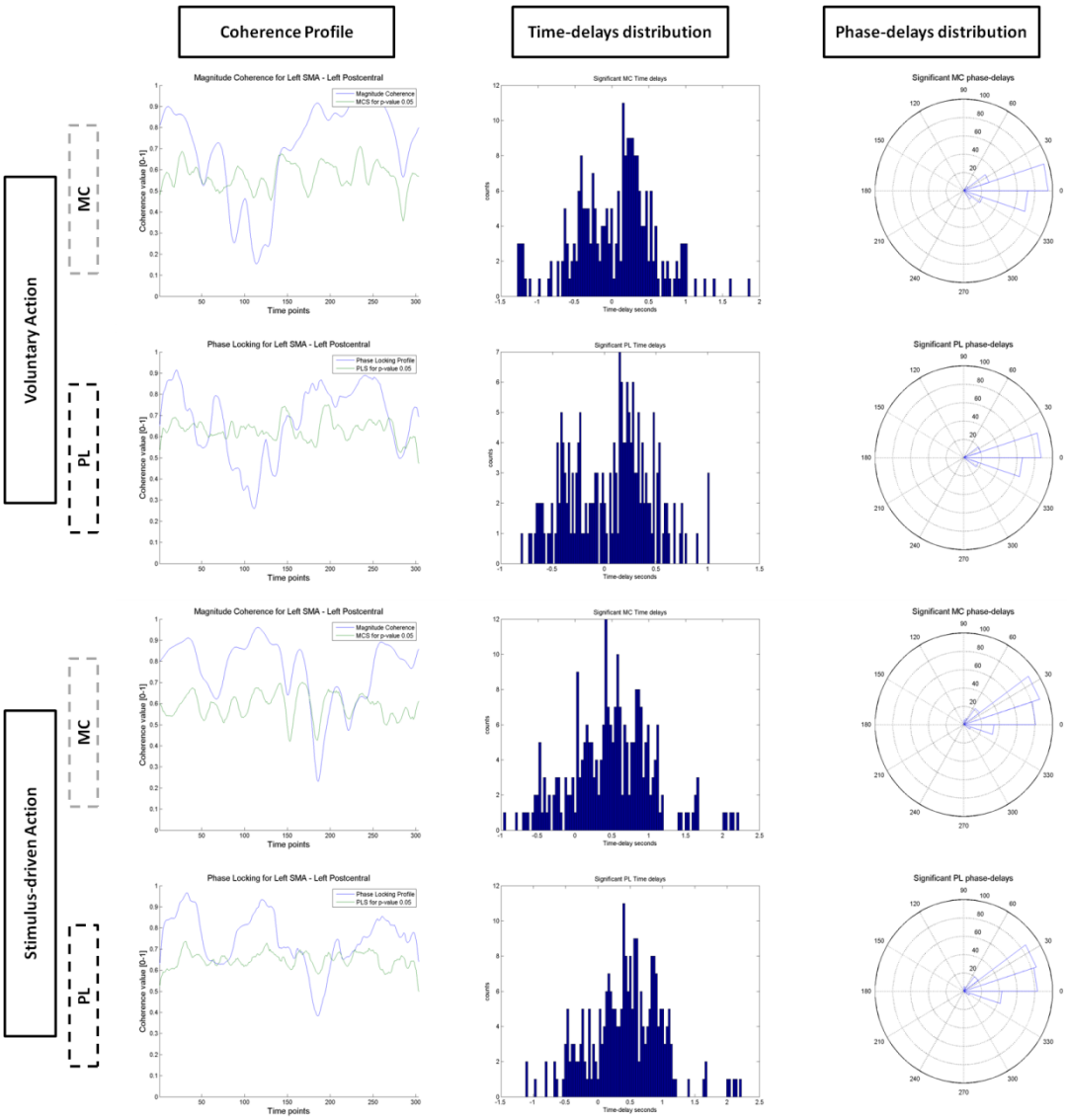

Figure 30- Results for L_SMA-L_postcentral area during voluntary and stimulus-driven finger movement states. On the left column: Magnitude and Phase-Locking profiles over all time-points; On the middle column: time-delays distribution for both MC and PL measures; On the right column: phase-delays distribution for both MC and PL measures.

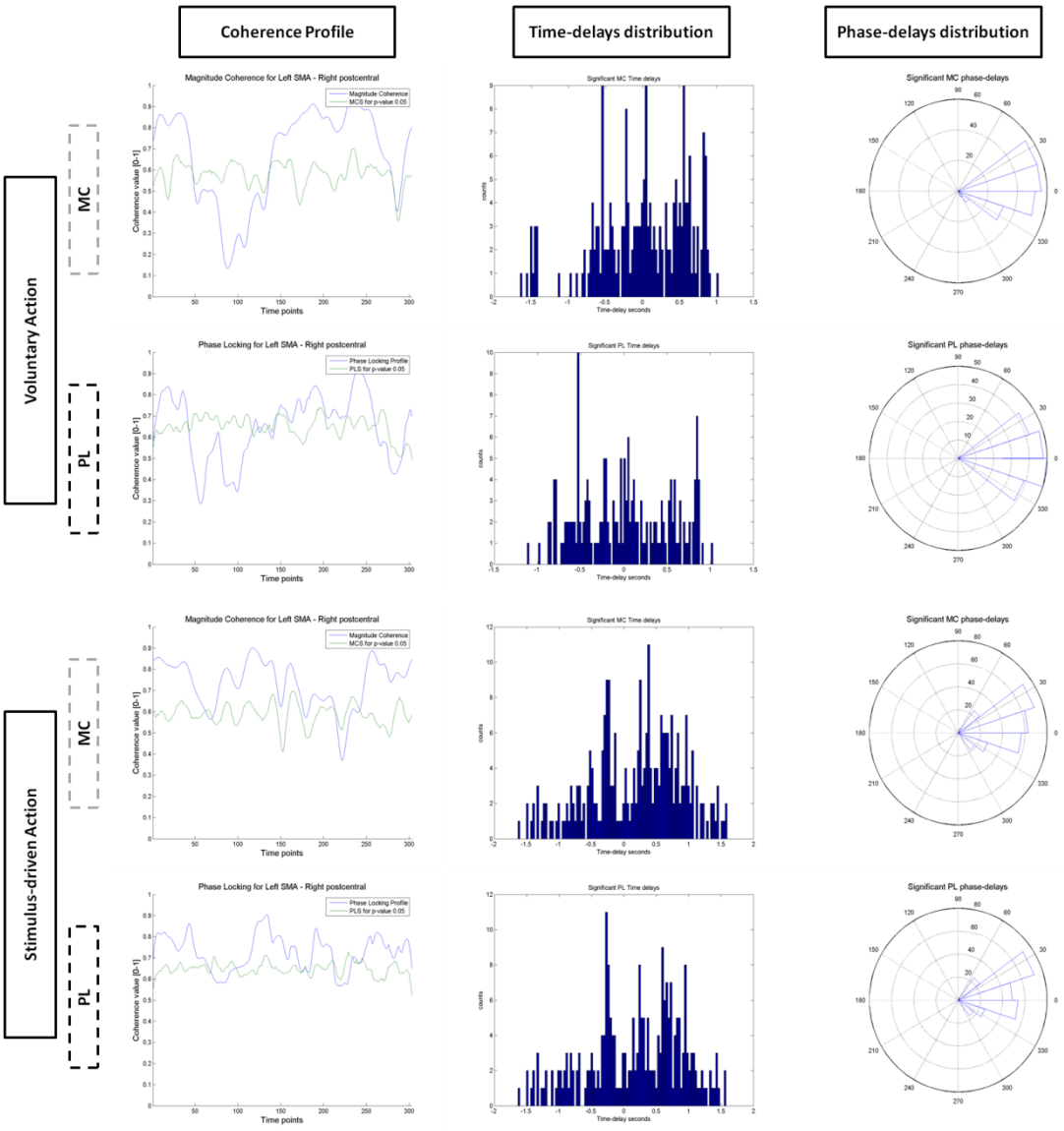

Figure 31- Results for L_SMA-R_postcentral area during voluntary and stimulus-driven finger movement states. On the left column: Magnitude and Phase-Locking profiles over all time-points; on the middle column: time-delays distribution for both MC and PL measures; on the right column: phase-delays distribution for both MC and PL measures.

Both time-delays and phase-delays distributions are composed of values corresponding to significant neuronal communication time-points. On Table 6 it is summarized the time-delays statistics for the analyzed pairs, L_SMA-M1/S1 areas, in terms of average, median and standard deviation, std, for time-windows/time-points of significant neuronal communication under the hypothesis of significant MC and under the hypothesis of significant PL measures for p-value=0.05, for both voluntary and stimulus-driven action states allowing a detailed inspection of time-delays statistics.

ROI pair	Neuronal Communication Measure (MC/PL)	State of Paradigm (Vol/Sti)	Averaged Time-delay (seconds)	Median Time-delay (seconds)	Std Time-delay (seconds)	Significant bins/Total bins=304
L-SMA-L_M1	MC	Vol	**-0.004**	-0.008	0.474	**287**
		Sti	**-0.054**	-0.021	0.429	**303**
	PL	Vol	**-0.042**	-0.034	0.442	**264**
		Sti	**-0.056**	-0.023	0.432	**298**
L_SMA-R_M1	MC	Vol	**-0.070**	-0.013	0.545	**249**
		Sti	**0.130**	0.097	0.527	**263**
	PL	Vol	**0.173**	0.025	0.427	**197**
		Sti	**0.128**	0.097	0.553	**248**
L_SMA-L_S1	MC	Vol	**0.046**	0.142	0.542	**238**
		Sti	**0.494**	0.504	0.559	**247**
	PL	Vol	**0.054**	0.141	0.393	**193**
		Sti	**0.426**	0.447	0.562	**249**
L_SMA-R_S1	MC	Vol	**0.001**	0.039	0.609	**212**
		Sti	**0.179**	0.286	0.709	**267**
	PL	Vol	**0.005**	0.006	0.524	**184**
		Sti	**0.172**	0.256	0.723	**239**

Table 6- Time-delays statistics for L_SMA-M1/S1 bilateral areas pairs, for both hypothesis of communication: MC-Magnitude Coherence and PL-Phase-Locking measures, and for both voluntarVol, and stimulus-driven,Sti, action states. Averaged, median and std statistics are calculated only for periods, time-points, above MCS and PLS for p-value=0.05. Those periods of communication are quantified and presented as significant bins.

3.4.2- Temporal lead and lag

3.4.2.1- FCMN and PPN regions

Based on the temporal lead and lag concept between brain regions pairs it is possible to establish the information flow chronometry. Considering FCMN regions, one expected scheme of information flow involves the Basal Ganglia, SMA and Precentral brain areas, see Figure 32.

Figure 32- ROIs scheme of chronometry-based information flow for brain regions belonging to the FCMN. Each color represents a brain area. Blue circle:Left Basal Ganglia (L_BG); Red:Left SMA(L_SMA) and Green: Left Precentral area. The black arrows show the information flow. On the left: posterior view; in the middle: lateral view and on the right: superior view of the human brain.

Focusing the left brain hemisphere, the Table 7 shows the time-delays statistics for the three subjects on voluntary action performance. For both subject 1 and 3 the averaged time-delays show that the left Basal Ganglia, BG, areas are activated before the Left SMA (positive time-delays values) meaning that BG is leading the left SMA. For subject 2 the results also show two BG areas leading the SMA, however for the 71 ROI, left caudate, the results are opposite. For the left SMA-left precentral pair, the results show negative averaged time-delays for all subjects.

Subject	Time-delay Statistic (seconds)	MC/PL-based	ROIs: 71-19	ROIs: 73-19	ROIs: 75-19	ROIs: 19-1
1	**Average**	**MC**	0.374	0.956	0.869	-0.004
		PL	0.458	0.974	0.802	-0.042
1	**Std**	**MC**	0.869	0.650	0.615	0.474
		PL	0.851	0.579	0.583	0.441
2	**Average**	**MC**	-0.372	0.053	0.360	-0.129
		PL	-0.382	0.092	0.306	-0.148
2	**Std**	**MC**	0.715	0.802	1.001	0.549
		PL	0.617	0.802	0.778	0.482
3	**Average**	**MC**	0.799	1.278	0.984	-0.398
		PL	0.638	1.037	0.848	-0.463
3	**Std**	**MC**	0.837	0.957	1.080	0.814
		PL	0.705	0.874	0.827	0.776

Table 7- Time-delay statistics (average and std values in seconds units) for all subjects during voluntary finger movement for both MC, magnitude coherence, and PL,phase-locking, measures of neuronal communication. The results are presented for four brain regions belonging to the FCMN , see **Figure 32**. The ROI pairs are defined by its AAL number, see Appendix 1- AAL brain regions .

Considering Figure 33, in both stimulus-driven and voluntary action performance, for the PPN regions the flow chronometry of information expected is represented by black arrows (from left postcentral area to left inferior parietal area and next to left SMA to finally achieve the left precentral area).

Figure 33- ROIs scheme of chronometry-based information flow for brain regions belonging to the PPN. Each color represents a brain area. Red circle:Left Postcentral; Grey: Left inferior parietal; Pink:Left SMA(L_SMA) and Green: Left Precentral area. The black arrows show the information flow chronometry. On the left: posterior view; in the middle: lateral view and on the right: superior view of the human brain.

The time-delay statistics for this case are presented on Table 8 and Table 9, for stimulus-driven and voluntary action, respectively.

Subject	Time-delay Statistic (seconds)	MC/PL-based	ROIs: 57-61	ROIs: 61-19	ROIs: 19-1
1	**Average**	**MC**	-0.523	-0.236	-0.054
		PL	-0.584	-0.175	-0.056
1	**Std**	**MC**	0.570	0.570	0.429
		PL	0.615	0.547	0.432
2	**Average**	**MC**	0.250	-0.182	-0.135
		PL	0.147	-0.211	-0.166
2	**Std**	**MC**	0.771	0.653	0.552
		PL	0.741	0.766	0.515
3	**Average**	**MC**	0.362	0.345	-0.392
		PL	0.248	0.265	-0.456
3	**Std**	**MC**	0.702	0.630	0.813
		PL	0.652	0.509	0.778

Table 8- Time-delay statistics (average and std values in seconds units) for all subjects during stimulus-driven finger movement for both MC, magnitude coherence, and PL,phase-locking, measures of neuronal communication. The results are presented for brain regions belonging to the PPN, see **Figure 33**. The ROI pairs are defined byits AAL number, see **Appendix 1- AAL brain regions** .

Subject	Time-delay Statistic (seconds)	MC/PL-based	ROIs: 57-61	ROIs: 61-19	ROIs: 19-1
1	**Average**	**MC**	-0.193	0.118	-0.004
		PL	-0.163	0.211	-0.042
1	**Std**	**MC**	0.660	0.699	0.474
		PL	0.592	0.599	0.441
2	**Average**	**MC**	0.529	-0.388	-0.129
		PL	0.512	-0.442	-0.148
2	**Std**	**MC**	1.050	0.639	0.549
		PL	1.076	0.662	0.482
3	**Average**	**MC**	0.151	0.509	-0.398
		PL	0.158	0.592	-0.463
3	**Std**	**MC**	0.800	0.600	0.814
		PL	0.797	0.609	0.776

Table 9- Time-delay statistics (average and std values in seconds units) for all subjects during voluntary finger movement for both MC, magnitude coherence, and PL,phase-locking, measures of neuronal communication. The results are presented for brain regions belonging to the PPN, see **Figure 33**. The ROI pairs are defined by its AAL number, see **Appendix 1- AAL brain regions** .

3.4.2.1- ACC and AIC regions

Table 10 shows the time-delay results for anterior cingulum cortex, ACC, (represented by ROIs number 31 and 32) and for anterior insular cortex, AIC, (represented by ROIs number 29 and 30) regarding to the left SMA. These results were taken for voluntary action.

Observing the results on Table 10 only for one case (subject 2: ROI pair 19-31) the time-delays are positive values. For all the other cases the results show negative averaged temporal delays between the left SMA and the ACC and AIC brain regions.

Subject	Time-delay Statistic (seconds)	MC/PL-based	ROIs: 19-31	ROIs: 19-32	ROIs: 19-29	ROIs: 19-30
1	**Average**	**MC**	-1.231	-0.874	-1.411	-1.314
		PL	-1.482	-1.283	-1.485	-1.373
1	**Std**	**MC**	0.776	0.867	0.770	0.748
		PL	0.492	0.529	0.776	0.662
2	**Average**	**MC**	0.109	-0.280	-0.246	-0.286
		PL	0.242	-0.622	-0.273	-0.370
2	**Std**	**MC**	0.561	0.818	0.646	0.663
		PL	0.549	0.961	0.612	0.719
3	**Average**	**MC**	-0.403	-0.545	-0.951	-0.975
		PL	-0.347	-0.682	-1.221	-1.013
3	**Std**	**MC**	0.754	0.830	0.797	0.697
		PL	0.721	0.729	0.483	0.663

Table 10- Time-delay statistics (average and std values in seconds units) for all subjects during voluntary finger movement for both MC, magnitude coherence, and PL,phase-locking, measures of neuronal communication. The results are presented for the pairs: L-SMA/ right and left anterior cingulum and insula brain regions. The ROI pairs are defined by its AAL number, see **Appendix 1- AAL brain regions .**

3.4.2.1- AIC and Heschl regions: Stimulus action

Table 11 shows the time-delay results for anterior insular cortex, AIC, (represented by ROIs number 29 and 30) and for bilateral Heschl regions (represented by ROIs number 79 and 80) regarding to the left SMA. These results were taken for stimulus action where the stimulus consisted on an auditory sound.

For subjects 1 and 3 the results show negative averaged time-delays for both AIC and Heschl gyrus meaning that these regions are leading the left SMA. For subject 2 the results are opposite for three pairs.

Subject	Time-delay Statistic (seconds)	MC/PL-based	ROIs: 19-29	ROIs: 19-30	ROIs: 19-79	ROIs: 19-80
1	**Average**	**MC**	-0.429	-0.601	-1.074	-1.109
		PL	-0.319	-0.621	-1.143	-1.134
1	**Std**	**MC**	0.742	0.596	0.671	0.647
		PL	0.710	0.578	0.674	0.594
2	**Average**	**MC**	0.041	-0.319	0.010	0.008
		PL	0.048	-0.344	0.105	0.059
2	**Std**	**MC**	0.909	0.568	0.844	0.604
		PL	0.771	0.568	0.698	0.610
3	**Average**	**MC**	-0.238	-0.962	-0.280	-0.301
		PL	-0.476	-0.928	-0.186	-0.301
3	**Std**	**MC**	0.788	0.758	0.768	0.599
		PL	0.748	0.639	0.558	0.556

Table 11- Time-delay statistics (average and std values in seconds units) for all subjects during stimulus-driven finger movement for both MC, magnitude coherence, and PL, phase-locking, measures of neuronal communication. The results are presented for the pairs: L-SMA/ right and left anterior insula and Heschl brain regions. The ROI pairs are defined by its AAL number, see **Appendix 1- AAL brain regions .**

3.4.3- Preferable phases for communication

For an inspection of phase values preferred on communication, the Figure 34, Figure 35 and Figure 36 show, for voluntary action state, and for all available subjects the significant phase values for four different pairs, already mentioned as expected to be involved on such action. For subject 1 and 3, for both MC and PL measures, the phases distribution during significant periods of neuronal communication between the respective pairs of brain regions showed preference values on the range $[-\frac{\pi}{2}; 0]$. However, for subject 2 the values are not centered on the same range.

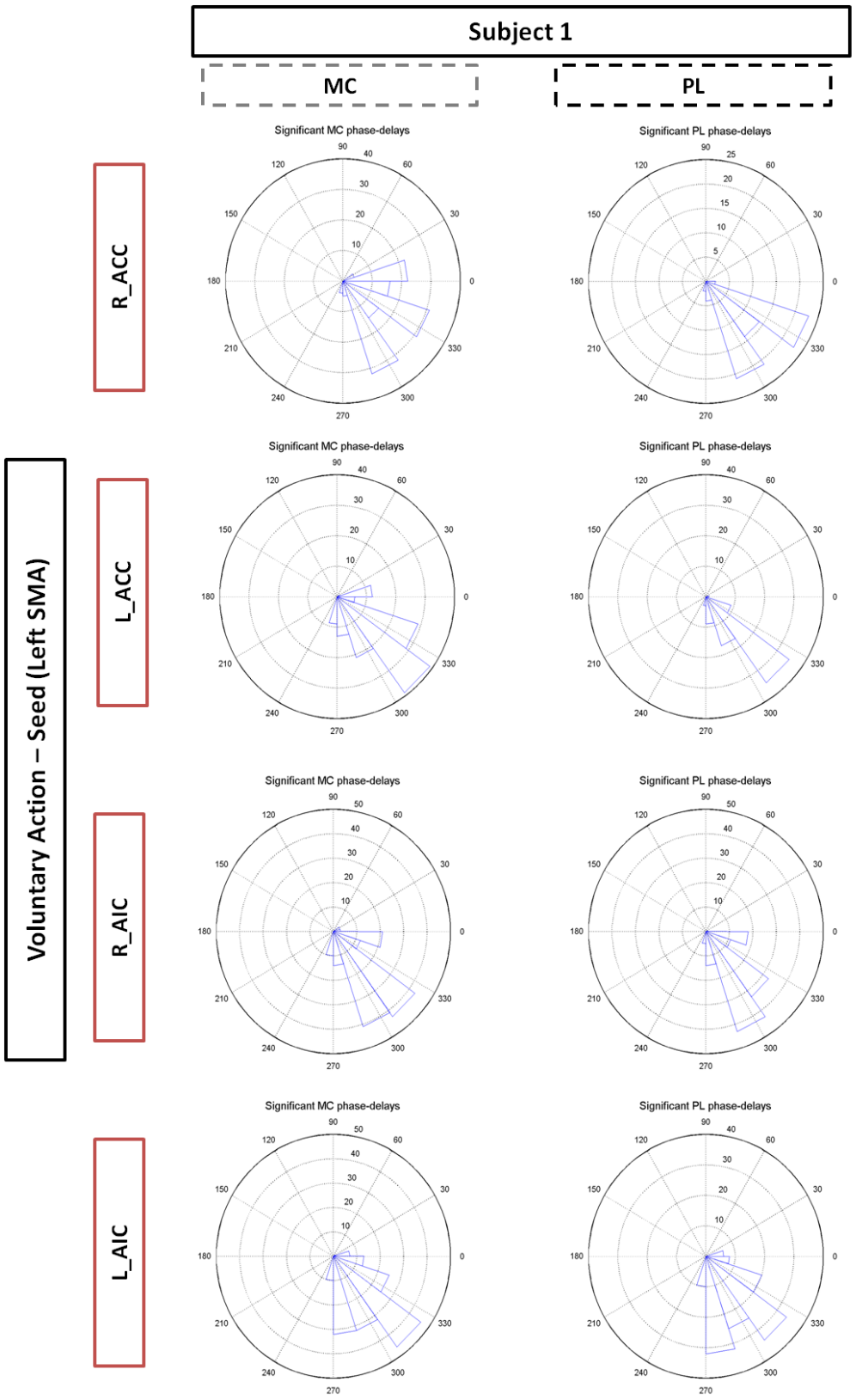

Figure 34- Phase distributions for voluntary action (subject 1). On the left column: significant values for MC-based neuronal communication and on the right column: significant values for PL-based neuronal communication PL. From top to bottom: L_SMA-right anterior cingulum; L_SMA-left anterior cingulum; L_SMA-right insula and L_SMA-left insula.

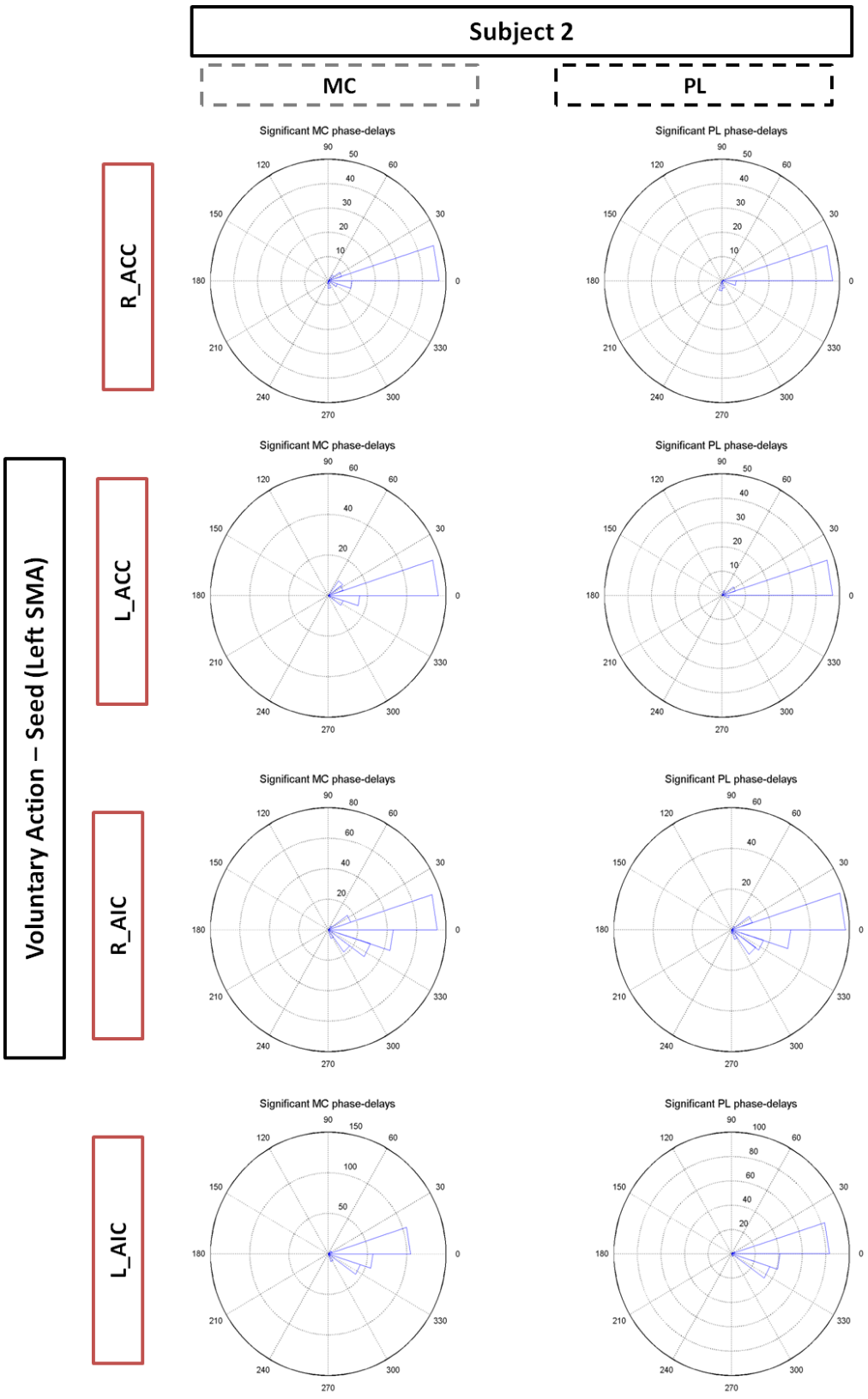

Figure 35- Phase distributions for voluntary action (subject 2). On the left column: significant values for MC-based neuronal communication and on the right column: significant values for PL-based neuronal communication PL. From top to bottom: L_SMA-right anterior cingulum; L_SMA-left anterior cingulum; L_SMA-right insula and L_SMA-left insula.

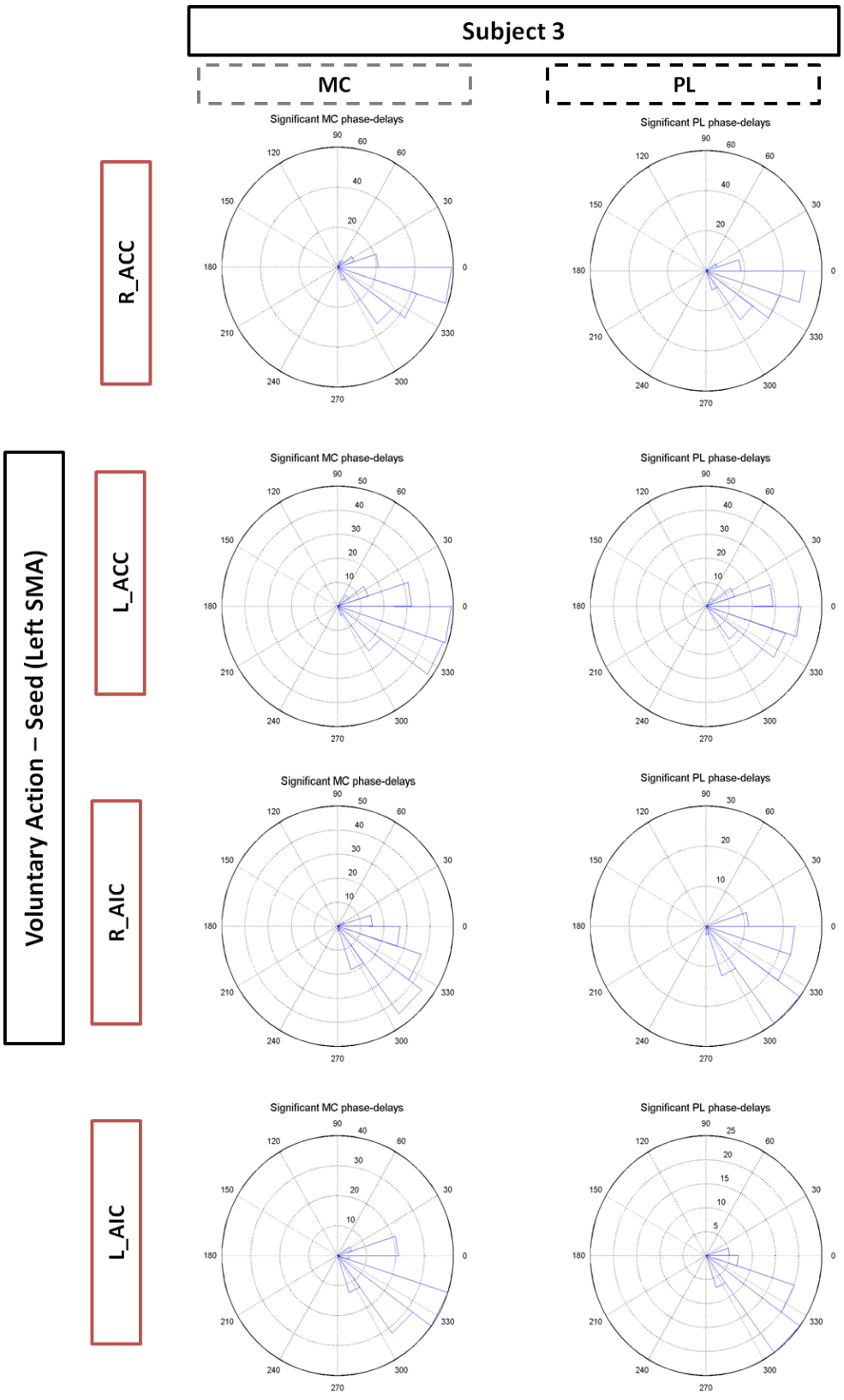

Figure 36- Phase distributions for voluntary action (subject 3). On the left column: significant values for MC-based neuronal communication and on the right column: significant values for PL-based neuronal communication PL. From top to bottom: L_SMA-right anterior cingulum; L_SMA-left anterior cingulum; L_SMA-right insula and L_SMA-left insula.

3.4.4- Rest versus tasks temporal delays

The bilateral M1 and bilateral posterior parietal cortex, PPC, in relation to the left SMA seed region, are used to investigate variations between resting state and both task conditions: stimulus driven action and voluntary action. On Figure 37 it is presented the results for the four mentioned pairs in terms of averaged time-delay, in seconds, for all subjects. For all cases the averaged time delays, based on MC and PL measures are very similar, for the same subject. The obtained values are quite different among the considered brain regions pairs within subject and for all subjects.

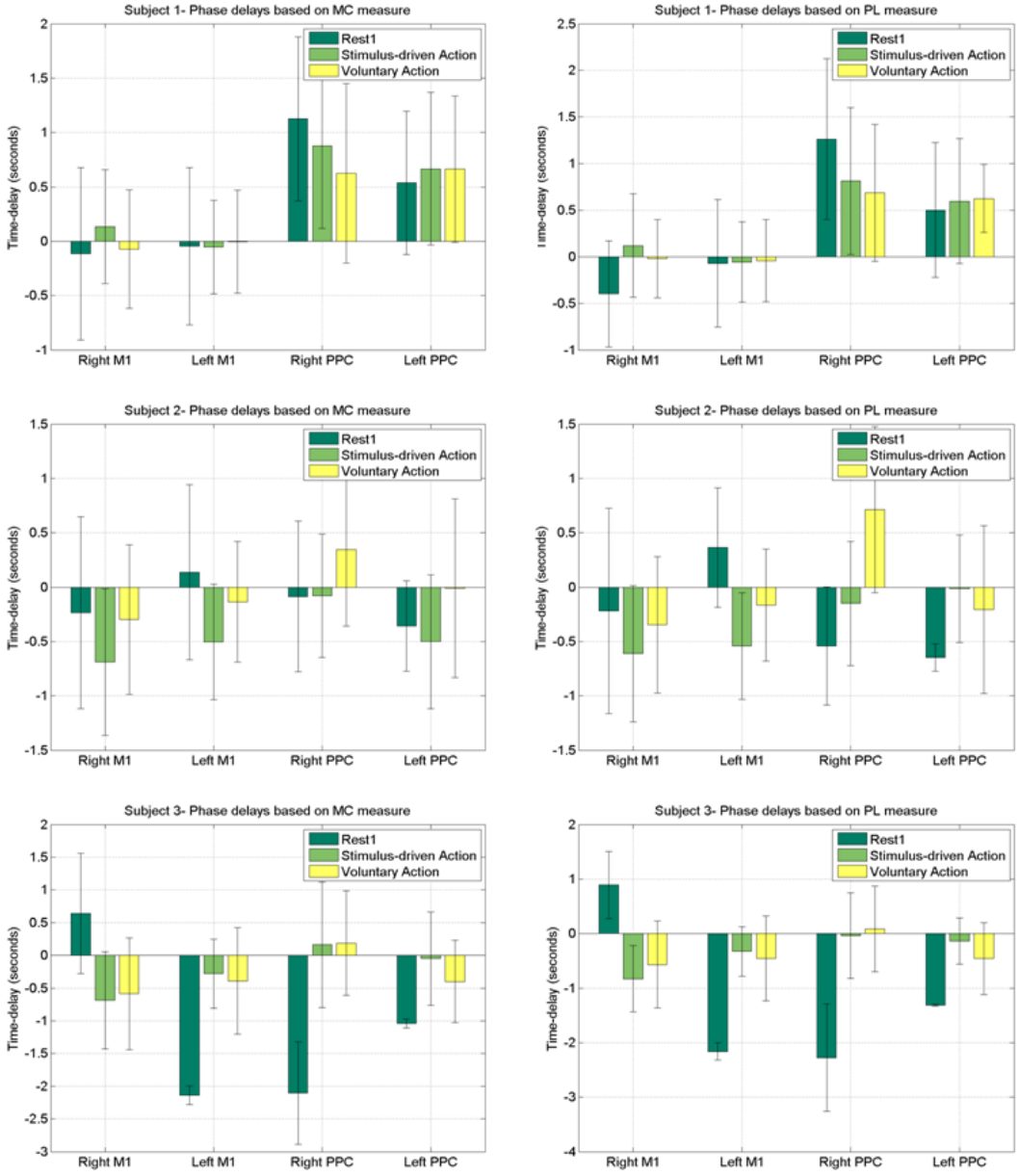

Figure 37- Averaged and standard deviation Phase-delays, in seconds units. On the first row: results of subject 1; on the second row: results for subject 2 and the third row presents the results for subject 3. The lef column presents the phase-delays values based on MC measure and the right columns shows the phase-delays values based on PL measure. For each case it is presented the results for Left SMA seed region in relation to Right M1, Left M1, Right PPC and Left PPC. Dark green bar: first resting state moment; green bar: stimulus-driven action (auditory-paced finger movement) and yellow bar: voluntary action (self-paced finger movement).

3.5- Time-delay Consistency across different TR values

It seems relevant to consider different TR values to analyze if there are different results, in terms of time-delays, for short and long TR values. So, using the three subjects from *B* dataset whose signals were acquired with a TR=0.92 seconds, much smaller than *A* dataset TR (=1.83s), it is performed a downsampling analysis to get the same signals, during resting state, with two different values of TR. Using a 3 factor for downsampling, the obtained TR is equal to 0.92×3, TR=2.76s. To interpret the results, it is plotted one scatter plot, for each pair of signals, showing the fitted linear regression between the time-delays obtained with TR=0.92 seconds and time-delays obtained with the mentioned downsampling. The downsampling was applied using the *downsample* function provided by MATLAB. The results are presented for different and random pairs of brain regions signals on Figure 38. The scatter plots are obtained using the *scatter* function and the linear regression is computed using the *lsline* function. The linear regression is estimated based on the commonly used least squares approach. The linear correlation between time-delays with and without downsampling is computed by *corr* function. On Figure 38, each row shows the results for a different random pair of brain signals and each column represents one different subject. It can be seen that, for subjects 2 and 3, R values are consistently larger than 0.5, implying strong correlation. On the other hand, subject 1 shows several instances where R<0.5, implying that there is a higher mismatch between the time-delay values computed from the original and the downsampled data.

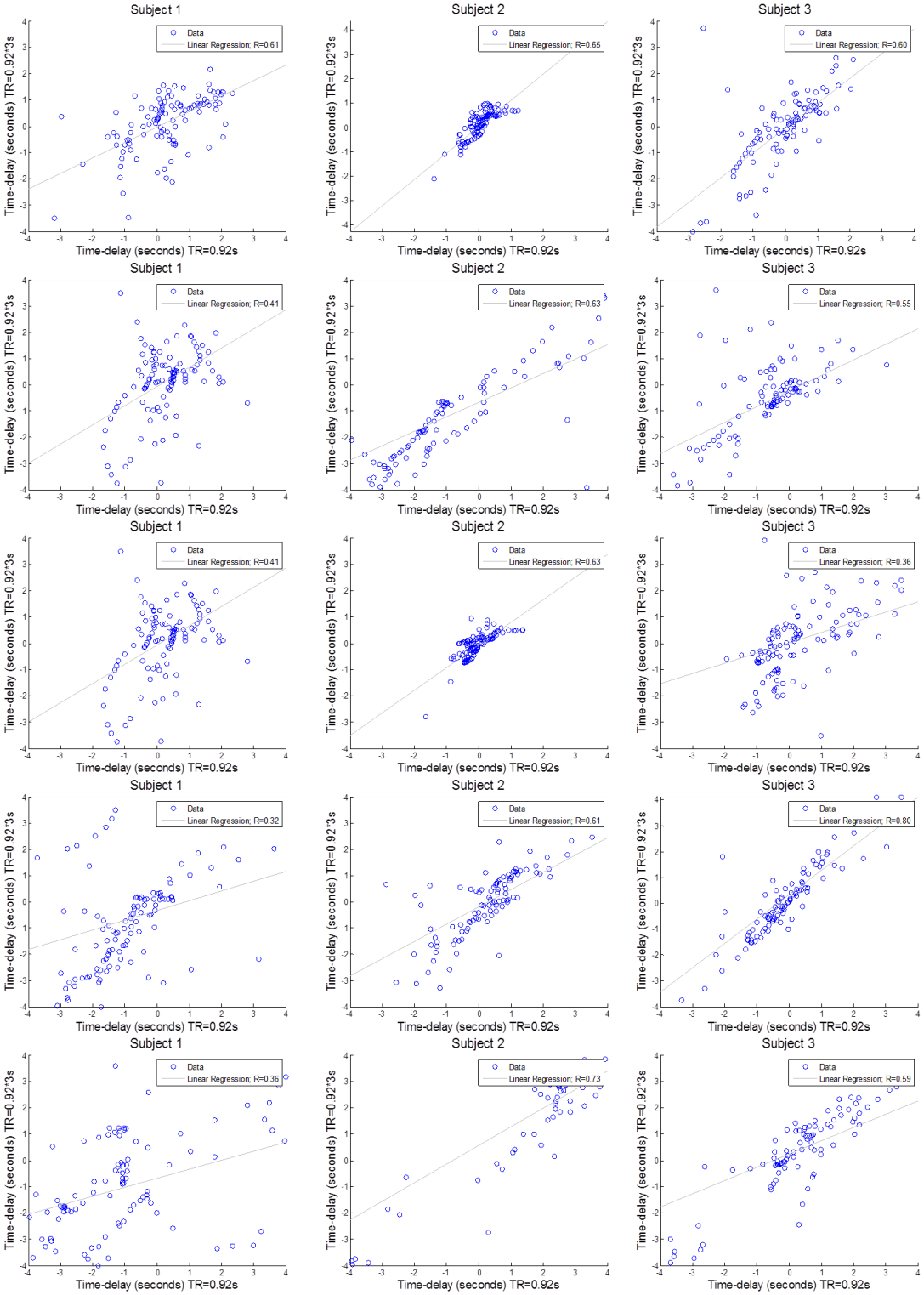

Figure 38- Scatter plot, linear regression and linear correlation values, represented by R, for different pairs signals time-delays. Each row refers to a random pair of brain signals. The columns show the results for subject 1, 2 and 3, respectively, from left to right. The units of time-delays are seconds.

3.6- Results for MC and PL measures relationship

The results for the relation between MC and PL profiles are based on both Pearson correlation and mutual information for a 95% level of significance applied with a Bonferroni correction for the Pearson correlation. For all available subjects of *A* dataset the Left SMA seed region and PPN/FCMN regions were used. For both voluntary and stimulus-driven actions, the results are presented on Figure 39 and Figure 40. All cases show a strong linear correlation and a strong mutual dependency between the variables MC and PL. All the correlation values are above 0.6 and the mutual information values are above 0.8.

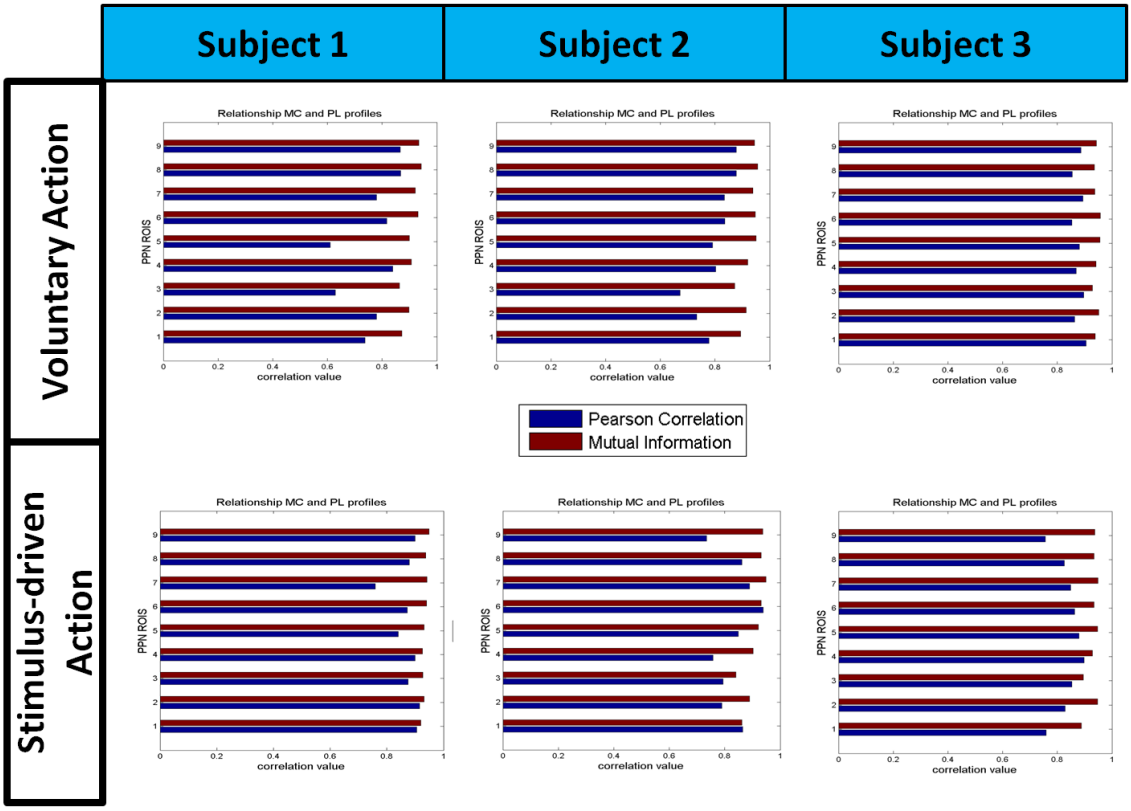

Figure 39- Relationship between MC and PL profiles measured by Pearson correlation and mutual information,MI. The MI values are normalized between [0-1]. Each column presents the results for each subject and the first row reggards to voluntary action, self-paced finger movement, whereas the second one refers to stimulus-driven action, auditory-paced finger movement. The blue bars show the Pearson correlation values whereas the red ones show the MI values for each region belonging to the PPN, see **Table 4.**

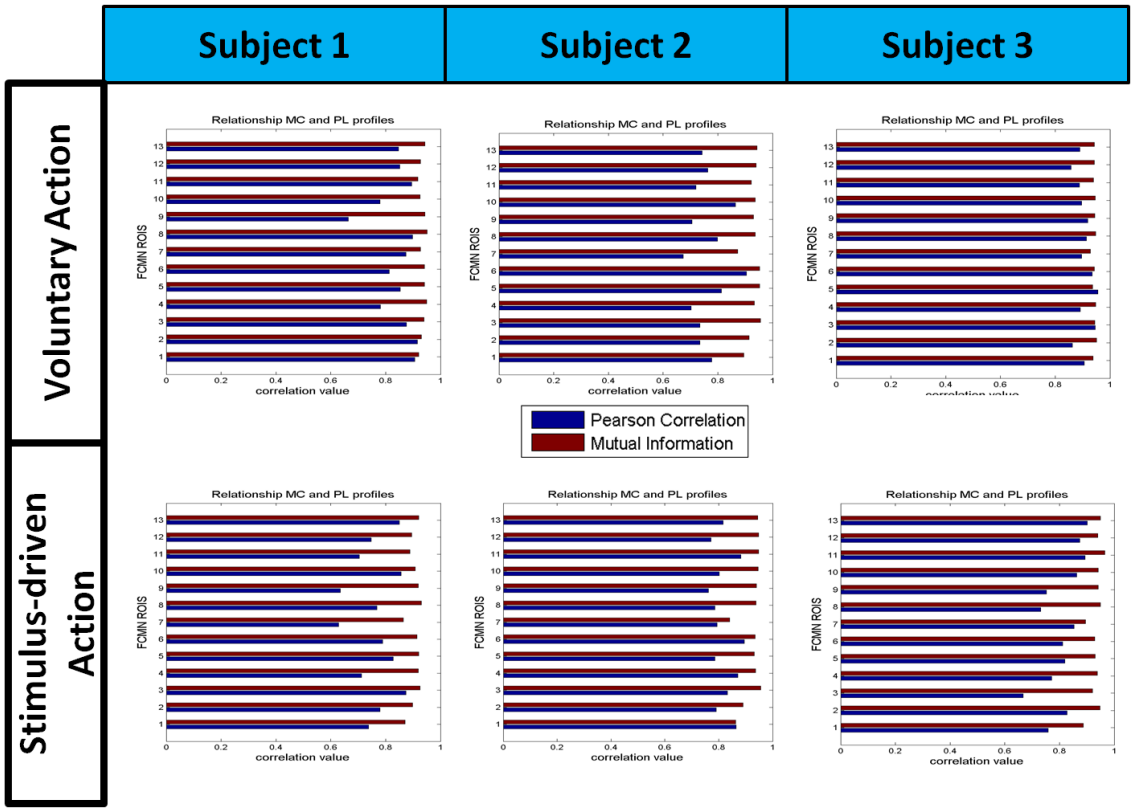

Figure 40- Relationship between MC and PL profiles measured by Pearson correlation and mutual information,MI. The MI values are normalized between [0-1]. Each column presents the results for each subject and the first row reggards to voluntary action, self-paced finger movement, whereas the second one refers to stimulus-driven action, auditory-paced finger movement. The blue bars show the Pearson correlation values whereas the red ones show the MI values for each region belonging to the FCMN, see **Table 4**.

4- DISCUSSION

4.1- Method features

4.1.1- Wavelet coherence - temporal resolution

Based on Lachaux (2002) the wavelet coherence can identify coherence variations within single trials combining a good temporal resolution. The time-frequency analysis allows the study of correlation with respect to frequency which is provided by the wavelet coherence. Wavelet coherence is based on a tradeoff between time and frequency resolution since the temporal resolution increases with frequency whereas the spectral resolution decreases with frequency. It uses an integration window which size is adaptable with the frequency leading to further gain in temporal resolution. However, one disadvantage related to such approach is related to a temporal resolution limitation due to the integration window which requires data recording before and after each time-window. This means that longer acquisitions are better for the wavelet coherence computation. For the *A* dataset subjects, during resting state acquisitions, all subjects had 160 functional echo-planar volumes taken from acquisition from which were removed the first 10 time-points, resulting on 150 time points for analysis. On the wavelet coherence analysis only the time points inside the influence cone are used. This means that for resting state only 134 time points were used during the coherence computation step. For subject 1, during both self-paced and auditory-paced finger movement, from the initial 330 volumes, only 304 are used on the coherence analysis. For subject 2, from the initial 366, 356 time points are indeed used and for subject 3, from 337 initial time-points, 327 are used for coherence computation. Since the longer the acquisition the better the results are, for both task condition both magnitude coherence and phase-locking measures over time are more accurately determine than in resting state condition. From longer scans it is possible to obtain more realistic neuronal communication behavior. The longer acquisitions were taken for task conditions which is favorable since it is expected that task condition involve more complex functional connectivity behavior (involving more brain regions communications during the processing of information).

4.1.2- Choice of input parameters

Over the implemented methodology steps there are some input parameters that must be discussed. The number of cycles for the WTC analysis step was set to 4 cycles. Since we are looking for oscillations close to 0.1Hz, each time-window corresponds to a ~40s period which is adequate based on Lachaux (2002) results. The number of surrogates was set to 1000 to get a reliable number of phase evolution simulations for each pair of brain regions to the statistical test analysis. A p-value of 0.05 was applied to MC and PL statistics, meaning that the selected Magnitude Coherence and Phase-Locking periods are statistically significant for a 95% level of

significance, which was considered an adequate choice that led to the identification of a satisfactory amount of coherence and PL episodes whilst controlling for false positives. All the results, for all subjects, are restricted to subject-specific narrow frequency bands close to 0.1Hz (see Table 3). (This choice was based in information obtained from G. Pfurtscheller, personal communication).

4.2- Magnitude Coherence and Phase-Locking profiles

The implemented methodology is focused on Magnitude Coherence and Phase-Locking measures of neuronal communication. In order to investigate the interactions between different brain regions both measures are used. So, it results on two different profiles of communication for each pair of brain regions as demonstrated on Figure 17. There are three interesting issues about MC and PL profiles: 1- Similarity; 2- Detection of real neuronal communication and 3- Stability, fluctuation and periodicity over time.

First, in relation to similarity the presented methodology used both Pearson correlation and Mutual Information to measure the relationship between a set of brain regions. For all three subjects, it was analyzed PPN and FCMN regions in relation to the left SMA seed, for both task conditions. While the Pearson correlation measures the linear degree dependence between variables, the Mutual Information measures the common information between variables. According to the results, MC and PL measures have a strong linear correlation (above 0.6 for all cases, p-value=0.05) and also a strong mutual dependency tested by mutual information (all values also above 0.8). This means that for all tested cases, 80% of the MC and PL distributions (both between 0 and 1), are common. So, MC and PL distribution share 80% of information. Using both measures it is expected that 80% of the analyzed time-windows have similar values of both MC and PL coherences. So, following the results there is a strong similarity between both measures of neuronal communication during PPN and FCMN regions in relation to the left SMA for both task conditions.

The implemented methodology does not identify which of the two metrics (MC and PL) best detect real neuronal communication periods. To perform such analysis it could be followed the work of Lachaux et al (1999). They used simulated signals with two well-defined phase-locked intervals. Figure 41 represents such analysis where the results show that phase-locking measure correctly detected both episodes, for a 95% level of significance. Whereas the magnitude coherence metric missed the first period of synchronization.

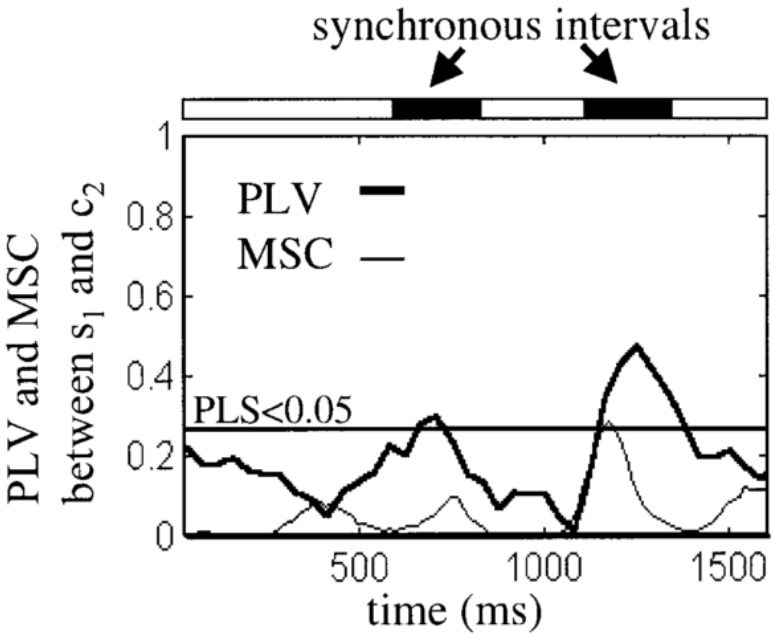

Figure 41- Comparison between neuronal synchrony detection based on both Magnitude coehrence and Phase-Locking measures. The black bold curve shows the PLV, phase-locking, profile over time and the other black curve shows the MSC, magnitude coherence profile, between s1 and c2 simulated signals with two specific synchronous intervals. PLS line corresponds to the statistical significant PLV in a 95% level of significance. Image taken from (Lachaux et al. 1999).

At last, regarding the stability issue, it is seen that both MC and PL profiles fluctuate over time, which is in accordance to the work performed by Handwerker (2012) showing that fMRI correlations fluctuate over time suggesting brain connectivity dynamics. Regarding the periodicity analysis, one possible way to expand these preliminary observations would be a temporal clustering analysis in order to group brain region signals with similar profiles, to detect brain region pairs with similar fluctuations and periodicities correlations over time. This would be followed by a periodicity transform to identify similar sequences over the profiles, following the work of Sethares & Staley (1999).

4.3- Slow oscillations around 0.1Hz

The results showed, for different pairs of brain regions, belonging to specific networks, spontaneous oscillations around 0.1Hz which is in accordance to Biswal et al. (1995) and Greicius et al. (2008). These slow oscillations were obtained during both rest and task conditions which is in accordance with previous findings (Gilden et al. 2001; Vanhatalo et al. 2004; Palva & Palva 2012). The presented fluctuations suggest a dynamic communication between brain regions around 0.1Hz during rest and task conditions acquisitions. These results are relevant since previous studies have already mentioned that ~0.1Hz oscillations are important in movement and decision making (Pfurtscheller et al. 2012).

4.4- Time and Phase-delays measure

There are different methods to investigate latencies across brain regions signals incorporating a variety of experimental paradigms. On the work performed by Sun (2005) the overall linear delay does not depend on a specific feature of the hemodynamic response such as onset or time-to-peak since the resulting value takes into account the entire time-series and not just a small portion of the time-series. The present method differs from Sun work since the resulting values of phase/time-delay are determined for a portion of the time series where it was identified significant magnitude coherence or phase-locking. Based on the phase-spectrum of a specific frequency range, the resulting value is an average from all time-windows of significant neuronal communication. It also does not depend on specific moments of hemodynamic response, but it ensures that the resulting phase/time-delay for neuronal communication is obtained from neuronal communication time-series periods. However, since averaged time-delay is computed for a variable number of values, for one case the averaged can result from for example 200 time-window values and for another case it can be a result from 10 time-windows and obviously the first one is much more accurate. The algorithm does not limit the minimum number of averaged time-points. The algorithm also displays measures of variability such as the standard deviation. The results for non static functional connectivity should consider variability measures and not only averaged quantities (Chang & Glover 2010).

Other methods depend upon a model of the hemodynamic response function, HRF, which has been shown to be highly variable across subjects and regions (Aguirre et al. 1998; Handwerker et al. 2004). The estimation of the time-delays would be dependent on how well the model of the HRF fits the data. Also these methods cannot be used to measure latencies for conditions where no specific timing information is available, such as delay periods during a memory task or rest periods (Biswal et al 1995; Sun et al. 2005). Since the presented methodology does not depend on HRF function modulation it is more easily adapt to a broad range of experimental designs.

The analysis of both MC and PL profiles, over time-windows, and the distribution of time and phase delays for those time-windows of significant magnitude coherence or phase-locking (indicating neuronal communication between two regions) allows to explore the dynamics of communication over time in a specific pair of regions. With such analysis it is possible to investigate if there are brain regions with preferential phase values for communication. The results can show if the phases are preferably distributed according to some distribution or if they are confined to a certain range. The results presented are taken only for a 3 subject dataset, with the goal of testing and illustrate the implemented methodology, so no far-reaching conclusion can be drawn. However, the results suggest some instances of inter-subject consistency: for two subjects, in voluntary action, the phase values during neuronal communication periods are

confined on the range $[-\frac{\pi}{2}; 0]$ for the left SMA in respect to anterior cingulum and anterior insula areas, see Figure 34, Figure 35 and Figure 36 for subject 1, 2 and 3, respectively. These areas are expected to be involved in such paradigm as mentioned on section 1.2.2.2- Task execution.

4.5- Time-delay Consistency across different TR values

The results on Figure 38, for subject 2 and 3, show a strong linear correlation between time-delays for TR=0.92s and for the same data downsampled by a 3 factor. So, this suggests that a shorter or longer TR does not cause major differences between time-delays values. This is reassuring because it suggests that a relatively long TR does not per se preclude the application of this method. However, this is not observed as clearly for Subject 1. There is no apparent reason why donwsampling would be more of an issue for a particular subject. Further probing is needed to ascertain the effects of low temporal sampling in time delay estimation.

4.6- Network dynamics during rest and tasks

4.6.1- Functional connectivity matrices

Observing both Figure 21 and Figure 22, functional matrices for both MC and PL metrics of neuronal communication show a clear relation between the averaged values, over all time-windows, obtained by the two measures. It is also possible to compare the different states of the paradigm and it is seen, for both action states, a globality of higher MC/PL values, suggesting a higher number of brain regions in connection during those states of acquisition. Observing also the Appendix 2- Functional connectivity matrices for subject 2 and 3, it is seen that all subjects present different connectivity matrices for all states of paradigm suggesting variations of neuronal communication among brain regions when executing the same tasks or resting. A visual comparison between MC and PL based matrices show strong similarities suggesting that both measures of functional connectivity can provide similar results of neuronal communication, at least on averaged values. Looking deeply to the presented matrices for the three subjects on all states of the paradigm, there is consistency regarding connected regions that can be part of specific known networks.

In Figure 23 and Figure 24 the functional connectivity within DMN regions for all resting states and for all subjects is analyzed. There seems to be no significant differences between MC and PL measures, however, there are significant differences between subjects matrices. The results on Figure 23 suggest that the focused brain regions, which belong to DMN, are indeed functionally connected with each other during rest. Comparing the presented values for MC and PL during the same paradigm state, as measures of functional connectivity, there seems to be no

significant differences. When looking to Figure 24 there is a clear decrease on both MC and PL measures for all resting states. These results suggest variability within subjects connectivity.

On Figure 25 the high values of MC and PL among FCMN regions suggest strong connection between those regions when performing a voluntary action. This network is expected to be involved in voluntary action as mentioned on 1.2.2.2- Task execution section which is, in this study, the execution of self-paced finger movement. The sub matrices show differences between subjects suggesting also variability within subjects connectivity. Regarding PPN brain regions, they are expected to be related with both voluntary and stimulus actions. Observing Figure 26 all regions present high values of functional connectivity for both MC and PL measures. Both subject 1 and 3 present higher global values of functional connectivity than subject 2. As far as this very small sample allows to infer, there is thus a substantial amount of inter-subject variability.

The developed method allows for detection of specific sets of highly connected brain regions. The reported high functional connectivity is expected in FCMN and PPN regions according to Haggard (2008).

4.6.2- Left SMA - PPN: task conditions

Observing Figure 27, the maps for left SMA-PPN show no significant differences between MC and PL based time-delays. For a 95% statistical level of significance all time-delays vary between -1 and 1 second. Focusing on the left precentral area, which works in association with other motor areas including the SMA and posterior parietal cortex, for all subjects and for both action states of the paradigm, the resulting averaged time-delays are negative. This means that the left SMA area is leaded by the left precentral region, and so it is activated after. According to Sun et al (2005) the M1 is delayed by several hundred milliseconds in relation to SMA and according to Haggard (2008) the SMA leads the M1. So, for these cases the obtained results are not in accordance.

In relation to left SMA and parietal cortex areas, the results are not consistent for the three subjects neither for the analyzed paradigm states. Also left SMA- postcentral areas have no consistency results across subjects. Regarding left SMA and right SMA brain areas, for subject 1, during both voluntary and stimulus-driven action, the neuronal communication seems to be lead by the left SMA (positive averaged time-delays between left and right SMA), however the results for subjects 2 and 3 show an opposite trend.

Recalling the functional matrices on Figure 26 based on averaged magnitude coherence and phase-locking values, over all time-windows, it is expected for cases of high averaged values of MC or PL functional connectivity a bigger number of significant time-windows of neuronal communication than for the cases of lower averaged values of MC and PL. Figure 27 presents

the averaged time-delays for both hypothesis of neuronal communication, meaning that time-delays are averaged only for the selected time-windows of significant communication. If the averaged value of MC/PL functional connectivity is high, it is expected that the neuronal communication between the two regions occurs during an elevated number of time-windows, contrary to the case of low values. This observation is important since the averaged time-delay is more accurate in cases of high number of time-windows presenting significant communication. Regarding the obtained functional sub-matrices for PPN regions, Figure 26, regions numbered from 1 to 6, corresponding to precentral, SMA and postcentral areas are highlighted. Focusing on left SMA row, for subject 1, also the parietal cortex areas present high values of functional connectivity (above 0,6). However, for subject 2 the parietal cortex areas have values below 0,6 for voluntary action, and also subject 3 presents lower values for parietal cortex. This means that the presented averaged time-delays for the left SMA- parietal areas pairs are not so accurate as for the cases of higher values of MC/PL connectivity, since they are obtained from an averaged over a small number of significant time-windows of neuronal communication.

4.6.3- Left SMA - sensorimotor areas: task conditions

Analyzing Figure 28-31, for subject 1, for both voluntary action and stimulus-driven action, the MC and PL profiles show, for all cases, dynamic neuronal communication over time. For the same acquisition state the MC and PL profiles seem quite similar suggesting a relationship between measures. It is also presented on the same figure both time-delay and phase-delay distributions for the time-windows of significant communication at a 95% level of statistical significance. For all cases, there are more than 50% selected time-windows for significant neuronal communication (p-value=0.05).

Regarding to the time-delays distribution in all cases there is a high value of time points selected having significant communication meaning that the averaged values results from a considerable average. All phases distributions, for a same pair, are very similar for MC and PL measures during a specific state of paradigm and quite similar for both voluntary and stimulus-driven actions maybe suggesting preferred phases values for neuronal communication. Analyzing the Table 6, for all cases it is seen that at least 50% of the available time points, Total bins=304, are selected, meaning that the averaged time-delays results from at least 152 values. For L_SMA-L_precentral area, for both MC and PL measures and for both action states, the averaged time-delays suggest that L_precentral area is activated before and it is leading the L_SMA, since the negative values. The averaged time-delays, -0.004s for MC-based measure, are very small and close to zero as the averaged time-delays resulting from PL-based measure,-0.054s. For the other presented ROI pairs, regarding to somatomotor areas, the averaged time-

delays are positive values meaning that the left supplementary motor area, SMA, is leading during both MC and PL neuronal communication periods.

For the other presented ROI pairs, regarding somatomotor areas, the averaged time-delays are positive values meaning that the left supplementary motor area, SMA, is leading during both MC and PL neuronal communication periods. According to Sun (2005) this early activation suggests that the SMA may be involved in initiating and coordinating subsequent motor process across the mentioned regions.

4.6.4- FCMN and PPN: Temporal lead and lag

Considering the Figure 32, and the results on Table 7, for both subject 1 and 3 the averaged time-delays show that the left Basal Ganglia, BG, areas are activated before the Left SMA (positive time-delays values) meaning that BG is leading the left SMA which agrees with the chronometry expected and mentioned in Haggard (2008). For subject 2 the results are also as the expected for two BG areas however for the 71 ROI, left caudate, the results show an opposite trend. It is important to mention that this case is the only one resulting from less than 50% of time-windows selected for significant neuronal communication for both MC and PL measures. Also for the left SMA and left precentral pair the results are opposite to what is expected (Left SMA leading left precentral area) for all subjects.

Regarding Figure 33, the results on Table 8 for stimulus-driven action show for subject 3 the expected chronometry for the ROIs pairs 57-61 and 61-19. However, between L_SMA and L_precentral areas the negative time-delays suggest that contrary to expected, the left precentral area is leading the left SMA for ~0.4 seconds. For both subject 1 and 2 some the results are also not according to the literature, Haggard (2008) review, in terms of the information flow chronometry, showing positive delays for 57-61 and 61-19 pairs. On Table 9, for voluntary action, subject 3 also presents the expected chronometry according to these pairs. The averaged time-delays show different latencies between the pairs of brain regions during stimulus-driven and voluntary action, thereby suggesting task-specific time delays between regions of a specific network, as postulated by Sun (2005).

4.6.5- AIC and ACC : Voluntary action

In relation to Anterior insular cortex and anterior cingulum cortex the obtained time- delays, presented on Table 10, are negative and consistent for almost cases, expect for left cingulum on subject 2. For all the other cases the results show that left SMA is activated before the anterior cingulum and insula regions showing consistency across subjects. For subject 2, ROI pair 19-31 is important to mention that the number of time-windows selected for both MC and PL measures are less than 50% of all time-windows suggesting that the average value can be an inaccurate measure.

Negative values mean that L SMA is leaded by bilateral insula and cingulum areas. So, the insula is leading the left SMA during voluntary action by ~1.5seconds for subject 1, ~0.3 seconds for subject 2 and ~1second for subject 3. The L SMA is leaded by anterior cingulum by ~1second to subject 1 and by ~0.7seconds to subject 3. These results show same variability among subjects as expected.

4.6.6- AIC and Heschl gyrus: Stimulus Action

Regarding the stimulus-driven action, attention is given to anterior AIC cortex and Heschl gyrus. For subjects 1 and 3 the results are consistent showing both left and right Heschl gyrus and anterior insula leading the left SMA. For subject 2 the results are contrary for three pairs. For those pairs less than 50% of time-windows were selected meaning less accurate measures.

4.6.7- M1 and PPC: Rest versus tasks conditions

On Figure 37 it is observed different averaged time-delays for all subjects in rest, stimulus-driven and voluntary action conditions. This again suggests condition-specific delays, as described by Sun (2005). This type of interaction is obtained for the M1 and PCC bilateral areas in relation to the Left SMA. The results are supported by the work performed by Sun (2005) which also reported a similar interaction for left SMA and left M1 brain areas. The results are quite variable among subjects. For subject 1, the SMA-PPC pairs presents less variable results, with the left SMA leading the bilateral PPC. However, for subjects 2 and 3 the results are quite variable among the three states. For stimulus-driven action, the left SMA is leaded by bilateral PPC, however the averaged time-delays are very different for both subjects 2 and 3. Regarding the bilateral M1 areas, for subject 1, the averaged time-delays are very close to zero in all considered states. For subject 2, the left SMA is leaded by the right M1 in all condition states. For left M1, in resting state, the left SMA is leading and for both action conditions the left SMA is leaded by the left M1. For subject 3 the results show that right M1 leads the left SMA in resting condition whereas the latter region leads in the movement conditions. For left M1, in all states, the left SMA is leaded by the left M1 brain area.

To determine the averaged time-delays between the left SMA and bilateral M1 brain areas, at least 50% of the time-windows were selected, meaning that for a 95% level of statistical significance at least 50% of the time-windows have significant magnitude coherence, MC and significant phase-locking, PL. So, these findings show that the left SMA is functionally connected to M1 at resting state. This is in accordance to Sun (2005) results and corroborates previous findings of correlations between M1 and SMA (Biswal et al. 1995; Xiong et al. 1999; Cordes et al. 2000).

4.7- Time-delays: Hemodynamic or neural delays?

Averaged time-delays values show between-subject variability which can be partially due to the known hemodynamic response variability between subjects. Controlling for this factor could involve for instance incorporating a breath-holding challenge in the paradigm (Chang et al. 2008). An interesting topic of discussion which is still investigated is whether fMRI delays between regions can be due primarily to hemodynamic differences or due to neuronal differences. The presented method cannot distinguish between both hypothesis, however, latency differences between rest and task conditions, as shown in Figure 37, suggest a neuronal source, because a strictly hemodynamic factor would not be expected to change consistently between tasks (Sun et al. 2005). Also according to Sun (2005), the finding of latency differences between homologous regions during task and rest support the neuronal delays. For subject 2, the latency between left SMA- left PPC is shorter than the latency of the right PPC in voluntary action, and the latency of the left SMA-right PPC is shorter than the latency on the left PPC in resting state. For subject 3, the latency between left SMA- left PPC is shorter than the latency of the right PPC in resting state, and the latency of the left SMA-right PPC is shorter than the latency on the left PPC in voluntary action. These results are also showed in Figure 37.

5- CLOSING REMARKS

The presented work was carried out in the context of the current interest in functional connectivity analysis and was able to provide new insights into the mechanisms of inter-regional brai communication. The implemented approach innovates by using a time and frequency analysis, based on wavelet transform coherence, to obtain magnitude coherence and phase-locking measures, for specific narrow frequency bands and, over time, for the study of BOLD fMRI signals. This methodology allowed to obtain temporal delay measures for significant periods of communication overcoming the problem of having single-trials. The presented work provides a set of outputs to global analysis for all brain regions and to individual analysis for specific pairs of brain regions. Since the available dataset is composed by only three subjects, the application of the implemented methodology had the goal of test and illustrate the potential of the work, without extending the conclusions about the connectivity dynamics during rest and task execution states to the population level. Some results are in accordance to previous results and other results are not. With a larger set of subjects it would be possible to perform statistical analysis over the results to more global conclusions. So, as future work, one step is to get a more realistic dataset in order to apply the developed method for neuronal communication analysis. The acquisition of a larger dataset is actually inderway within the context of the collaboration between the UT Grax and IBEB/FCUL. Also, the implementation of effective connectivity measures such as Granger causality would improve the work as well the implementation of a graph theory based approach to get an anatomical connectivity component. The combination of anatomical links, functional measures and effective connectivity approach will hopefully be a follow-up of the current work in the very near future and will lead to a more complete and in-depth insight into the mechanisms that underlie the inter-regional communication responsible for the implementation of voluntary motion. It should also be stressed that the methodological approach that was described in the current work can be applied to virtually any brain process that requires synchronized interaction between brain regions.

REFERENCES

Aguirre, G.K., Zarahn, E. & D'esposito, M., 1998. The Variability of Human, BOLD Hemodynamic Responses. *NeuroImage*, 8(4), pp.360–9. Available at: http://www.ncbi.nlm.nih.gov/pubmed/9811554.

Aizenstein, H.J. et al., 2004. The BOLD Hemodynamic Response in Healthy Aging. *Journal of Cognitive Neuroscience*, 16(5), pp.786–93. Available at: http://www.ncbi.nlm.nih.gov/pubmed/15200706.

Andrew, C. & Pfurtscheller, G., 1996. Event-related coherence as a tool for studying dynamic interaction of brain regions. *Electroencephalography and clinical neurophysiology*, 98(2), pp.144–8. Available at: http://www.ncbi.nlm.nih.gov/pubmed/8598174.

Beckmann, C.F., DeLuca, M., Devlin, J.T., Smith, S.., 2005. Investigation into resting state connectivity using independent component analysis. *Philosophical Transactions of the Royal Society B: Biological Sciences*, 360, pp.1001–1013.

Biswal, B. et al., 1995. Functional connectivity in the motor cortex of resting human brain using echo-planar MRI. *Magnetic Resonance in Medicine*, 34, pp.537–541.

Biswal, B., 2012. Resting state fMRI: A personal history. *NeuroImage*, 62(2), pp.938–44. Available at: http://www.ncbi.nlm.nih.gov/pubmed/22326802 [Accessed May 25, 2014].

Bluhm, R.L. et al., 2007. Spontaneous low-frequency fluctuations in the BOLD signal in schizophrenic patients: anomalies in the default network. *Schizophrenia Bulletin*, 33(4), pp.1004–12. Available at: http://www.pubmedcentral.nih.gov/articlerender.fcgi?artid=2632312&tool=pmcentrez&rendertype=abstract [Accessed July 20, 2014].

Brass, M. & Haggard, P., 2007. To do or not to do: the neural signature of self-control. *The Journal of neuroscience*, 27(34), pp.9141–5. Available at: http://www.ncbi.nlm.nih.gov/pubmed/17715350 [Accessed July 12, 2014].

Cabeza, R.& N.L., 2000. Imaging Cognition II: An Empirical Review of 275 PET and fMRI Studies. *J. Cognit. Neurosci.*, 12, pp.1–47.

Cabral, J. et al., 2011. Role of local network oscillations in resting-state functional connectivity. *NeuroImage*, 57(1), pp.130–9. Available at: http://www.ncbi.nlm.nih.gov/pubmed/21511044 [Accessed November 29, 2013].

Chang, C., Cunningham, J.P. & Glover, G.H., 2009. Influence of heart rate on the BOLD signal: the cardiac response function. *NeuroImage*, 44(3), pp.857–69. Available at: http://www.pubmedcentral.nih.gov/articlerender.fcgi?artid=2677820&tool=pmcentrez&rendertype=abstract [Accessed May 27, 2014].

Chang, C. & Glover, G.H., 2010. Time-frequency dynamics of resting-state brain connectivity measured with fMRI. *NeuroImage*, 50(1), pp.81–98. Available at: http://www.pubmedcentral.nih.gov/articlerender.fcgi?artid=2827259&tool=pmcentrez&rendertype=abstract [Accessed November 8, 2013].

Chang, C., Thomason, M.E. & Glover, G.H., 2008. Mapping and correction of vascular hemodynamic latency in the BOLD signal. *NeuroImage*, 43(1), pp.90–102. Available at: http://www.pubmedcentral.nih.gov/articlerender.fcgi?artid=2587338&tool=pmcentrez&rendertype=abstract [Accessed September 22, 2014].

Chao-Gan, Y. & Yu-Feng, Z., 2010. DPARSF: A MATLAB Toolbox for "Pipeline" Data Analysis of Resting-State fMRI. *Frontiers in Systems Neuroscience*, 4(May), p.13. Available at: http://www.pubmedcentral.nih.gov/articlerender.fcgi?artid=2889691&tool=pmcentrez&rendertype=abstract [Accessed July 11, 2014].

Corbetta, M & Shulman, G.L., 2002. Control of goal-directed and stimulus-driven attention in the brain. *Nature Reviews Neuroscience*, 3, pp.201–215.

Cordes, D. et al., 2000. Mapping Functionally Related Regions of Brain with Functional Connectivity MR Imaging. *AJNR. American Journal of Neuroradiology*, 21(9), pp.1636–44. Available at: http://www.ncbi.nlm.nih.gov/pubmed/11039342.

Cunnington, R. et al., 2002. The preparation and execution of self-initiated and externally-triggered movement: a study of event-related fMRI. *NeuroImage*, 15(2), pp.373–85.

Curtin, F. & Schulz, P., 1998. Multiple Correlations and Bonferroni 's Correction. *Biological Psychatry*, 44, pp.775–777.

Damoiseaux, J.S. et al., 2006. Consistent resting-state networks across healthy subjects. *Proceedings of the National Academy of Sciences of the United States of America*, 103 (37), pp.13848–13853.

Dum, R.P. & Strick, P.L., 2002. Motor areas in the frontal lobe of the primate. *Phisiology & Behavior*, 77, pp.677–682.

Fox, M.D. et al., 2005. The human brain is intrinsically organized into dynamic, anticorrelated functional networks. *Proceedings of the National Academy of Sciences of the United States of America*, 102(27), pp.9673–8. Available at: http://www.pubmedcentral.nih.gov/articlerender.fcgi?artid=1157105&tool=pmcentrez&rendertype=abstract.

Fries, P., 2005. A mechanism for cognitive dynamics: neuronal communication through neuronal coherence. *Trends in Cognitive Sciences*, 9(10), pp.474–80. Available at: http://www.ncbi.nlm.nih.gov/pubmed/16150631 [Accessed July 9, 2014].

Gabor, D., 1945. Theory of Communication. *The Journal of The Institute of Electrical Engineers*, pp.429–457.

Gervain, J. et al., 2011. Near-infrared spectroscopy: A report from the McDonnell infant methodology consortium. *Developmental Cognitive Neuroscience*, 1(1), pp.22–46. Available at: http://www.ncbi.nlm.nih.gov/pubmed/22436417 [Accessed November 7, 2013].

Ghuman, A.S., van den Honert, R.N. & Martin, A., 2013. Interregional neural synchrony has similar dynamics during spontaneous and stimulus-driven states. *Scientific reports*, 3, p.1481. Available at:

http://www.pubmedcentral.nih.gov/articlerender.fcgi?artid=3601606&tool=pmcentrez&rendertype=abstract [Accessed June 2, 2014].

Gilden, D.L., Thornton, T. & Mallon, M.W., 2001. 1/f Noise in Human Cognition. *Science*, 267(5205), pp.1837–1839.

Greicius, M.D., Kiviniemi, V., Tervonen, O., Vainionpaa, V., Alahuhta, S., Reiss, A.L. & Menon, V., 2008. Persistent default-mode network connectivity during light sedation. *Human Brain Mapping*, 29, pp.839–847.

Grinsted, A., Moore, J.C, Jevrejeva, S., 2004. Application of the cross wavelet transform and wavelet coherence to geophysical time series. *Nonlinear Processes in Geophysics*, 11, pp.561–566.

Gusnard, D.A. & Raichle, M.E., 2001. Searching for a baseline: Functional imaging and the resting human brain. *Nature Reviews Neuroscience*, 2, pp.685–694.

Haggard, P., 2008. Human volition: towards a neuroscience of will. *Nature Reviews Neuroscience*, 9(12), pp.934–46. Available at: http://www.ncbi.nlm.nih.gov/pubmed/19020512 [Accessed July 17, 2014].

Hampson, M. et al., 2006. Brain connectivity related to working memory performance. *The Journal of neuroscience*, 26(51), pp.13338–43. Available at: http://www.pubmedcentral.nih.gov/articlerender.fcgi?artid=2677699&tool=pmcentrez&rendertype=abstract [Accessed July 15, 2014].

Handwerker, D. a, Ollinger, J.M. & D'Esposito, M., 2004. Variation of BOLD hemodynamic responses across subjects and brain regions and their effects on statistical analyses. *NeuroImage*, 21(4), pp.1639–51. Available at: http://www.ncbi.nlm.nih.gov/pubmed/15050587 [Accessed August 17, 2014].

Hurtado, J.M., Rubchinsky, L.L. & Sigvardt, K.A., 2004. Statistical method for detection of phase-locking episodes in neural oscillations. *Journal of Neurophysiology*, 91(4), pp.1883–98. Available at: http://www.ncbi.nlm.nih.gov/pubmed/15010498.

Jenkins, I.H. et al., 2000. Self-initiated versus externally triggered movements. II. The effect of movement predictability on regional cerebral blood flow. *Brain: A Journal of Neurology*, 123, pp.1216–1228. Available at: http://www.ncbi.nlm.nih.gov/pubmed/10825359.

Lachaux, J. et al., 2002. Estimating the time-course of coherence between single-trial brain signals: an introcuction to wavelet coherence. *Neurophysiol Clin*, 32, pp.157–174.

Lachaux, J.P. et al., 1999. Measuring Phase Synchrony in Brain Signals. *Human Brain Mapping*, 8(4), pp.194–208. Available at: http://www.ncbi.nlm.nih.gov/pubmed/10619414.

Mcintyre, M. et al., 2003. Blood oxygenation level dependent functional magnetic resonance imaging. *Concepts in Magnetic Resonance*, 16A(1), pp.5–15. Available at: http://doi.wiley.com/10.1002/cmr.a.10049 [Accessed May 31, 2014].

McKiernan, K.A., Kaufman, J.N. , Kucera- Thompson, J. & Binder, J.R., 2003. A parametric manipulation of factors affecting task-induced deactivation in functional neuroimaging. *Journal of Cognitive NeuroscienceNeurosci.*, 15, pp.394–408.

Van Milligen, B. et al., 1995. Wavelet bicoherence: A new turbulence analysis tool. *Physics of Plasmas*.

Muller, K., Lohmann, G., Mildner, T., von Cramon, D.Y., 2003. Investigating the stimulus-dependent temporal dynamics of the BOLD signal using spectral methods. *Journal of Magnetic Resonance Imaging*, 17, pp.357–82.

Muller, K., Lohmann, G., Neumann, J., Grigutsch, M., Mildner, T., von Cramon, D.Y., 2004. Investigating the wavelet coherence phase of the BOLD signal. *J. Magn. Reson. Imaging*, 20, pp.145–152.

Muller, K., Lohmann, G., von Cramon, D.Y., 2001. On multivariate spectral analysis of fMRI time series. *NeuroImage*, 2, pp.347–356.

Niedermeyer, E. & Lopes da Silva, F., 2005. *Electroencephalography: Basic Principles, Clinical Applications and Related Fields* Sixth. D. L. Schomer MD. & F. L. Silva, eds., Hardcover.

Ossadtchi, A. et al., 2013. Mutual information spectrum for selection of event-related spatial components. Application to eloquent motor cortex mapping . *Frontiers in Neuroinformatics*, (7:53). Available at: http://www.frontiersin.org/Journal/Abstract.aspx?s=752& name=neuroinformatics&ART_DOI=10.3389/fninf.2013.00053.

Palva, J.M. & Palva, S., 2012. Infra-slow fluctuations in electrophysiological recordings, blood-oxygenation-level-dependent signals, and psychophysical time series. *NeuroImage*, 62(4), pp.2201–11. Available at: http://www.ncbi.nlm.nih.gov/pubmed/22401756 [Accessed November 14, 2013].

Pfurtscheller, G., Daly, I., et al., 2012. Coupling between intrinsic prefrontal HbO2 and central EEG beta power oscillations in the resting brain. *PloS one*, 7(8), p.e43640. Available at: http://www.pubmedcentral.nih.gov/articlerender.fcgi?artid=3427164&tool=pmcentrez&rendertype=abstract [Accessed November 22, 2013].

Pfurtscheller, G., Bauernfeind, G., et al., 2012. Does conscious intention to perform a motor act depend on slow prefrontal (de)oxyhemoglobin oscillations in the resting brain? *Neuroscience letters*, 508(2), pp.89–94. Available at: http://www.ncbi.nlm.nih.gov/pubmed/22206841 [Accessed September 24, 2014].

Pluim, J.P.W., Maintz, J.B.A. & Viergever, M. a, 2003. Mutual information based registration of medical images: a survey. *IEEE Transactions on Medical Imaging*, 20(8), pp.986–1004. Available at: http://www.ncbi.nlm.nih.gov/pubmed/12906253.

Raichle, M.E., 2003. Functional brain imaging and human brain function. *The Journal of neuroscience : the official journal of the Society for Neuroscience*, 23(10), pp.3959–62. Available at: http://www.ncbi.nlm.nih.gov/pubmed/12764079.

Roche-Labarbe, N. et al., 2007. Coupled oxygenation oscillation measured by NIRS and EEG. *NeuroImage*, 36(3), pp.718–727.

Roelfsema, P.R. et al., 1997. Visuomotor integration is associated with zero time-lag synchronization among cortical areas. *Nature*, 385, pp.157–161.

Saab, M., 2009. DC-EEG in Psychophysiology Applications – A Technical and Clinical Overview. *Neurofeedback*. Available at: http://www.bmedreport.com/archives/3739.

Sasai, S. et al., 2012. Frequency-specific functional connectivity in the brain during resting state by NIRS. *NeuroImage*, 63(1), pp.179–193.

Sethares, W. a. & Staley, T.W., 1999. Periodicity transforms. *IEEE Transactions on Signal Processing*, 47(11), pp.2953–2964. Available at: http://ieeexplore.ieee.org/lpdocs/epic03/wrapper.htm?arnumber=796431.

Shannon, C. & Weaver, W., 1964. *The Mathematical Theory of Communication* First., The University of Illinois Press.

Simpson, J. R. J., Snyder, A. Z. Gusnard, D. A. & Raichle, M.E., 2001. Emotion- induced changes in human medial prefrontal cortex: I. During cognitive task performance. *Proc. Natl. Acad. Sci.*, 98, pp.683–687.

Sporns, O., 2007. Brain Connectivity. *scholarpedia*. Available at: http://www.scholarpedia.org/article/Brain_connectivity.

Sporns, O., 2011. *Networks of the Brain* First., Cambridge, London: The MIT Press.

Strother, S.C., 2006. Evaluating fMRI Preprocessing pipelines. *IEEE Engineering in Medicine and Biology Magazine*, 25(2), pp.27–41.

Sun, F.T., Miller, L.M. & D'Esposito, M., 2005. Measuring temporal dynamics of functional networks using phase spectrum of fMRI data. *NeuroImage*, 28(1), pp.227–37. Available at: http://www.ncbi.nlm.nih.gov/pubmed/16019230 [Accessed July 29, 2014].

Torrence C., Compo, G., 1998. A practical guide to wavelet analysis. *Bulletin of the American Meteorological Society*, 79, pp.61–78.

Tzourio-Mazoyer, N. et al., 2002. Automated anatomical labeling of activations in SPM using a macroscopic anatomical parcellation of the MNI MRI single-subject brain. *NeuroImage*, 15(1), pp.273–89. Available at: http://www.ncbi.nlm.nih.gov/pubmed/11771995 [Accessed May 25, 2014].

Vanhatalo, S. et al., 2004. Infraslow oscillations modulate excitability and interictal epileptic activity in the human cortex during sleep. *Proceedings of the National Academy of Sciences of the United States of America*, 101(14), pp.5053–7. Available at: http://www.pubmedcentral.nih.gov/articlerender.fcgi?artid=387372&tool=pmcentrez&rendertype=abstract.

Varela, F.J., 1995. Resonant cell assemblies: a new approach to cognitive functions and neuronal synchrony. *Biol Res.*, 28, pp.81–95.

Vieira, G., 2011. *Modelagem matemática-computacional da conectividade cerebral em ressonância magnética funcional para o estudo do estado de repouso*. São Paulo University.

Witt, S.T., Meyerand, M.E. & Laird, A.R., 2009. Functional neuroimaging correlates of finger tapping task variations: An ALE meta-analysis. *NeuroImage*, 42(1), pp.343–356.

Witte, H. et al., 2004. On the spatio-temporal organisation of quadratic phase-couplings in tracé alternant EEG pattern in full-term newborns. *cCinical Neurophysiology*, 115(10), pp.2308–15.

Xiong, J. et al., 1999. Interregional connectivity to primary motor cortex revealed using MRI resting state images. *Human Brain Mapping*, 8(2-3), pp.151–156. Available at: http://www.ncbi.nlm.nih.gov/pubmed/10524607.

Yuan, H. et al., 2013. Correlated slow fluctuations in respiration, EEG, and BOLD fMRI. *NeuroImage*, 79, pp.81–93. Available at: http://www.ncbi.nlm.nih.gov/pubmed/23631982 [Accessed November 11, 2013].

Zheng, F., Sassaroli, A. & Fantini, S., 2010. Phasor representation of oxy- and deoxyhemoglobin concentrations. *Journal of Bomedical Optics*, 15(4).

APPENDIX

Appendix 1- AAL brain regions used on DPARSF

Number	Regions	Regions
1	Precentral_L	Precental gyrus
2	Precentral_R	Precental gyrus
3	Frontal_Sup_L	Superior frontal gyrus, dorsolateral
4	Frontal_Sup_R	Superior frontal gyrus, dorsolateral
5	Frontal_Sup_Orb_L	Superior frontal gyrus, orbital part
6	Frontal_Sup_Orb_R	Superior frontal gyrus, orbital part
7	Frontal_Mid_L	Middle frontal gyrus
8	Frontal_Mid_R	Middle frontal gyrus
9	Frontal_Mid_Orb_L	Middle frontal gyrus, orbital part
10	Frontal_Mid_Orb_R	Middle frontal gyrus, orbital part
11	Frontal_Inf_Oper_L	Inferior frontal gyrus, opercular part
12	Frontal_Inf_Oper_R	Inferior frontal gyrus, opercular part
13	Frontal_Inf_Tri_L	Inferior frontal gyrus, triangular part
14	Frontal_Inf_Tri_R	Inferior frontal gyrus, triangular part
15	Frontal_Inf_Orb_L	Inferior frontal gyrus, orbital part
16	Frontal_Inf_Orb_R	Inferior frontal gyrus, orbital part
17	Rolandic_Oper_L	Rolandic operculum
18	Rolandic_Oper_R	Rolandic operculum
19	Supp_Motor_Area_L	Supplementary motor area
20	Supp_Motor_Area_R	Supplementary motor area
21	Olfactory_L	Olfactory cortex
22	Olfactory_R	Olfactory cortex
23	Frontal_Sup_Medial_L	Superior frontal gyrus, medial
24	Frontal_Sup_Medial_R	Superior frontal gyrus, medial
25	Frontal_Mid_Orb_L	Superior frontal gyrus, medial orbital
26	Frontal_Mid_Orb_R	Superior frontal gyrus, medial orbital
27	Rectus_L	Gyrus rectus
28	Rectus_R	Gyrus rectus
29	Insula_L	Insula
30	Insula_R	Insula
31	Cingulum_Ant_L	Anterior cingulate and paracingulate gyri
32	Cingulum_Ant_R	Anterior cingulate and paracingulate gyri
33	Cingulum_Mid_L	Median cingulate and paracingulate gyri
34	Cingulum_Mid_R	Median cingulate and paracingulate gyri
35	Cingulum_Post_L	Posterior cingulate gyrus
36	Cingulum_Post_R	Posterior cingulate gyrus
37	Hippocampus_L	Hippocampus
38	Hippocampus_R	Hippocampus
39	ParaHippocampal_L	Parahippocampal gyrus
40	ParaHippocampal_R	Parahippocampal gyrus
41	Amygdala_L	Amygdala
42	Amygdala_R	Amygdala
43	Calcarine_L	Calcarine fissure and surrounding cortex
44	Calcarine_R	Calcarine fissure and surrounding cortex
45	Cuneus_L	Cuneus
46	Cuneus_R	Cuneus

47	Lingual_L	Lingual gyrus
48	Lingual_R	Lingual gyrus
49	Occipital_Sup_L	Superior occipital gyrus
50	Occipital_Sup_R	Superior occipital gyrus
51	Occipital_Mid_L	Middle occipital gyrus
52	Occipital_Mid_R	Middle occipital gyrus
53	Occipital_Inf_L	Inferior occipital gyrus
54	Occipital_Inf_R	Inferior occipital gyrus
55	Fusiform_L	Fusiform gyrus
56	Fusiform_R	Fusiform gyrus
57	Postcentral_L	Postcentral gyrus
58	Postcentral_R	Postcentral gyrus
59	Parietal_Sup_L	Superior parietal gyrus
60	Parietal_Sup_R	Superior parietal gyrus
61	Parietal_Inf_L	Inferior parietal
62	Parietal_Inf_R	Inferior parietal
63	SupraMarginal_L	Supramarginal gyrus
64	SupraMarginal_R	Supramarginal gyrus
65	Angular_L	Angular gyrus
66	Angular_R	Angular gyrus
67	Precuneus_L	Precuneus
68	Precuneus_R	Precuneus
69	Paracentral_Lobule_L	Paracentral lobule
70	Paracentral_Lobule_R	Paracentral lobule
71	Caudate_L	Caudate nucleus
72	Caudate_R	Caudate nucleus
73	Putamen_L	Lenticular nucleus, putamen
74	Putamen_R	Lenticular nucleus, putamen
75	Pallidum_L	Lenticular nucleus, pallidum
76	Pallidum_R	Lenticular nucleus, pallidum
77	Thalamus_L	Thalamus
78	Thalamus_R	Thalamus
79	Heschl_L	Heschl gyrus
80	Heschl_R	Heschl gyrus
81	Temporal_Sup_L	Superior temporal gyrus
82	Temporal_Sup_R	Superior temporal gyrus
83	Temporal_Pole_Sup_L	Temporal pole: superior temporal gyrus
84	Temporal_Pole_Sup_R	Temporal pole: superior temporal gyrus
85	Temporal_Mid_L	Middle temporal gyrus
86	Temporal_Mid_R	Middle temporal gyrus
87	Temporal_Pole_Mid_L	Temporal pole: middle temporal gyrus
88	Temporal_Pole_Mid_R	Temporal pole: middle temporal gyrus
89	Temporal_Inf_L	Inferior temporal gyrus
90	Temporal_Inf_R	Inferior temporal gyrus
91-108	Cerebelum	Cerebelum
109-116	Vermis	Vermis

Appendix 2- Functional connectivity matrices for subject 2 and 3

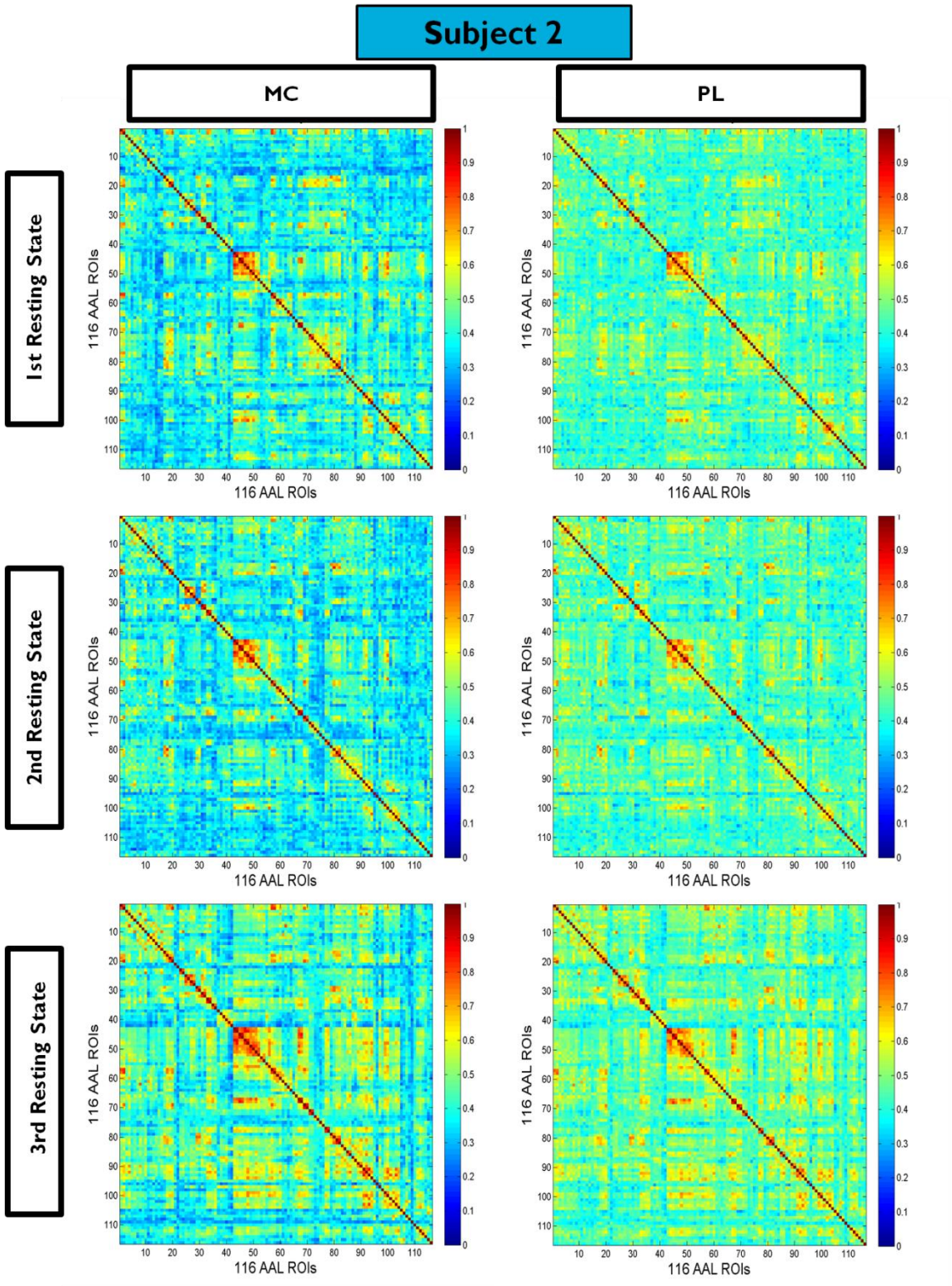

Figure 42- Functional Connectivity matrices for all resting states (for subject 2). On the left: functional measure based on Magnitude Coherence metric and on the right: functional measure based on Phase-Locking. From top to bottom: 1st resting state; 2nd resting state; and 3rd resting state moment of the analyzed paradigm.

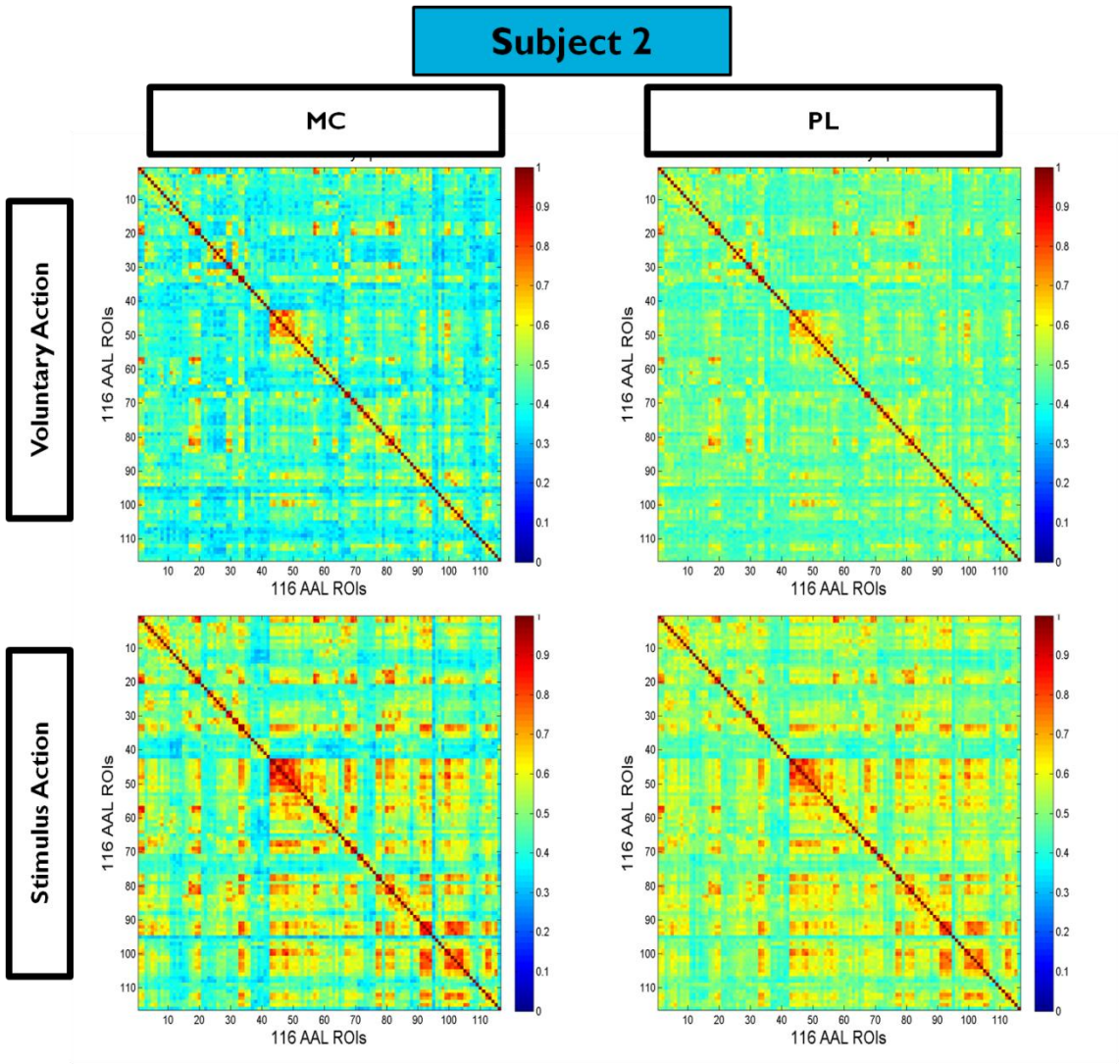

Figure 43- Functional Connectivity matrices for action states (for subject 2). On the left: functional measure based on Magnitude Coherence metric and on the right: functional measure based on Phase-Locking metric. From top to bottom: Voluntary action corresponding to self-paced finger movement and Stimulus action corresponding to auditory-paced finger movement.

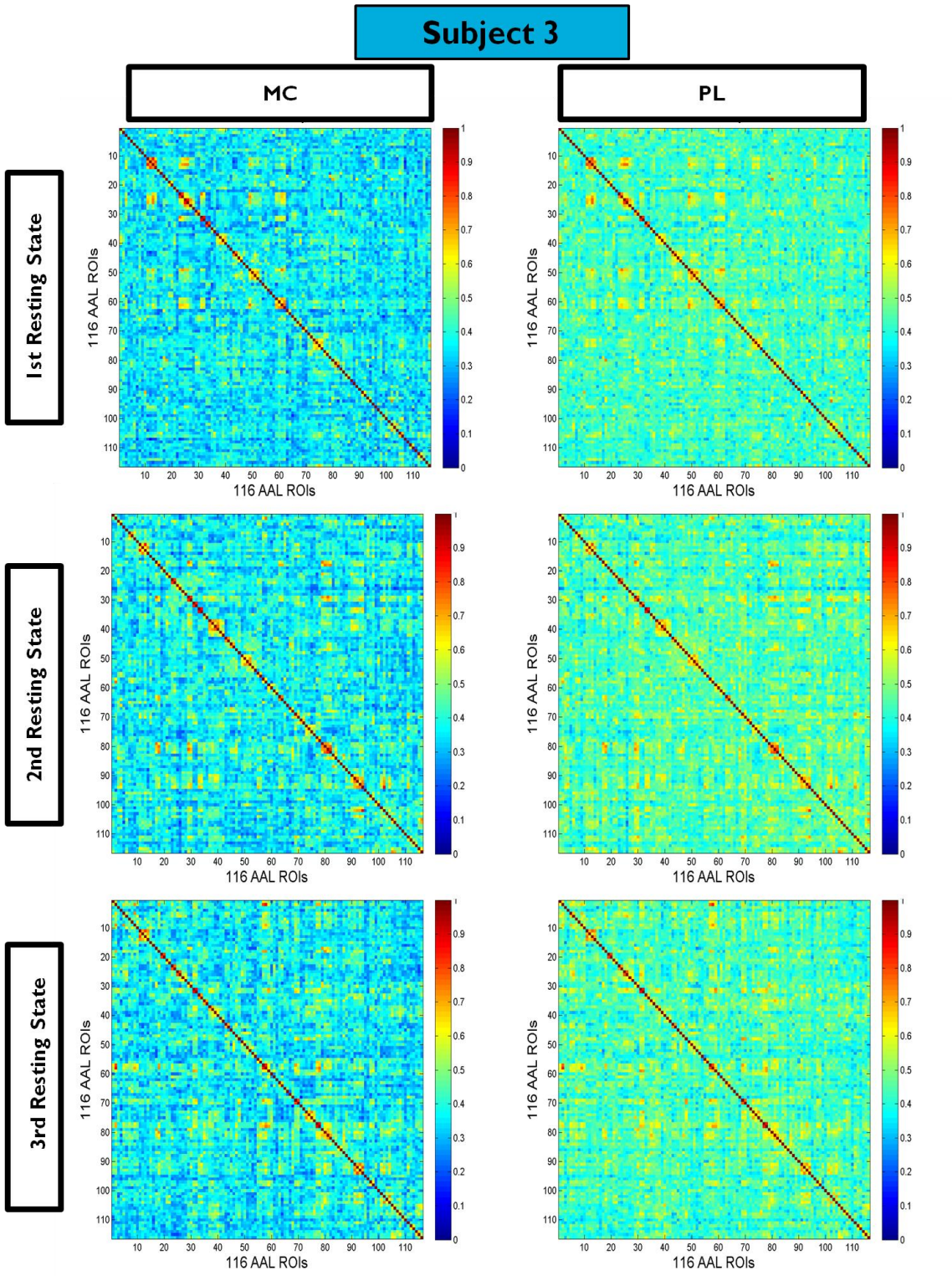

Figure 44- Functional Connectivity matrices for all resting states (for subject 3). On the left: functional measure based on Magnitude Coherence metric and on the right: functional measure based on Phase-Locking. From top to bottom: 1st resting state; 2nd resting state; and 3rd resting state moment of the analyzed paradigm.

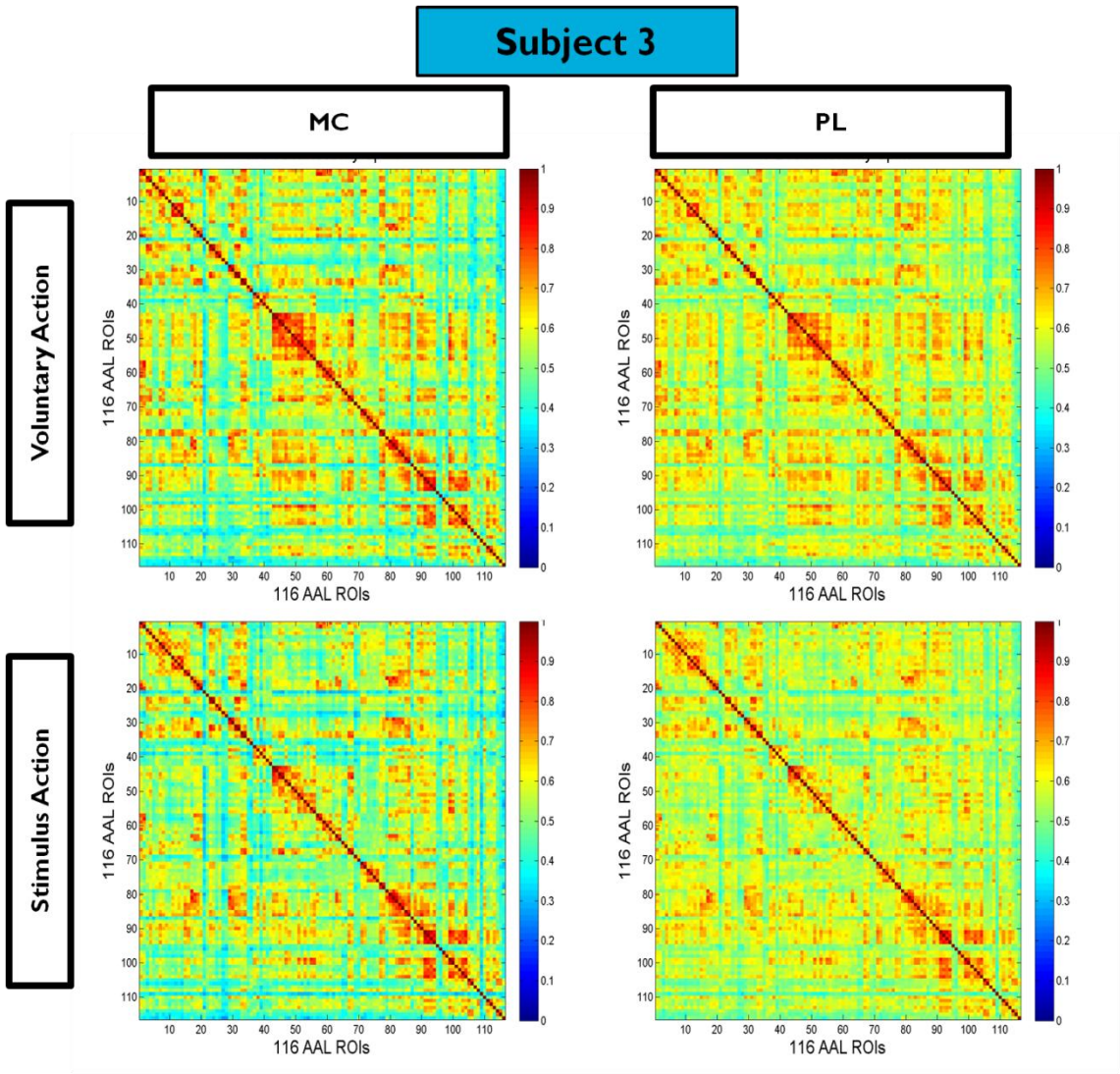

Figure 45- Functional Connectivity matrices for action states (for subject 3). On the left: functional measure based on Magnitude Coherence metric and on the right: functional measure based on Phase-Locking metric. From top to bottom: Voluntary action corresponding to self-paced finger movement and Stimulus action corresponding to auditory-paced finger movement.